Investigation of Application of Wavelets to Detect Minor Insulation Failures during Impulse Tests on Power Transformers

by

Sudath Namal Fernando

A dissertation submitted to the Faculty of Graduate Studies in partial fulfillment of the requirements for the degree of

Doctor of Philosophy

The Department of Electrical and Computer Engineering

The University of Manitoba

Winnipeg, Manitoba, Canada

THE UNIVERSITY OF MANITOBA

FACULTY OF GRADUATE STUDIES

*****

COPYRIGHT PERMISSION

INVESTIGATION OF APPLICATION OF WAVELETS TO DETECT MINOR INSULATION FAILURES DURING IMPULSE TESTS ON POWER TRANSFORMERS

BY

Sudath Namal Fernando

A Thesis/Practicum submitted to the Faculty of Graduate Studies of The University of Manitoba in partial fulfillment of the requirement of the degree

Of

Doctor of Philosophy

Acknowledgements

I express my deep gratitude and appreciation to my thesis advisor, Dr. M.R. Raghuveer, for suggesting the thesis topic, and for his constant guidance, encouragement and support.

I am indebted to Prof. Rohan Lucas (University of Moratuwa, Sri Lanka) for his encouragement to do higher studies and arranging the opportunity to do so.

I appreciate and acknowledge Dr. W. Ziomek (Pauwels Canada) and Dr. F. A. M. Rizk (formerly with IREQ, Quebec) for their input to this work, and Mr. Daryl Hamelin for his assistance in performing laboratory experiments.

Funding from Manitoba Hydro, the University of Manitoba, and the National Science and Engineering Research Council are gratefully acknowledged. I also acknowledge support given by Pauwels Canada Inc. and Carte International Inc. by providing their test facilities for the research work.

I would like to thank his colleagues for many stimulating discussions, particularly Chandana and Nandaka for helping with experimental work.

This acknowledgement would be incomplete without thanking my wife and parents for continuous support, understanding and encouragement in all aspects.

Namal Fernando

August 2008

Summary

Several signal analysis methods have been proposed to overcome the limitations associated with conventional techniques for fault detection during the impulse tests on power transformers. One such group of methods employs wavelet transforms with which test waveforms are analyzed to localize the disturbance in both time and frequency. There have been several reported studies on the application of wavelet transforms to identify insulation failures during impulse tests. Some of these studies have utilized simulated waveforms in which the fault is introduced by a mathematical model. Others have used experimental data that do not realistically simulate minor insulation failures during impulse tests.

This thesis presents results of an investigative study to evaluate the applicability of wavelet-based techniques to detect minor insulation failures during impulse tests on power transformers, by considering experimentally generated waveforms obtained using low-voltage and high-voltage tests on model and actual high voltage coils. The results show that wavelet-based techniques are capable of detecting certain impulse test failures that may not be detected by using conventional techniques.

Based on experimental data and analysis, it is shown that wavelet transform can be successfully applied to detect short-duration temporary faults, which occur within the first 2 μs of the neutral current waveforms. This is not possible by the use of the conventional neutral-current method. It was also found that apart from short-duration temporary faults which occur within the first 2 μs, turn-to-turn faults can be detected using neutral current method. Furthermore, results presented in the thesis do not support the conclusion in some published literature that wavelets can detect minute faults that can not be detected by the neutral-current method.

Table of Contents

List of Figures

List of Tables

Chapter 1

Introduction

The objective of this research was to investigate the suitability of wavelet transform application for detection of minor insulation failures during impulse tests on power transformers. This chapter provides the background and motivation behind the research, the objectives of the investigation, and an overview of the thesis.

1.1 Testing of Power Transformers

The reliability of a power system greatly depends on the reliable operation of power transformers in the power system. Reliability of power transformers can be improved by subjecting them to rigorous testing, in accordance with a well defined test plan with effective test specifications resulting from a joint effort between the manufactures and users of power transformers. The written test plan and specifications should take into consideration the anticipated operating environment of the transformer, including factors such as atmospheric and environmental conditions, type of grounding, characteristics of the protective devices, presence of capacitor banks, power system conditions (short circuits, load rejection, resonance) as well as lightning and switching transients. In addition to rating data of a transformer, the user should include in the specifications and test plan any information or requirements pertaining to service conditions, usual and/or unusual, which may have impact on operational characteristics of the transformer. Selection of appropriate tests and the specifications of correct test levels, which ensure transformer reliability in service, are part of the joint effort [1]. There are several national and international standards available for transformer testing [2–7].

1.2 Impulse Tests on Power Transformers

Impulse testing began on commercial basis in 1933 when the first rules were formulated pertaining to its conduct [8]. The purpose of conducting impulse tests on a transformer is to give a reasonable demonstration that the transformer will withstand electrical stresses due to transient overvoltages in practice. Low frequency dielectric tests do not demonstrate impulse strength because the low frequency test voltage is of lower magnitude and is uniformly distributed throughout the winding, whereas lightning voltage is generally of much higher magnitude and may cause a radical departure from a uniform distribution. Therefore, impulse tests, will give a more adequate demonstration of the sufficiency of the dielectric strength of transformer for service conditions.

There are two types of impulse tests; lightning impulse test and switching impulse test. The purpose of the lightning impulse test is to check the dielectric strength of transformer insulation against overvoltages of atmospheric origin, while the aim of the switching impulse test is to verify the dielectric strength of transformers against switching surges [9].

In switching impulse tests (Section 2.7), owing to a better, nearly linear, distribution of voltage throughout the winding, the fault normally involves major deterioration in the form of a short circuit between sections, parts of a winding or even between windings or to ground. These types of faults cause significant changes in the voltage wave either as a complete collapse of the wave or a shortening of the tail or, sometimes, as a temporary dip in the trace. Hence, the voltage records on switching impulse tests are commonly considered to be sufficiently sensitive to enable the detection of most faults, and will not be investigated in the current research.

Lightning impulse voltage test simulates travelling waves due to lightning strikes and line flashovers. The standard full-wave lightning impulse voltage wave shape is one where the voltage reaches crest magnitude in 1.2 μs, then decays to 50% of the crest magnitude in 50 μs. Such a wave is said to have a wave shape of 1.2/50 μs. In this thesis "impulse test" is used to describe lightning impulse voltage test. More details on impulse tests are given in Chapter 2.

Given the nature of impulse test failures, one of the most important matters to consider is the detection of such failures. The most common method of fault detection is the *neutral-current method*, which consists in comparing the neutral currents produced when a standard lightning impulse is applied to the HV winding terminal at the basic insulation level (BIL) and at a reduced level. Assuming a constant shape of the test impulse over the test-voltage range, the neutral currents are expected to have the same form, provided the test object remains linear. Any nonlinearity observed at higher test voltages implies a disqualifying internal breakdown in the winding, which can be revealed by a usually minor difference between the compared current oscillograms. Section 2.5 deals with different techniques for the interpretation of impulse test results in detail.

Several signal analysis methods have been proposed and some have been implemented to overcome the limitations associated with the fault detection techniques based on the neutral current method. The implementation of these methods have been made possible by considerable improvements in the processing capacity, and data collection hardware. One such group of methods employs *frequency-response* analysis. These methods analyze the captured waveforms in the frequency domain and one such method which has been included into standards [6] is the *transfer-function* method.

In the *transfer-function* method [10, 11], the frequency domain graphs deconvoluted from the test-voltage and neutral current records obtained respectively at full and reduced test levels are compared. The transfer function of a transformer is a characteristic feature and, is in theory, independent of the shape of the applied voltage impulse. The difference between the transfer functions recorded at BIL and at the reduced test level manifests itself as either a frequency shift or pole-height attenuation; empirical interpretation attributes the former to a local breakdown and the latter to partial discharge. This distinction is of great practical importance, since even a minor local breakdown disqualifies the transformer whereas a partial discharge may be tolerated at the BIL, provided the insulation is not damaged [10].

Another type of methods may be categorized as *time-frequency* analysis. In these methods, the waveforms acquired during impulse test are analyzed to localize the disturbance in both time and frequency. One such method is the *wavelet transform* (WT). In the current research work, the main focus was on the applicability of WT to detect minor insulation failures, which occur during impulse tests on power transformers.

1.3 Motivation Behind the Research

Due to the multiresolution property of WT, it can zoom in on the particular details of a signal. One direct consequence of such treatment will be the possibility of accurately locating in time all abrupt changes in the signal and estimating their frequency components as well. Therefore, the use of WT has been suggested in previous work [12, 13] for the detection of insulation failures during impulse tests.

There have been several studies [12–17] on the application of WT to identify insulation failures during impulse tests. Some of these studies have utilized simulated waveforms in which the fault is introduced by a mathematical model. One of these models, simulates the fault current by superimposing a short duration, low amplitude, fast decaying and oscillating signal onto the neutral current. Others have used experimental waveforms for their research work in which faults were simulated by shorting the turns of a coil or a transformer model. These research efforts replicate *permanent faults* within transformer windings.

Following are some of the limitations of the research work carried out in this area and reported in literature.

1. Some have proposed WT for detection of minor insulation failures during impulse using simulated waveforms [12, 13, 15]. The main limitation is the lack of experimental verification using an appropriate method to create minor insulation failures during impulse tests.

2. The neutral current with minor fault due to a minor insulation failure during an impulse test has been simulated using a mathematical model [12, 13], the appropriateness of which has not been verified by experimental results.

3. There are other published works [14, 16, 17] that have used experimental results

to demonstrate the suitability of WT to detect faults. However, they have used *permanent faults* to create neutral currents with minor fault. i.e. minor insulation failures during impulse tests are created by shorting the turns or winding discs using a copper wire.

4. Although the published work demonstrates the use of wavelet functions in this particular application, unfortunately all studies using wavelet analysis have suffered from an apparent lack of *quantitative* results. Also, more work is required in this area to select an optimum wavelet function for fault detection.

1.4 Objectives of the Research

The objective of this research work was to investigate the applicability of WT to detect minor insulation failures during impulse tests on power transformers, by considering experimentally generated waveforms. The experimental waveforms, in the current research, were generated by utilizing a low-voltage (LV) experimental setup using a recurrent surge generator (RSG), and a high-voltage (HV) experimental setup using a 50 kV impulse generator. In the current investigation, the following were achieved in order to reach the main objective of this research.

1. **Development of a LV experimental setup to generate neutral current waveforms with minor insulation failures during impulse tests.** Minor insulation failures were created on a model transformer using neon lamps and a 1000 V RSG. Since these faults due to minor insulation failures last only a short time, faults created using neon lamps are termed *temporary faults.* Wavelets are suitable for analyzing signals that last for a few microseconds and have relatively high frequency components. When faulty neutral currents are gener-

ated by using the method proposed in the current research work, they create disturbances in the neutral current that are ideal for WT detection.

2. **Development of a HV experimental setup to generate neutral current waveforms with minor insulation failures during impulse tests.** The minor faults between sections of an actual transformer coil were created by using miniature sphere gaps and a 50 kV impulse generator. Artificial faults created by using a sphere gap also produced temporary faults and wavelet-based techniques are suitable for analyzing such signals. Because of lower turn-on voltage of neon lamps, it was planned to use them if the voltage created was insufficient to cause sparkover of sphere gap.

3. **Development and implementation of statistical analysis technique to select the best basis for fault detection.** A quantitative method is proposed to select best basis functions for fault detection. This method assumes that perturbations due to minor insulation failures could be simulated by a short duration, low amplitude, fast decaying and oscillating signal.

4. **Development and implementation of wavelet-based algorithm for de-noising of experimental waveforms.** The proposed algorithm consists of the selection of the wavelet function, number of levels of decomposition, and the threshold rule for a wavelet-based noise reduction technique. Validity of the algorithm will be demonstrated using experimental data.

5. **Analysis of LV and HV experimental results for fault detection using wavelet-based techniques.** Impulse test results were analyzed by using continuous wavelet transform, multiresolution signal decomposition, and wavelet packets.

6. Comparison of the features of proposed wavelet-based techniques with neutral-current method and transfer-function method.

7. Examination of the sensitivity of wavelet-based techniques, and whether or not it represents an improvement over existing techniques.

1.5 Thesis Overview

Chapter 2 is an introduction to impulse tests on power transformers in some detail. The windings of a power transformer are exposed to different types of overvoltages. These overvoltages, their effect on the windings, and a brief overview of the methods to determine transient response of transformers are discussed. This chapter also provides a comprehensive overview of lightning impulse tests as per most recent technical standards. Finally, a short introduction to switching impulse tests is included.

An overview of wavelet theory is given in Chapter 3. In order to understand the wavelet transform better, the Fourier transform is briefly explained. Generally, there are no explicit formulas for the basis functions $\phi(t)$ and $\psi(t)$. Hence most algorithms concerning scaling functions and wavelets are formulated in terms of the filter coefficients. This chapter includes an example of computing the function values of $\phi(t)$ and $\psi(t)$ for the Daubechies 4-coefficient scaling function and wavelet (db2).

A detailed review, in chronological order, of published research work on the application of time-frequency based methods to detect minor faults during impulse tests on power transformers is given in Chapter 4. This is followed by a general discussion which highlights the limitations of the published work, and provides a rationale for the motivation behind the present research. This chapter also provides a brief review of the transfer-function method for detection of impulse test failures.

Chapter 5 describes low-voltage (LV) impulse tests on a model transformer, which was used in the current research to generate neutral current waveforms. The neutral currents were analyzed using wavelet-based techniques to detect artificially created minor insulation failures, and results are reported in Section 5.5. Since the efficiency of WT to detect faults depends on the wavelet function, this chapter proposes a quantitative method to select the optimum wavelet function for impulse failure detection. This chapter also provides an algorithm for denoising. Proposed algorithm consists of basis function, threshold method, and decomposition level. Validity of the algorithm is demonstrated using experimental data.

Chapter 6 describes high-voltage (HV) impulse tests on an actual transformer coil. Minor insulation failures were artificially created by using sphere gaps, and neon lamps. Neutral-current waveforms were analyzed using different wavelet-based techniques. These results were compared with other methods, where faults are detected in analyzing waveforms in the time-domain and frequency-domain. Sensitivity of the proposed methods for fault detection is explored by considering faults at different locations along the coil.

Finally, in Chapter 7 conclusions are drawn and the contribution of the research are pointed out. Suggestions are given for future work covering the areas which need further research. Appendices A and B provide details of the impulse generator, technical specifications of the instrumentations used for the experimental work, and HV transformer coil. At the end of the appendices, all the acronyms used in this thesis have been listed.

Chapter 2

Power Transformer Impulse Tests

The windings of power transformers are exposed to voltage surges arising from lightning or switching. Depending on the waveshape of the surges, the internal voltage distribution, thus, the voltage stress on different parts of the insulation system varies. To prevent damage to the transformer due to the breakdown in its insulation system, the equipment must be designed to withstand surges, the peaks of which may be many times the working voltage of the power system. Impulse tests are performed on the power transformer to verify the design of the insulation system for anticipated surges as specified in customer's technical specifications.

2.1 Voltage Appearing Across the Transformer Terminals

Dielectric tests on power transformers should demonstrate the ability of the transformer to survive different types of voltages that appear across its terminal, and it should not damage the insulation. Type of dielectric tests and their magnitudes should be based upon the conditions that the transformer will experience during its operating lifetime. Fig. 2.1, based on IEC 60071-1 2006 [18], shows the voltage or overvoltage shapes in the system, and corresponding standard voltage shapes applied in a standard withstand voltage test. The voltages to which a transformer's terminals are subjected can be broadly classified as low-frequency and transient.

The majority of the voltages that a transformer experiences during its operational life are low-frequency, e.g., the voltage is within $\pm 5\%$ of nominal, and the frequency is within 1% of rated. Sustained relatively lower-frequency (10 to 500 Hz) overvoltage can result from Ferranti rise, load rejection, and ferroresonance. These effects can produce abnormal turn-to-turn and phase-to-phase stresses. Then again, line-to-ground faults can result in unbalance and very high terminal-to-ground voltages, depending upon system grounding. Low-frequency dielectric tests which consist of the applied voltage test, induced test, and partial discharge test demonstrate that the strength of the transformer insulation system has the necessary dielectric strength to withstand the voltages indicated in the tables of standards [3, 5, 7] for low-frequency tests.

Transient voltage refers to a class of excitation caused by events like lightning surges, switching events, and line faults causing voltages with a chopped waveform [19]. Normally, these are aperiodic waves. There are the following three types of transient overvoltage waves that a transformer may be subjected during it life.

2.1.1 Slow-front Transients

Slow-front transient overvoltages are referred to as switching overvoltages. Their frequency depends on the natural frequency of the system and they are produced by some switching-in or switching-out operation or by a network fault. Most of these overvoltages are highly damped phenomena of relatively short duration. According to IEC 60071-1 2006 [18], the shape of a slow-front overvoltage is usually unidirectional

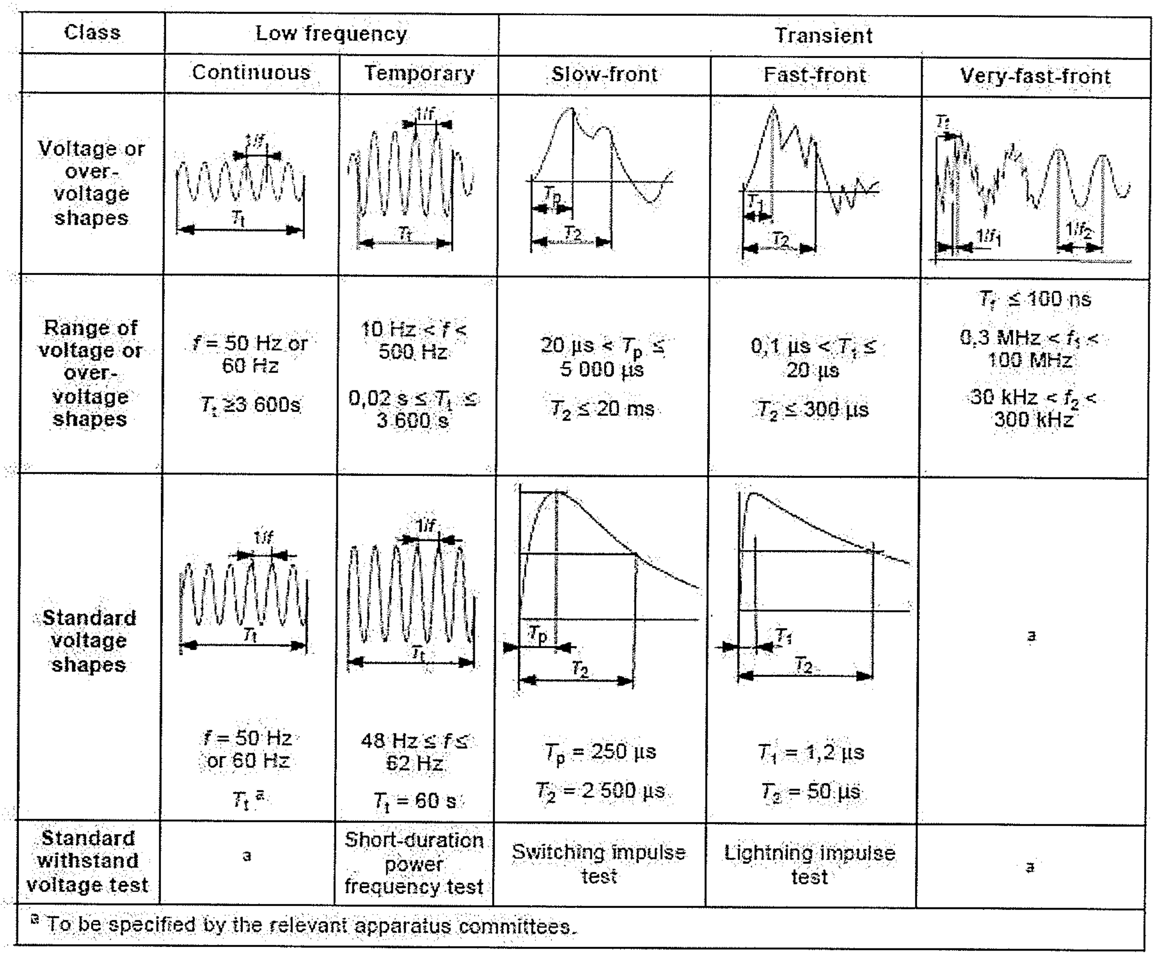

Class	Low frequency		Transient		
	Continuous	Temporary	Slow-front	Fast-front	Very-fast-front
Voltage or over-voltage shapes					
Range of voltage or over-voltage shapes	f = 50 Hz or 60 Hz $T_t \geq$ 3 600s	10 Hz < f < 500 Hz 0,02 s $\leq T_t \leq$ 3 600 s	20 µs < $T_p \leq$ 5 000 µs $T_2 \leq$ 20 ms	0,1 µs < $T_1 \leq$ 20 µs $T_2 \leq$ 300 µs	$T_f \leq$ 100 ns 0,3 MHz < f_1 < 100 MHz 30 kHz < f_2 < 300 kHz
Standard voltage shapes	f = 50 Hz or 60 Hz T_t [a]	48 Hz $\leq f \leq$ 62 Hz T_t = 60 s	T_p = 250 µs T_2 = 2 500 µs	T_1 = 1,2 µs T_2 = 50 µs	a
Standard withstand voltage test	a	Short-duration power frequency test	Switching impulse test	Lightning impulse test	a

[a] To be specified by the relevant apparatus committees.

Figure 2.1: Classes and shapes of overvoltages, standard voltage shapes and standard withstand voltage tests

with time to peak between 20 to 5,000 μs; the total duration is less than 20 ms.

Overvoltages due to switching surges generally have crest magnitudes, which range from about 1.0 to 3.0 pu for phase-to-ground surges and from about 2.0 to 4.0 pu for phase-to-phase surges (in pu of the phase-to-ground crest voltage base) with higher values sometimes encountered as a result of a system resonant condition. Waveshapes vary considerably with rise times ranging from 50 to thousands of microseconds, and times to half value in the range of hundreds of microseconds to thousands of microseconds [20].

The switching surge distributes voltage inside the transformer inductively almost from the beginning, and causes no oscillations of high magnitude. Because of its longer duration, for the same voltage, it imposes more severe stress on the winding to ground insulation compared to a fast-front transient [21].

The ability of the transformer to withstand slow-front transient voltages is readily demonstrated by factory switching surge tests at levels a reasonable margin above those it will experience in service. Switching impulse tests are discussed in Section 2.7 in detail.

2.1.2 Fast-front Transients

The duration of overvoltages of atmospheric (external) origin is even shorter than that of internal overvoltages, and caused mainly by lightning strikes. Such overvoltages appearing in high voltage networks may either be due to direct strikes on the line or to strikes to ground (indirect strikes) very close to the line. The travelling waves thus produced are unidirectional voltage pulses with time to peak between 0.1 to 20 μs; the total duration is less than 300 μs.

Overvoltage due to lightning has a great effect on insulation between parts of a winding (between turns, between taps, between layers or sections), largely because of the initial capacitively distributed voltages and of the subsequent oscillatory transient voltages, which occur between the parts during the interval between the initial capacitive distribution and the final inductive voltage distribution [21].

For testing the strength of the transformer insulation to withstand overvoltages of external origin a test voltage having a wave shape closely similar to that caused by a lightning strikes, termed a lightning impulse voltage, is applied. The lightning impulse test is the main focus of this thesis, and is discussed in Section 2.4 in detail.

2.1.3 Very-fast-front Transients

Disconnecting switch operations in Gas Insulated Substations (GIS) generate steep front transient overvoltages characterized by a very fast front overvoltage, which is usually unidirectional with time to peak less than 0.1 μs, total duration less than 3 ms, and with superimposed oscillations at frequency 30 kHz $< f <$ 100 MHz. In practice, the term VFT is restricted to describe transients with frequencies above 1 MHz [20].

The 50% breakdown probability voltage of oil-paper insulation is lower for steep fronted GIS transients than for lightning impulses [22]. The oil-paper insulated equipment like transformers or their bushings, subjected to GIS transients, may fail at voltages below the lightning impulse level. Hence, the insulation of transformers for the GIS application must be designed with due consideration to these steep fronted transients. Furthermore, due to steep fronted wave impulses, directly connected transformers can experience an extremely nonlinear voltage distribution along the high-voltage winding, connected to the oil-SF_6 bushings, and high resonance voltages due to transient oscillations generated within the GIS. Transformers can generally withstand these stresses; however, in critical cases, it may be necessary to install surge arresters to protect tap changers [23].

There is, as yet, no standard waveshapes for testing a transformer insulation for VFT.

2.2 Initial Voltage Distribution

The initial voltage distribution in the winding of a power transformer during a transient disturbance depends on the internal capacitances of the transformer winding and the capacitances between windings and grounded structures. The initial charging current diminishes to zero when the capacitance network is charged. The time required for charging is a very small fraction of a microsecond [24]. This justifies the assumption that, during the initial period, the highly inductive transformer winding draws no significant current and may be considered as though if open-circuited.

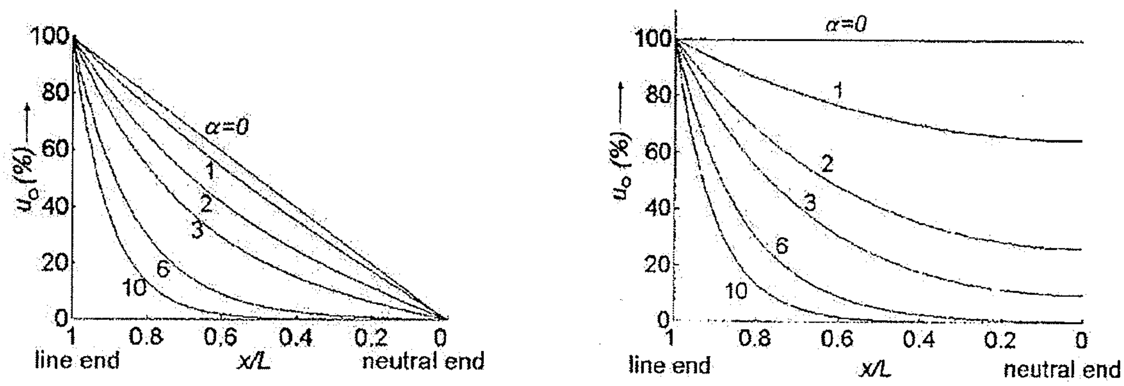

(a) Grounded neutral (b) Isolated neutral

Figure 2.2: Hyperbolic voltage distribution within transformer winding.

Depending on whether the other end of the winding is isolated or grounded, the equation governing the voltage distribution, at the end of the initial charging period, takes the following forms.

For grounded neutral (Fig. 2.2(a))

$$v_x = V\frac{\sinh(\alpha x)}{\sinh(\alpha)} \tag{2.1}$$

and for an isolated neutral (Fig. 2.2(b))

$$v_x = V\frac{\cosh(\alpha x)}{cosh(\alpha)} \tag{2.2}$$

In both the above equations

$$\alpha = \sqrt{\frac{C_g}{C_s}} \tag{2.3}$$

where

x	distance along the coil stack as a fraction of the stack height
v_x	voltage to ground at point x
α	winding gradient
C_g	capacitance of winding to ground
C_s	effective series capacitance

The presence of capacitance to ground causes a non-uniform voltage distribution as shown in Fig. 2.2. The higher the value of α, the deviation between the initial and final voltage distributions are larger; also the amplitudes of oscillations which occur between the two distributions are greater. For plain disk windings, α generally varies from 5 to 15. An outer coil has a lesser value of α compared to a similar inner coil as the latter faces two ground planes (i.e. higher C_g) [25].

When the applied voltage is maintained for a sufficient time (50 to 100 μs), appreciable current begins to flow in the inductances eventually leading to a uniform voltage distribution. The difference between the initial and final voltage distributions are shown in Fig. 2.3.

The nonlinearity of the initial voltage distribution can be improved by using *electrostatic shields* at the line end of a disc winding. These shields are electrically connected to the end-section. The initial voltage distribution in the end-section becomes more linear, because of the large capacitance between the shield and the turns

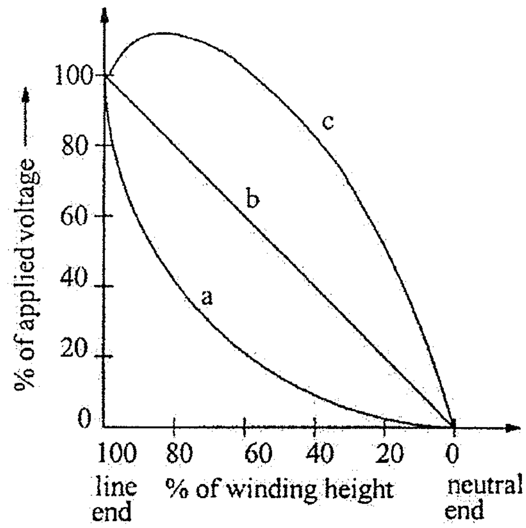

Figure 2.3: Impulse Voltage distribution (a) initial distributions (b) final distribution (c) maximum voltage to ground

of the end-section. Another method is the use of *interleaved disc windings*, which attempt to increase C_s. A detailed analysis of interleaved transformer windings is given in [26]. The other approach is to use *Shielded layer windings*, in which nonlinearity is reduced by decreasing C_g.

The initial voltage distribution can be determined experimentally by applying a voltage wave with a fairly fast rise time (e.g. 0.5 μs) and measuring the normalized distribution within the winding structure at an intermediate time (e.g. 0.3 μs). The initial distribution can be computed analytically by injecting a current into the excited node and determining the normalized voltage throughout the transformer winding structure. This computational method is outlined in detail by Degeneff and Kennedy [27].

2.3 Response of Transformer Windings to Transient Voltages

Considerable research has been devoted to determining the transformer's internal transient voltage distribution . These attempts started at the beginning of the 1900's and have continued at a steady pace for almost 100 years [28]. The objective of this section, based on article written by Degeneff in [20], is to provide a brief overview of the methods to determine the transient response of transformers.

2.3.1 Lumped Parameter Model

A device's transient response is a result of the flow of energy between the distributed electrostatic and electromagnetic characteristics of the device. For all practical transformer winding structures, this interaction is quite complex and can only be realistically investigated by constructing a detailed lumped parameter model of the winding structure and then carrying out a numerical solution for the transient voltage response. The most common approach is to subdivide the winding into a number of segments (or groups of turns). The method of subdividing the winding can be complex and, if not addressed carefully, affects the accuracy of the resultant model. The resultant lumped parameter model is composed of inductances, capacitance, and losses. Starting with these inductances, capacitances, and resistive elements, equations reflecting the transformers transient response can be written in numerous forms. Two of the most common are the basic admittance formulation of the differential equation and the state variable formulation. The admittance formulation [29] is given by :

$$[I(s)] = \left[\frac{1}{s}[\Gamma_n] + [G] + s[C]\right][E(s)] \tag{2.4}$$

The general state-variable formulation is given by Vakilian [30, 31] describing the transformers lumped parameter network at time t:

$$\begin{bmatrix} L & 0 & 0 \\ 0 & C & 0 \\ 0 & 0 & U \end{bmatrix} \begin{bmatrix} di_e/dt \\ de_n/dt \\ df_e/dt \end{bmatrix} = \begin{bmatrix} -r & T^t \\ -T & -G \\ -r & T^t \end{bmatrix} \begin{bmatrix} i_e \\ e_n \end{bmatrix} - \begin{bmatrix} 0 \\ I_s \\ 0 \end{bmatrix} \tag{2.5}$$

where the variables in Equation (2.4) and (2.5) are:

i_e	Vector of currents in the winding segments
e_n	Models nodal voltages vector
f_e	Windings flux-linkages vector
r	Diagonal matrix of windings series resistance
T	Windings connection matrix
T^t	Transpose of T
C	Nodal capacitance matrix
U	Unity matrix
$[I(s)]$	Laplace transform of current sources
$[E(s)]$	Laplace transform of nodal voltages
Γ_n	Inverse Nodal Inductance Matrix = $[T][L]^1[T]^t$
L	Matrix of self and mutual inductances
G	Conductance matrix, for resistors connected between nodes
I_s	Vector of current sources

In a linear representation of an iron core transformer, the permeability of the core is assumed constant regardless of the magnitude of the core flux. This assumption allows the inductance model to remain constant for the entire computation. Equations (2.4) and (2.5) are based on the assumption that the transformer core is linear and the various elements in the model are not frequency dependent. Work in the last decade has addressed both the nonlinear characteristics of the core and the frequency dependent properties of the materials. Much progress has been made, but their inclusion adds considerably to the model's complexity and computational difficulty. If the core is nonlinear, the permeability changes as a function of the material properties, past history, and instantaneous flux magnitude. Therefore, the associated inductance model becomes time dependent. The basic strategy for solving the transient response of the nonlinear model in Equation (2.4) or Equation (2.5) is to linearize the transformer's nonlinear magnetic characteristics at an instant of time based on the flux in the core at that instant.

Two other model formulations should be mentioned. De Leon addressed the transient problem using a model based on the idea of duality [32]. The finite element method has found wide acceptance in solving for electrostatic and electromagnetic field distributions. In some instances it is very useful in solving for the transient distribution in coils and windings of complex shape.

2.3.2 Frequency Domain Solution

A set of linear differential equations representing the transient response of the transformer can be solved either in the time or frequency domain. If the model is linear, the resultant solution will be the same for either method. The frequency domain solution requires that the components of the input waveform at each frequency be determined. These individual sinusoidal waves are then applied individually to the transformer and the resultant voltage response throughout the winding is determined. Finally, the total response in the time domain is determined by summing the component responses at each frequency applying superposition. An advantage of this method is that it allows the recognition of frequency-dependent losses to be addressed easily. Disadvantages of this method are that it does not allow the modelling of time-dependent switches, nonlinear resistors like ZnO, or the recognition of nonlinear magnetic core characteristics.

2.3.3 Solution in the Time Domain

The following briefly discusses the solution of Equation (2.4) and Equation (2.5). There are numerous methods to solve Equation (2.4) but it has been found that when solving the stiff differential equation model of a transformer, a generalization of Dommels method [29, 33] works very well. A lossless lumped parameter transformer model containing n nodes has approximately $n(n+1)/2$ inductors and $3n$ capacitors. Since the total number of inductors far exceeds the number of capacitors in the network, this methodology reduces storage and computational time by representing each capacitor as an inductor in parallel with a current source. The following system of equations results:

$$[\hat{Y}][F(t)] = [I(t)] - [H(t)] \tag{2.6}$$

where

$[F(t)]$	nodal integral of the voltage vector
$[I(t)]$	nodal injected current vector
$[H(t)]$	past History current vector

and

$$[\hat{Y}] = \frac{4}{\Delta t^2}[C] + \frac{2}{\Delta t}[G] + [\Gamma_n] \tag{2.7}$$

The lumped parameter model is composed of capacitances, inductances, and losses computed from the winding geometry, permittivity of the insulation, iron core permeability, and the total number of sections into which the winding is divided. The matrix $[\hat{Y}]$ is then computed using the integration step size, Δt. At every time step, the above system of equations is solved for the unknowns in the integral of the voltage vector. The unknown nodal voltages, $[E(t)]$, are calculated by taking the derivative of $[F(t)]$. Δt is selected based on the detail of the model and the highest resonant frequency of interest. Normally, Δt is smaller than one-tenth the period of this frequency.

Most transformer winding models can simulate the actual winding behaviour with a reasonable accuracy up to 100 kHz. This is considered sufficient to represent the frequency spectrum of the standard lightning impulse, and the transients generated by the transmission system [34, 35].

2.4 Lightning Impulse Tests

The purpose of the lightning impulse test is to check the dielectric strength of transformer insulation against overvoltages of atmospheric origin. IEC recommends this test to be performed as a type test on transformers with HV winding having $U_m \leq 72.5\ kV$ (U_m is the highest voltage rating for the equipment), and as a routine test on transformers of higher voltage ratings, by applying a standard negative-polarity 1.2/50 μs impulse voltage wave described in Section 2.4.1. The extension of the lightning impulse test to include impulses chopped on the tail as a special test is recommended in cases where the transformer is directly connected to GIS by means of oil/SF_6 bushings or when the transformer is protected by rod gaps. The peak value of the chopped impulse shall be 10% higher than for the full impulse [5]. The test sequence consists of one impulse of a voltage between 50% and 75% of the full test voltage, and three subsequent impulses at full voltage.

According to IEEE standards, impulse tests are routine for Class II power transformers (power transformers with HV windings from 115 kV through 765 kV). The test sequence consists of voltage applications in the following order: one reduced full wave, two chopped waves, and one full wave. The time interval between application of the last chopped wave and the final full wave should be minimal to avoid recovery of dielectric strength if a failure were to occur prior to the final full wave. When front-of-wave (FOW) tests are also specified, impulse tests are generally applied in the following order: one reduced full wave, two FOW, two chopped waves, and one full wave. IEC standards do not recommend the use of FOW.

The actual sequence of impulse tests depends on the transformer purchasers' requirement. The following test sequence is typical for Manitoba Hydro:
For windings without non-linear resistors:

- one reduced full wave impulse, typically 50% BIL
- one reduced chopped wave impulse,
- two 110% chopped wave impulses,
- two 100% full wave impulses

For windings with non-linear resistors:

- one reduced full impulse,
- one 80% full wave impulse,
- one 100% full wave impulse,
- one reduced chopped wave impulse,
- two 110% chopped wave impulses,
- two 100% full wave impulses,
- one 80% full wave impulse,
- one reduced full wave impulse

This sequence also applies to neutral terminals suitable for ungrounded operation, otherwise, the neutral receives a reduced and two full waves, however, with slower wave (longer front time up to 13 μs). The sequence of impulse voltage application to the transformer terminal shall be from the highest to the lowest voltage ratings. Each unit shall be tested with its own bushing in place. In case where a bushing has to be replaced, this bushing shall be impulse tested as an individual unit.

2.4.1 Lightning Impulse Wave Shapes

Under the present lightning impulse test standards [4,6] there are the following three types of voltage waves applied to a winding terminal.

Full wave

If a lightning disturbance travels some distance along the transmission line before it reaches the transformer, its wave shape approaches a full wave as shown in Fig. 2.4(a), and is described by its time to crest and its time to half value of the tail [36]. The virtual front time (T_1) of a lightning impulse is 1.67 times the time interval between the instants when the impulse is 30% and 90% of the peak value, corresponding to points A and B in Fig. 2.4(a). If oscillations are present on the front, points A and B should be taken on the mean curve drawn through these oscillations. The virtual time to half-value (T_2) of a lightning impulse is the time interval between the virtual origin (O_1) and the instant on the tail when the voltage has decreased to half of the peak value. The standard lightning impulse is a full lightning impulse having a virtual front time of 1.2 μs and a virtual time to half-value of 50.0 μs. It is described as a 1.2/50.0 μs impulse. The tolerance on time to crest should normally be $\pm 30\%$, and the tolerance on time to half of crest shall normally be $\pm 20\%$ [3,5].

In the case of impulse test on neutral terminal, IEC allows a longer duration of the front time, up to 13 μs. IEEE restricts the duration of the front to 10 μs [3].

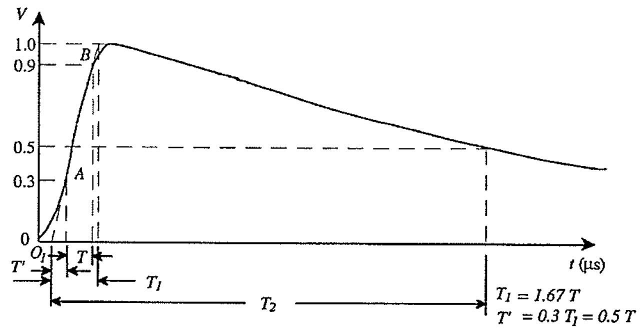

(a)

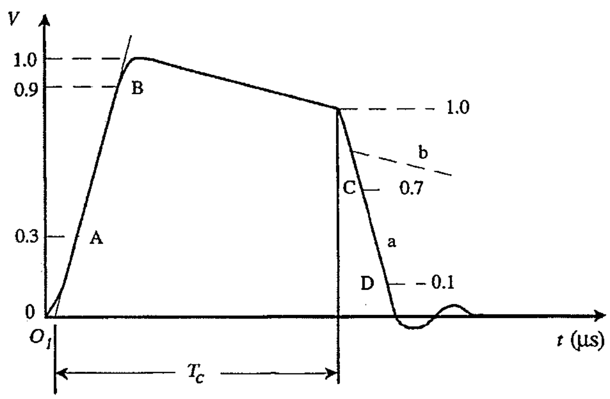

(b)

Figure 2.4: Different waveforms (a) Full-wave (b) Chopped wave

The full wave, because of its relatively long duration, causes major oscillations to develop in the winding and consequently stresses not only the turn-to-turn and section-to-section insulation throughout the winding, but also develops relatively high voltages, compared to power frequency stresses, across large portions of the winding and between the winding and ground (core or adjacent windings).

Chopped Wave

A lightning surge travelling along the transmission line might result in a flashover across an insulator or might cause a failure of an adjacent apparatus in a substation after the crest of the wave has been reached. This type of wave shape is called a *chopped wave*, and its wave shape is shown in Fig. 2.4(b). The duration of the total voltage collapse is 0.1 to 0.2 μs [9].

The chopped wave employs the same wave shape as a full-wave lightning impulse, except that its crest value is 10% greater than that of the full-wave. Different times to chopping T_c (as defined in IEC 60060-2), will result in different stresses (voltage and duration) in different parts of the winding(s) depending on the winding construction and arrangement employed. Hence, it is not possible to state a time to chopping which is the most onerous either in general or for any particular transformer. The time to chopping is therefore not regarded as a test parameter provided that it is within the limits of 2 to 6 μs as required by IEC 60076-3 [5]. The IEEE standards restrict the time to chopped between 2 μs and 5 μs [4]. The chop in the voltage wave is accomplished by the flashover of a rod gap or by using a chopping gap, connected in parallel with the transformer being tested.

The chopped wave test is justified because other equipment in the station can fail and produce a chopped wave at the transformer's terminals. This can occur only at, or below, the surge arrester protective level, so that the chopped wave and full wave tests may be specified to have equal crest magnitudes. Recognizing, however, the possible effect of operating voltage and the impulse voltage distribution in some windings, the relevant standards recommend that the chopped wave tests be made at 110% of the full wave test voltage [37, 38]. For an example, if the arrester discharges as the wave is increasing, the effective front may be far steeper than 1.2 μs to the crest. Further, the voltage may be appreciably higher across the terminals of the transformer than across the arrester, and if there is a poor value of α, so that there is a concentration of voltage at the line, and if the impulse is of opposite polarity to the existing service voltage, an appreciable increase in severity over test conditions could result [39].

The chopped wave, because of its shorter duration, does not allow major oscillations to develop as fully and generally does not produce as high voltages across large portions of the windings or between the winding and ground. However, because of its greater amplitude, it produces higher voltages at the line end of the winding; and because of the rapid change of voltage following flashover of the test gap, it produces higher turn-to-turn and section-to-section stress. The higher the factor of α of a winding, i.e. the higher the amplitude of the internal voltage oscillations, the greater the difference between the shape of these voltages and that of the applied impulse voltage. Also the internal voltage difference arising under the effect of a chopped wave can be considered as produced by superposition of internal voltage difference brought about by two full waves [40].

Front-of-wave

Following a severe lightning stroke directly to a transformer terminal or very close to it, a surge voltage may rise steeply until it is relieved by a flashover, causing sudden, very steep collapse of voltage. This type of wave shape is called *front-of-wave* (FOW), and is chopped on the front of the wave before the prospective crest value is reached. The rate of rise of voltage of the wave is approximately 1000 kV/μs [41]. Chopping occurs at a chop time corresponding to an assigned instantaneous crest value.

In some applications front-of-wave impulse tests are specified in addition to the usual chopped-wave and full-wave tests [2]. This practice may find justification for transformer windings that connect to circuits highly exposed to direct lightning strokes and especially where the frequency of lightning occurrence is high. IEC standards do not include this type of waveforms.

The front-of-wave is still shorter in duration and produces still lower winding-to-ground voltages deep within the winding. However, at the line end, its greater amplitude produces higher voltages from winding-to-ground. This, combined with the rapid change of voltage on the front and following flashover, produces a high turn-to-turn and section-to-section voltage near the line end of the winding.

There are many who argue that front-of-wave test is an anachronism and should be relegated to history [21,42]. The front-of-wave test was specified in transformer testing when lightning voltages having very steep fronts were allowed to enter the station and were then chopped by the transformer bushing or by a rod-gap attached to the transformer bushing. Transformers installed in modern shielded EHV stations, protected by modern lightning arresters, will not be exposed to transients that rise as rapidly, reach as high a crest voltage, or chop as abruptly as the front-of-wave test.

2.4.2 Lightning Impulse Test Circuit

For impulse failure detection analysis to be accurate, it is important that careful attention be paid to the test set-up, specially with respect to grounding, external clearances, and induced voltages produced by impulse currents. Fig. 2.5 illustrates the proper physical arrangement of the impulse generator, chopping gap, test object, and voltage divider [6]. High voltages and currents at high frequencies in the main circuit and the chopping circuit can produce rapidly changing electromagnetic fields, capable of inducing unwanted noise and error voltages in the low-voltage signal circuits connected to the impulse recorder inputs. The purpose of this physical arrangement is to minimize these effects.

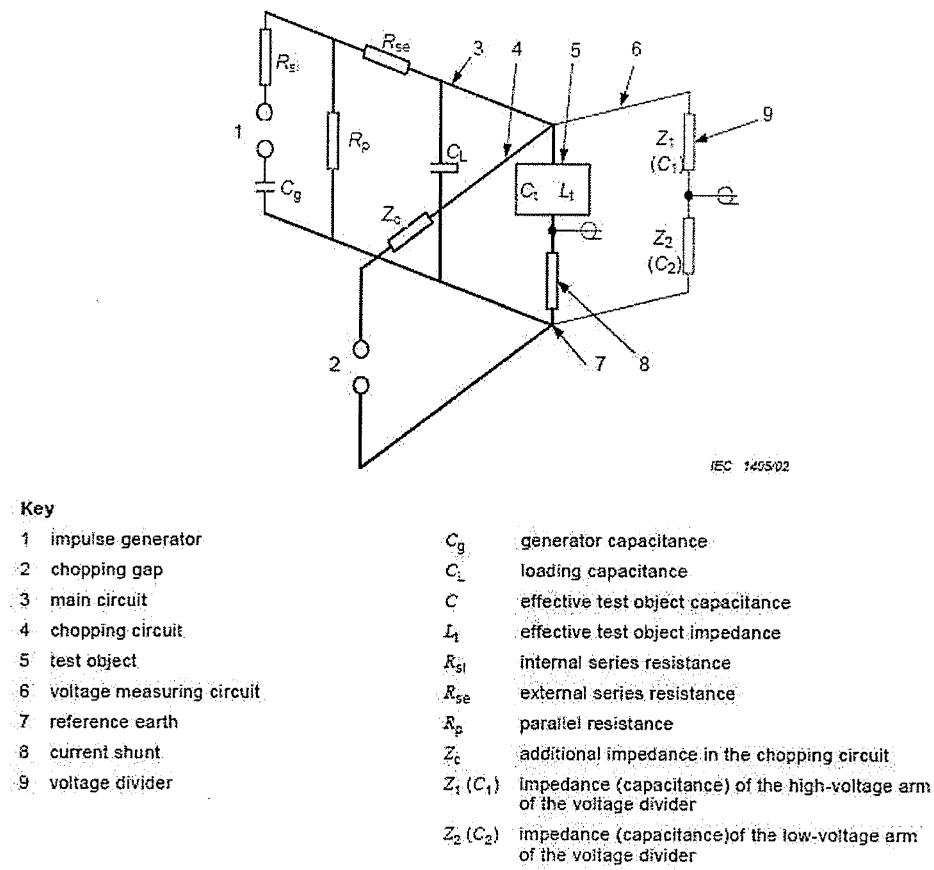

Figure 2.5: Typical impulse test circuit.

Impulse Generators

The circuit most commonly used by all impulse generator manufacturers is the multi-stage Marx circuit and is shown in Fig. 2.6. In this circuit, several energy storage stage capacitors are charged in parallel and discharged in series. The rated voltage of each capacitor is in the range of 100 to 200 kV and the stage capacitance is of the order of 0.5 μF. The discharge is arranged to give a total output voltage equal to the sum of all the individual stage capacitor voltages.

A DC power supply is used to charge the stage capacitors through charging resistors R_{ch}. The front and tail resistors are represented by R_f and R_t, while C_L

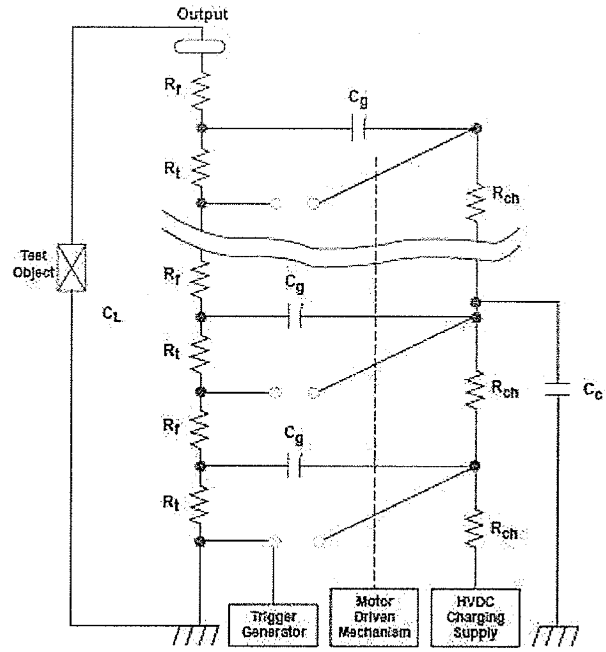

Figure 2.6: Schematic diagram of a impulse generator

is the test object. During charging, current flows into the capacitors through R_{ch}. When the stage capacitors have been charged to the required voltage, the discharge of the impulse generator is begun by the breakdown of the first gap. This triggering is initiated by injection of a HV pulse into a third electrode of the first stage gap. Sequentially, the upper stages are triggered by natural overvoltage. The output waveshape into the test object is determined by the net generator stage capacitance during discharge, the values of R_f and R_t, the inductance of the generator and test circuit connection, and C_L.

Grounding

Impulse testing of transformers require simultaneous measurement of voltage and current waveforms; these two signals are brought to the measuring instrument from the divider and shunt by coaxial cables [43]. The grounding points of the divider and shunt are connected to the laboratory grounding mesh at different locations separated by a distance of several meters. Considerable potential difference can be developed between these locations under transient conditions. The transient voltage drop on the grounding mesh impedance is caused by the current flowing in this mesh. The capacitive current is injected to the grounding mesh by a rapid rise of the potential of the impulse generator high voltage electrode. Considering the magnitude of the current flowing in the laboratory grounding system and high current derivatives, metal plates or metal grid laid on or embedded in the impulse test area are essential to reduce the transient voltage difference between the input end of the voltage divider and shunt coaxial cable. A theoretical analysis of grounding plate and grid as ground return, and a basis for the selection of a metal grid is reported in [44].

For the high-voltage experimental setup, which is discussed in Chapter 6, a grounding plate was used as the ground return and broad copper straps instead of round conductors were used as connections on the ground side. For the same amount of metal, a strip has lower inductance than a round conductor; and lower inductance means lower induced voltages in case of rapidly varying variables.

2.4.3 Measurement of Impulse Voltages & Currents

There are three basic types of dividers that are suitable for impulse testing. They are resistance, capacitance, and compensated. As the name implies, the resistance divider utilizes the principle that the voltage across a resistor varies directly with the resistance, while the capacitance divider, the voltage varies inversely with the capacitance. Compensated dividers are a combination of resistance, and sometimes inductance; IEEE 4-1995 [36] gives more details on the various dividers.

There are four mechanisms of interference-coupling in the signal measuring circuit [45]. The interferences arise due to conductive, inductive, capacitive, and electromagnetic modes.

The mechanism of conductive coupling requires a continuous conductive path between the divider and shunt cable ends, and also between the ground point of the waveform recorder. The ground current flows in the grounding mesh and in the coaxial cable shield, which forms a parallel path. The voltage drop developed by the cable shield current across the cable shield resistance represents the interference due to conductive coupling. This interference shows up in the form of high frequency oscillation which often masks pertinent details of the recorded voltage and current forms. This interference can be reduced by (a) selection of high quality coaxial cables, which are characterized by a low resistance of the coaxial cable (b) reduction in the current flowing in the shield, which results in an increase in the ground efficiency. i.e. ratio between the cable shield current to the grounding mesh current which depends on the respective inductive impedance of the two paths. Although high grounding efficiency, 60 dB (1:1000), is desirable, many practical grounding systems are characterized by a modest grounding efficiency of 40 dB [43]. Interference due to current flowing in the shield of the measuring cable may be reduced by an adequate grounding at the voltage divider side, by using triaxial cable with outer shield grounded at both input and instrument ends, and/or by cable running through a metallic conduit connected at both ends to the local grounds [46]. In this research work, measurement of the neutral current waveforms were brought to the measuring instrument from the shunt by triaxial cable.

Interference due to potential differences, induced or applied between the terminals of the measuring cable, may be reduced by using input voltage as high as possible, namely by operating the instrument at its maximum range, or by inserting an external attenuator between the receiving end of the cable and the instrument.

Signal transmission by fiber optic cables may be used to reduce the interference provided the characteristics of any such link are adequate to meet the requirements of the IEC 60060-2 [47].

Interference due to electromagnetic field penetrating directly into the instrument may be reduced by placing the instrument in a Faraday cage having sufficient attenuation in the frequency range of interest. The methods of shielding a high-voltage laboratory and a simplified method for shielding calculation are reported in [48, 49].

A shunt or an impulse current transformer may be used to measure the neutral current for fault detection. Design aspects of different types of shunts (tubular and wirewound) are addressed in [50, 51]. The type of shunt to use for neutral current recording depends on which current component is considered the most important for fault detection. In most cases, it is a pure ohmic shunt with an added parallel capacitor to limit the amplitude of the capacitive component at the beginning of the trace. In the current research work, a non-inductive resistive shunt and an high-frequency current monitor were used.

2.4.4 Digital Recorders

A digital recorder stores waveforms as a record of points characterized by discrete values of amplitude and time. The sampling rate and resolution are basic characteristics of a digitizer, as they determine the size of the recording errors inherent in the analog-to-digital conversion process. In other words, the sampling rate and resolution of a digitizer define the magnitudes of the errors which could be present even if the digitizer was to operate in an ideal fashion [52].

Following are the minimum requirements for digitizers as per relevant standards [46, 53]:

Sampling Rate The sampling rate shall not be less than $30/T_X$ samples/s where T_X is the time interval to be measured [e.g., when then front time (T_1) is to be determined the T_X=0.6 T_1 and not T_1]. For full lightning impulses, the permitted range of the front time (± 30% or from about 0.8 μs to about 1.6 μs) requires a sampling rate of at least 60 million samples/s (corresponding to the lower limit of T_X of 0.5 μs). To measure the front oscillations, the sampling rate shall be not less than $4f_{max}$ where f_{max} is the maximum frequency that can occur in the test circuit. Bandwidth and spectra of different measuring devices and test impulses are shown in Fig. 2.7 [43].

Rated Resolution A rated resolution of 2^{-8} (0.4% of the full-scale deflection) or better is required for tests where the impulse parameters are to be evaluated. For tests which involve signal processing other than impulse parameter evaluation, a rated resolution of 2^{-9} (0.2% of the full-scale deflection) or better is recommended. i.e. 9-bit or better digitizer is recommended.

The commercially available impulse analyzing systems have digitizers with 12-bit vertical resolution at 120 million samples/s or better. In this research work, a digital oscilloscope with 9-bit resolution (separate digitizer for each channel) and sampling rate of 5000 million samples/s was used.

2.5 Interpretation of Lightning Impulse Test Results

Interpretation of oscillograms or digital recordings is based on comparison of the waveshapes of voltages and current records between reduced and rated test voltages

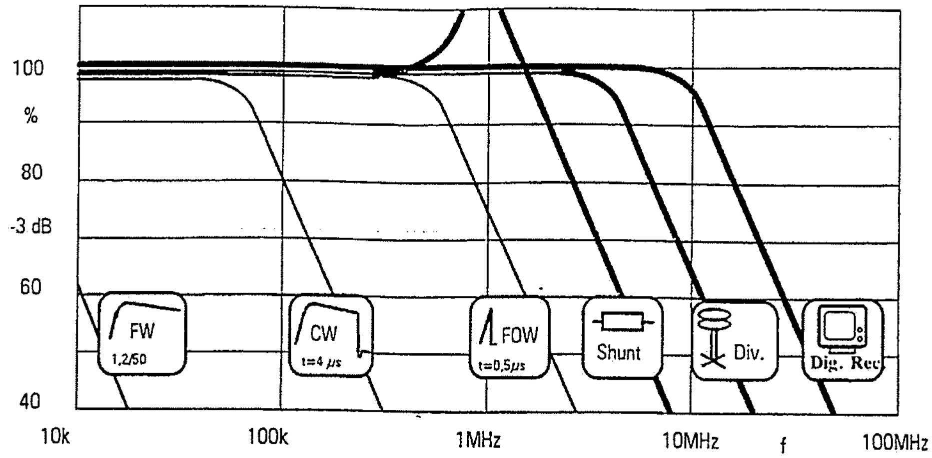

Figure 2.7: Bandwidth and spectra of different measuring devices and test impulses: full-wave lightning impulse, chopped-wave, front-chopped wave, shunt typical high voltage measuring coaxial shunt, typical divider, digital recorder.

or between successive records at rated test voltage. This is a skilled task and it is often difficult to decide the significance of discrepancies, even with considerable experience, because of the large number of possible disturbance sources. Discrepancies of any kind are of concern and should be investigated [6].

Following are few instances where a discrepancy does not mean a impulse failure.

- disturbance due to the test circuit, the measuring circuit and grounding methods: In multi-stage generators, differences in the firing times of the individual stages may give rise to minute changes in the amplitude of current records with high-frequency initial oscillations (without changing the basic frequency).

- sometimes discrepancies after the peak may originate from the generator, with multiple parallel stage operation, if the discharge circuits are not coincident in time. This may require new setting of the discharge gaps on generators which have both series and parallel gaps.

- discrepancy due to core grounding or any non-linear elements within the test object are not the source of the disturbances. Non-gapped, non-linear resistors may produce a logical and progressive development or change with increasing voltage levels.

The detection of the faults is the most important phase of impulse testing. The detection of failure with oscillograms or digital recordings is the most effective and sensitive. Following are some methods that can be used for detection of insulation failures during impulse tests.

2.5.1 Voltage Oscillograms

Examination of the oscillograms or digital recordings of the applied voltage provide relatively insensitive means for failure detection. Thus, the detectable discrepancies indicate major faults in the insulation or in the test circuit [6].

The voltage oscillograms give a perfect indication of faults between winding and grounded structures. Direct breakdowns to ground are indicated as a more or less by a sharp fall of the voltage recorded. Breakdowns along creepage surfaces are extended over longer times during which the voltage drops in a very irregular manner. All faults to ground are thus very clearly indicated. Internal faults in the winding are also clearly indicated, provided the breakdown occurs over larger parts of the winding, the indications being irregularities over the wave shape such as oscillations or shortening of the tail of the wave. Smaller faults between turns and coils are difficult to detect by the voltage oscillogram [54, 55].

Comparison of the chopped-wave recordings after the instant of chopping is not normally possible unless the instants of chopping are almost identical (e.g., within 0.1 μs of each other). For some transformers, even small differences in the instant of chopping can give rise to marked differences in the oscillation pattern after the chop (this pattern being a superposition of the transient phenomena due to the front of the original impulse and the chopping), and these differences may confuse comparison between the records of successful applications and those where a fault exists.

2.5.2 Neutral Current Oscillograms

Comparison of neutral current oscillograms offers a more sensitive means for failure detection compared to comparison of impulse voltage oscillograms. The neutral current (ground current) method was first proposed by Hagenguth in 1944 [56]. Since then there have been several reports [38, 54, 55] prepared by CIGRE in the 1950's which deal with the subject of fault detection using neutral current oscillograms. The neutral current method consists of inserting a non-inductive resistive current shunt between a terminal that would otherwise be grounded and the impulse generator-system ground. A record of the current is made during the application of the reduced full wave, at the beginning of a test sequence, and again during the full wave. These oscillograms are then compared by superposition for differences that may indicate the existence of a fault.

The neutral current method is based on the fact that successive applications of impulse voltages do not change the neutral current wave shape as long as no failure (e.g., turn-to-turn fault, breakdown between discs, breakdown or flashover to a grounded part, etc.) occurs. Under the effect of a breakdown between two conductive parts normally isolated from each other, the winding characteristics (capacitances and inductances) influencing the lightning impulse phenomenon will be subject to a sudden change, and consequently the current will be different from that of a healthy winding. Thus, from the change observable in the oscillogram showing the shape

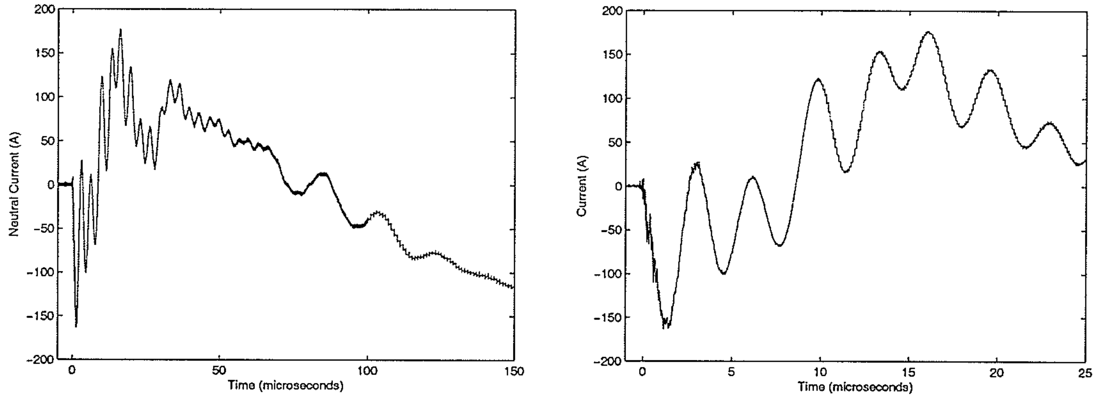

Figure 2.8: Neutral current waveform of an actual impulse test for different time scales.

of current flowing to ground at the end of the winding, a conclusion can be drawn about the fault occurring within the winding. In the case of momentary faults lasting for a short time compared to the duration of an impulse voltage wave, the shape of the oscillograms is dominated by the change of capacitances. If, however, the fault persists for a longer time, then the effect of the change of inductance also makes its presence felt. Correspondingly, a fault of short duration will cause a minor distortion in the shape of the curve, whereas a longer fault will result in an increased current and a displacement of the current curve with respect to the zero line [9].

A significant increase, combined with a change in superimposed frequency in a neutral current is indicative of a fault within the tested winding while a decrease indicates a fault from the tested winding to an adjacent winding or to ground.

Fig. 2.8 shows neutral current waveform from an impulse test on a 240 MVA, 132/79 kV transformer, which passed the impulse test. The magnitude and wave shape of the neutral current is a function of the surge characteristics of the winding tested. Generally, the following three main components can be distinguished in the neutral current [4]:

1. The capacitive component that represents the current charging the distributed series capacitance of the winding. This component appears at the very beginning of the trace as a more or less steeply rising wave with possibly some oscillations.

2. A period of small oscillations, due to mutual inductance couplings and capacitance between turns or discs of a winding, that follows the capacitive component.

3. The inductive component that flows through the inductance of the winding. This component very often includes superimposed large amplitude oscillations due to travelling waves in the winding. It is the last to appear on the trace.

Depending on the type of winding tested, the relative prominence of these three components can vary widely; for example, a multilayer winding of an instrument transformer will have negligible inductive components, while the capacitive component will be very large. A non-interleaved disc winding of a power transformer, on the other hand, will have a relatively small capacitive component, with the inductive current with large amplitude oscillations (travelling wave) being the most prominent one. Trace sweep speeds should be selected so as to display all three components, if possible, but for full-wave impulse tests the inductive component is the first choice.

The capacitive component of the neutral current can give an early indication of the failure, provided the failure can produce detectable change in the magnitude of this component. This depends on the extent of the breakdown and on the value of the series capacitance of the winding. The larger the series capacitance, the more dependable the fault indication will be. The period of small oscillations due to mutual inductance coupling is not very useful for fault detection because of its small amplitude relative to the other two components. The magnitude of the inductive components relative to the capacitive one varies with the type of winding and with terminal conditions of the untested windings. Short-circuiting of untested windings increases the inductive component of the current several times. A typical disc winding as employed in medium and large power transformers reduces the sensitivity of fault detection, for faults comprising a small percentage of the winding. Experience and tests show, however, that the neutral-current method is sensitive enough to detect one short-circuited turn in a typical disc winding even with all other winding terminals short-circuited and grounded. This applies also to low-voltage helical or layer winding of the power transformer.

This is not necessarily true for multilayer high-impedance windings such as those used in potential and distribution transformers. Due to the large inductance of these windings, the inductive current change may be negligible even with several turns of the winding short-circuited.

The first 2 μs of the neutral current trace cannot be expected to be matched (reduced & full-wave) because of the great probability of voltage pick-up from the high-voltage circuits. They should be therefore be disregarded for the purpose of analyzing test traces [4]. Apart from the first 2 μs, any deviation between two traces superimposed may indicate a failure in the transformer under test and shall be carefully analyzed. The type of discrepancy will vary with the type of fault and type of winding tested. A ground fault will tend to reduce the magnitude of the neutral current to zero from the moment it occurs. Faults in the minor insulation of the winding will tend to increase the current magnitude by lowering the impedance of the winding. With power-transformer windings, this will invariably be accompanied by changes in the oscillations superimposed on the inductive part of the current. When the inductive component alone shows an increase, without any other visible discrepancy in the shape or phase of the oscillations, it may indicate magnetic core saturation rather than a dielectric failure. This could happen with small power or distribution transformers and may require demagnetization prior to the application of the full wave. Effect of magnetic core saturation during impulse test on distribution transformers are reported in [57].

Sometimes the increase in the inductive current will not be apparent, but changes in the shape of the oscillations will normally indicate a failure. The increase in the inductive component may not be visible if the fault encompasses only a small number of turns and all the untested windings are short-circuited. Even a fault involving one turn, however, in a power transformer winding would cause visible change in the oscillations.

Small, local, jagged disturbances, perhaps spread over 2 μs or 3 μs, are a possible indication of severe discharge or partial breakdown in the insulation between turns or coils or coil connections. For windings of small series capacitance, that is, exhibiting essentially travelling wave behaviour, it may be possible to identify the source of disturbances by evaluating the time difference between the arrival at the neutral of the capacitive and the travelling wave disturbances.

2.5.3 Transfer-function Method

In the *transfer-function* method [10, 11], the frequency domain graphs deconvoluted from the test-voltage and neutral-current records obtained respectively at full and reduced test levels are compared. The transfer function of a transformer is a characteristic feature and, is in theory, independent of the shape of the applied voltage impulse. The difference between the transfer functions recorded at BIL and at the reduced test level manifests itself as either a frequency shift or pole-height attenuation;

empirical interpretation attributes the former to a local breakdown and the latter to partial discharge. This distinction is of great practical importance, since even a minor local breakdown disqualifies the transformer whereas a partial discharge is tolerated at the BIL, provided the insulation is not damaged. A brief review of transfer-function method is included in Chapter 4. Chapter 6 presents comparison of the WT and transfer-function methods.

2.5.4 Acoustic Measurement

Unusual noise within the transformer at the instant of applying the impulse is an indication of a possible failure and should be investigated. Efforts have been made to develop a method based on acoustics to detect impulse test failures, when such failures are not as obvious as a loud noise.

Beldi [58] proposed a fault detection by means of the electro-acoustic method. All discharges in a liquid are accompanied by pressure and sound waves. Beldi proposed instrumentation that was capable of converting hydrodynamic phenomena due to a fault into electrical signals. These signals can be measured by direct reading of the instruments or recorded by means of oscillograph.

A method to detect insulation failure during impulse tests based on sonar techniques of triangulation and ranging is reported in [59]. It is known that corona and spark breakdowns produce both audible and ultrasonic pressure waves in the medium surrounding the discharge.

2.5.5 Time-frequency Analysis

In *time-frequency analysis*, test waveforms are analyzed to localize the disturbance in both time and frequency. One such method is the *wavelet transform*. Introduction to these methods and a critical review are included in Chapter 3 and Chapter 4 respectively. In this research the main focus is on the investigation of wavelet-based methods for detection of minor insulation failures, which occur during lightning impulse tests on power transformers.

2.6 Fault Location

The location of the fault after an indication of a breakdown is often a long and tedious procedure which may involve the complete dismantling of the transformer and even then a turn-to-turn or layer-to-layer fault may escape detection. Any indication of the approximate position in the winding of the breakdown will help to reduce the time spent in the location of the fault [60].

The location of the fault indicated on a voltage oscillogram is obtained by calculating the length of the winding to the fault taking into consideration that the wave has passed the distance twice [54].

The neural current oscillogram may give an indication of this position by a burst of high-frequency oscillations or a divergence from the no-fault wave shape. Since the speed of propagation of the wave through a winding is about 150 m/μs, the time interval between the entry of the wave through a winding and the fault location can be used to obtain the approximate positions of the fault, provided the breakdown has occurred before a reflection from the end of the winding has taken place. Distortion of the voltage oscillogram may also help in the location of a fault but it generally requires a large fault current to distort the voltage wave and the breakdown is then usually obvious.

With the resistance type shunt, the part of the trace at which the discrepancy begins to show can give some indication as to the location of the fault in terms of winding length from the impulsed end. With the capacitive shunt, such as those used for testing high impedance, low kVA multilayer windings, any sustained minor insulation failure will only cause a gradual increase in the current, which builds up over a fairly long time. Location of the failure by measuring the time of its occurrence is not usually possible.

The main advantage of the wavelets based methods for failure detection is its ability to localize oscillations in the neutral current due to minor insulation failures. Such information can be used to locate the position of the impulse failure.

2.7 Switching Impulse Tests

When higher transmission voltages (500 kV and above) were introduced, it became apparent that switching impulses play a greater role in their overall effect on the power system than at lower voltages. The switching impulse test is a routine test for windings rated at 300 kV and above [5].

The time to reach the crest amplitude and total time duration of these switching impulses are much longer than those of lightning impulses [4]. Fig. 2.9 shows typical shape of the switching impulse. Since their time to crest and the total time duration are much longer than those of the lightning impulses, the voltage distribution of these switching impulses within the winding of the transformer will be more uniform. The distribution will be essentially on a volts per turn basis, approaching the uniform distribution of low-frequency steady-state voltages. Because there may be non-linearity in some windings, it cannot be generalized that the distribution will be uniform in all situations.

Since the switching impulse wave shape is somewhere between the low frequency and lightning impulse wave shapes, the assumption is usually made that a transformer

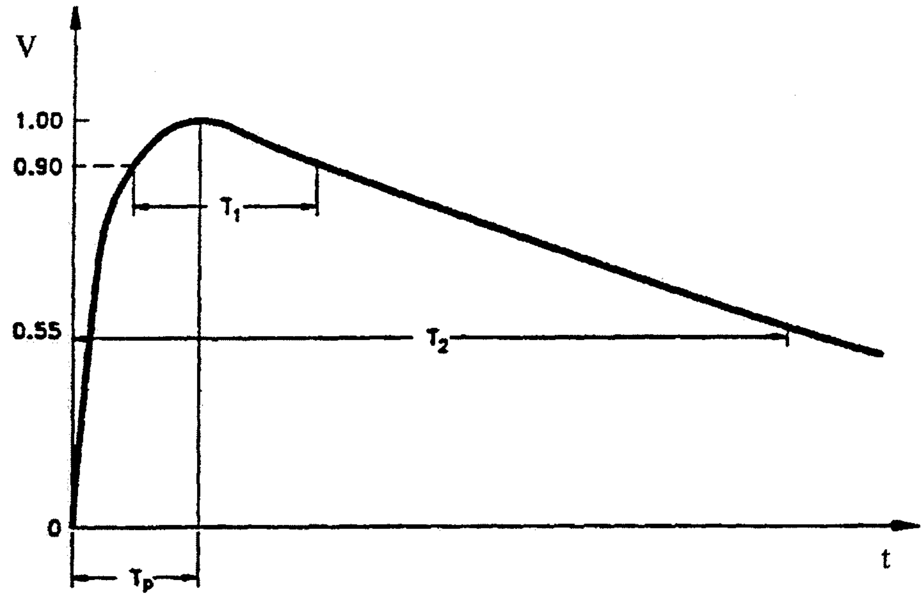

Figure 2.9: Full Switching Impulse

that withstand both the low-frequency and lightning impulse tests will also withstand the switching impulses if the magnitude of the switching impulse crest is in the order of 80% to 85% of BIL. However, industry experience shows that this assumption does not hold true in all cases, and the switching impulse withstand capability of a transformer cannot be merely interpolated from other tests. For this reason, switching impulse testing of high-voltage power transformers is recommended.

The generally accepted crest value, also defined as the basic switching impulse level (BSL), for the switching impulse is 83% of the BIL as outlined in IEEE Std C57.12.00-2000 [2]. The "83 percent BIL" formula was based on the studies that were initiated to determine the waveshapes of typical switching surge voltage transients. It was determined from tests that the ratio of the crest of the switching surge voltage transient withstand to the crest of the low-frequency voltage withstand was a minimum of 1.3:1. This is equivalent to approximately 83% of the BIL for higher voltage classes [61, 62]. However, lightning impulse and switching impulse tests are each based upon the maximum impulse and switching surge voltages allowed by the lightning arrester to reach the transformer. These test voltages are 15% or more greater than the lightning arrester protective level. They are nearly alike (line-to-ground) because the protective characteristics of modern arresters are flat for transient voltage waves ranging from fast impulses that crest in a few microseconds to long slow switching transients that crest in hundreds of microseconds [21].

An impulse generator is used to apply the switching impulse voltage to the transformer. The wave shape and amplitude are obtained with the impulse generator adjustments, wave shaping resistor, and possibly an external load capacitance. Basic impulse generator characteristics are discussed in section 2.4.2.

The test sequence consists of one calibration switching impulse at a voltage level between 50% and 75% of the full test voltage, and three subsequent switching impulses at full voltage. Oscillograph records are taken of at least the impulse wave shape on the line terminal being tested. The neutral current oscillogram records are generally not necessary for failure detection but can provide useful information to confirm suspected failure, and aid in diagnostics [4]. The test is successful if there is no collapse of the voltages as indicated by the oscillograms but it should be noted that due to the influence of magnetic saturation successive oscillograms may differ in the wave shape. The wave tail shortening due to fault in general, is clearly distinguishable from the variation in the wave tail length due to magnetization of the core. The voltage records of switching impulse tests are a sufficiently sensitive means for detection of most faults, and was not investigated in the current research.

Chapter 3

Time-Frequency Analysis

A key concept of signal analysis is the notion of "localization" in time and frequency [63]. Time-frequency analysis of a non-stationery signal (i.e. signals whose frequency varies with time) indicates the time instant at which various frequency components of the signal are present. One direct consequence of such treatment will be the possibility of accurate location in time of all abrupt changes in the signal and estimation of their frequency components as well. It is this very application i.e. to locate low magnitude abrupt changes in the neutral current waveforms, that has created interest to use time-frequency analysis to detect faults. A number of techniques are available to examine a signal by time-frequency analysis such as, *short time Fourier transformation* (STFT), Wagner Distribution, Gaber transformation, bilinear transforms and *wavelet transformation* (WT).

This chapter provides a general introduction to STFT and WT. More detailed mathematical analysis can be found in articles on this subject by Daubechies [64,65], Mallat [66,67], Rioul and Vetterli [68], and Farge [69]. An excellent review of the recent published works dealing with industrial applications of wavelets and, more generally speaking, multiresolution analysis are given in [70].

3.1 Fourier Transform

The Fourier transform's utility lies in its ability to analyze a signal in the time domain for its frequency content. The transform works by first translating a function in the time domain into a function in the frequency domain. The signal can then be analyzed for its frequency content because the Fourier coefficients of the transformed function represent the contribution of each sine and cosine function at each frequency. An inverse Fourier transform transforms data from the frequency domain into the time domain.

3.2 Short-Time Fourier Transform

The Fourier transform is widely used in signal analysis and processing. When the signal is periodic and sufficiently regular, the Fourier coefficients decay quickly with increase in frequency. For nonperiodic signals, the Fourier integral yields a continuous spectrum. The Fast Fourier transform (FFT) permits efficient numerical Fourier analysis.

In the application of transformer fault detection during impulse testing, given a signal f, the main interest is in its frequency content locally in time. The standard Fourier transform

$$X(f) = \int_{-\infty}^{+\infty} x(t)\ e^{-j2\pi ft}\ dt \tag{3.1}$$

also gives a representation of the frequency content of f, but information concerning time-localization, e.g. high frequency burst due to a fault, can not be read easily.

The Fourier spectrum analysis is global in time and is basically not suitable to analyze non-stationary and fast varying transient signals. Signals are stationary if their properties do not change during the course of the signals. Many temporal aspects of the signal, such as the start and end of a finite signal and the instant of appearance of a singularity in a transient signal, are not preserved in the Fourier spectrum. The Fourier transform does not provide any information regarding the time evolution of spectral characteristics of the signal. The STFT, or called the Gabor transform, the Wigner distribution, and the ambiguity function are usually used to overcome the drawback of the Fourier analysis for nonstationary and fast transient signals.

An intuitive way to analyze a nonstationary signal is to perform a time-dependent spectral analysis. A non-stationary signal is divided into a sequence of time segments in which the signal may be considered as quasistationary. Then, the Fourier transform is applied to each of the local segments of the signal.

The short-time Fourier transform is associated with a window of fixed width. Gabor in 1946 was the first to introduce the short-time Fourier transform which is known as the sliding window Fourier transform. The transform is defined as

$$STFT(\tau, f) = \int x(t)\; g^*(t-\tau)\; e^{-j2\pi ft}\; dt \tag{3.2}$$

where $g(t)$ is a square integrable short-time window, which has a fixed width and is shifted along the time axis by a factor τ.

In the STFT, the signal is multiplied by a sliding window that localizes the signal in the time domain, but results in a convolution between the signal spectrum and the window spectrum; that is, a blurring of the signal in the frequency domain. The narrower the window, the better we localize the signal and the poorer we localize its spectrum.

The width Δt of the window $g(t)$ in time domain and the bandwidth Δf of the window $G(\Delta f)$ in frequency domain are defined respectively as

$$\Delta t^2 = \frac{\int t^2 |g(t)|^2 dt}{\int |g(t)|^2 dt} \qquad \Delta f^2 = \frac{\int f^2 |G(f)|^2 df}{\int |G(f)|^2 df} \tag{3.3}$$

where the denominator is the energy of the window in time and frequency domains. The two sinusoidal signals can be discriminated only if they are more than Δf apart. Thus, Δf is the resolution in the frequency domain of the short-time Fourier transform. Similarly, two pulses in time domain can be discriminated only if they are more than Δt apart. Note that once a window has been chosen for the STFT, the time and frequency resolutions given by (3.3) are fixed over the entire time-frequency plane. The STFT is a fixed window Fourier transform.

The time-frequency joint representation has an intrinsic limitation, the product of the resolutions in time and frequency is limited by the uncertainty principle:

$$\Delta t \Delta f \geq \frac{1}{4\pi} \tag{3.4}$$

This is also referred to as the Heisenberg inequality, familiar in quantum mechanics and important for time-frequency joint representation. A signal can not be represented as a point in the time frequency space. One can only determine its position in the time-frequency space within a rectangle of $\Delta t \Delta f$.

The time-bandwidth product $\Delta t \Delta f$ must obey the uncertainty principle. We can only trade time resolution for frequency resolution or vice versa. Gabor proposed the Gaussian function as the window function. The Gaussian function has the minimum time-bandwidth product determined by the uncertainty principle (3.4). The Fourier transform of the Gaussian window is still a Gaussian as

$$g(t) = \frac{1}{\sqrt{2\pi} s} exp(-\frac{t^2}{2s^2}) \quad and \quad G(f) = exp(-\frac{s^2(2\pi f)^2}{2}) \tag{3.5}$$

which have a minimum spread. A simple calculation shows that

$$\Delta t^2 = \frac{s^2}{2} \quad and \quad \Delta f^2 = \frac{1}{s^2(2\pi)^2} \tag{3.6}$$

which satisfies the uncertainty principle (3.4) and achieves the minimum time-bandwidth product $\Delta t \Delta f = 1/4\pi$. The short-time Fourier analysis depends critically on the choice of the window. Its application requires a priori information concerning the time evolution of the signal properties in order to make a priori choice of the window function. Once a window is chosen, the width of the window along both time and frequency axes are fixed in the entire time-frequency plane.

3.3 Wavelets

A wavelet is a mathematical function used to divide a given function into different frequency components and study each component with resolution matches its scale [71]. The fundamental idea behind wavelets is to analyze them according to scale. This involves creating mathematical structures that vary in scale [72].

Thus, wavelets are functions that satisfy certain mathematical requirements and are used in representing data or other functions. A real or complex-value function $\psi(t)$ is defined as a wavelet if:

1) The integral of $\psi(t)$ is zero

$$\int_{-\infty}^{+\infty} \psi(t)\, dt = 0 \tag{3.7}$$

This means that a wavelet must have zero average value in the time domain (or zero dc component) and that the wavelet must be a bandpass function. Therefore, it must be oscillatory (must be a wave).

2) The integral of $\psi^2(t)$ is unity

$$\int_{-\infty}^{+\infty} \psi(t)^2 \, dt = 1 \tag{3.8}$$

(The third requirement will be discussed a little later.)

There are several functions that meet these requirements. Some popular wavelets include [45]:

the Morlet wavelet (modulated Gaussian):

$$\psi(t) = e^{j\omega_0 t} \, e^{-\frac{t^2}{2}} \tag{3.9}$$

the Haar wavelet (named after German mathematician Alfred Haar):

$$\psi(t) = \begin{cases} 1, & 0 \leq t \leq 0.5 \\ -1, & 0.5 \leq t \leq 1 \\ 0, & \text{otherwise} \end{cases} \tag{3.10}$$

the Shannon wavelet:

$$\psi(t) = \frac{\sin(\frac{\pi t}{2})}{\frac{\pi t}{2}} \cos(\frac{3\pi t}{2}) \tag{3.11}$$

the Mexican hat wavelet (second derivative of a Gaussian):

$$\psi(t) = n(1 - t^2) \, e^{-\frac{t^2}{2}} \tag{3.12}$$

where n is a normalization factor. There are several other wavelets such as Bessel, Cauchy, Coifman, cubic-spline, Daubechies, Dubuc, Franklin, Lagrange, Lazy, Lemarie, Maar, and Meyer wavelets. New wavelets are being discovered on a regular

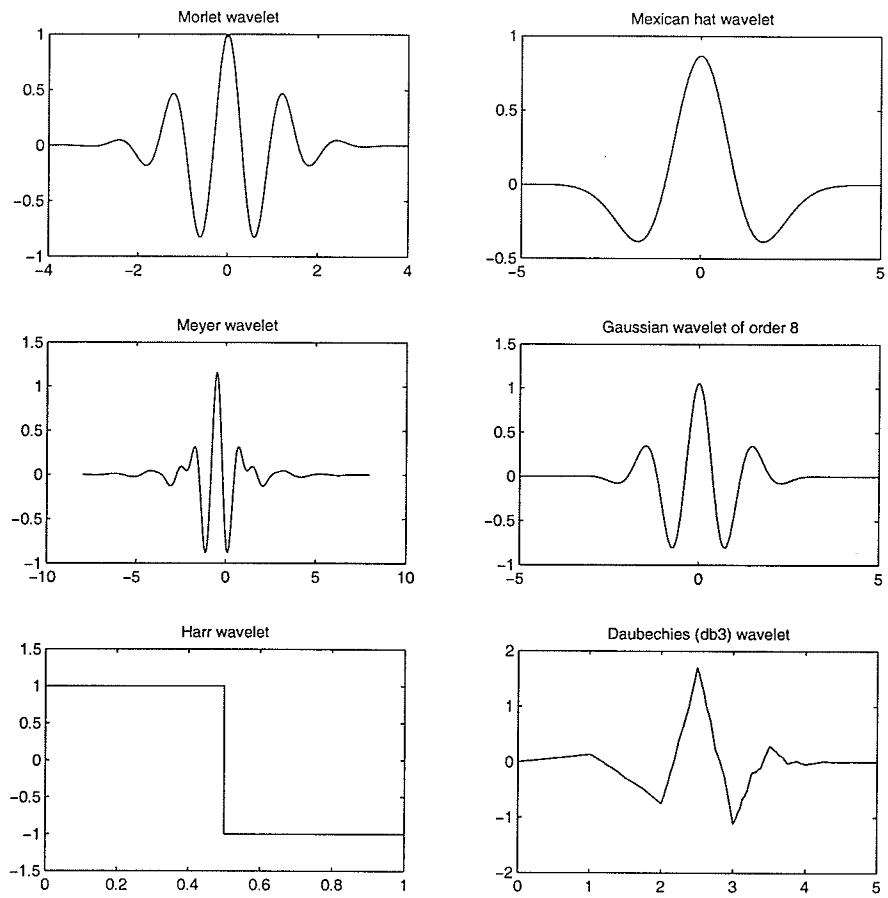

Figure 3.1: Some examples of wavelet functions.

basis. The particular application dictates which wavelet is selected. Few of these wavelets are shown in Fig. 3.1, and are known as *mother wavelets.*

Each of the mother wavelets can be used to generate other wavelets to form a set of basis functions. This is achieved by

a) translation/shifting:

$$\psi(t) \longrightarrow \psi(t+k) \tag{3.13}$$

b) dilation/scaling:

$$\psi(t) \longrightarrow \psi(at) \tag{3.14}$$

where k is the translation factor and a is the scaling factor. Thus, other wavelets are generated from a single basic wavelet $\psi(t)$, the so-called *mother wavelet*, by scaling and translation according to (3.13) and (3.14).

Fig. 3.2 shows an example of translation and dilation of the mother wavelet. Scaling, as a mathematical operation, either dilates or compresses a signal. Larger scales correspond to dilated (or stretched out) signals and small scales correspond to compressed signals. Fig. 3.2(a), $a = 1/4$ is the smallest scale, and $a = 1$ is the largest scale which is similar to the scale used in maps. As in the case of maps, high scales correspond to a non-detailed global view (of the signal), and low scales correspond to a detailed view. Similarly, in terms of frequency, low frequencies (high scales) correspond to a global information of a signal (that usually spans the entire signal), whereas high frequencies (low scales) correspond to a detailed information of a hidden pattern in the signal (that usually lasts a relatively short time) [73]. The term translation is related to the location of the window, as the window is shifted through the signal. As shown in Fig. 3.2(b) this term corresponds to time information in the transform domain.

The third important property is orthogonality. The basis functions generated are required to be orthogonal

$$\int \psi_i(t)\psi_j(t)\, dt = \begin{cases} n, & i = j \\ 0, & i \neq j \end{cases} \tag{3.15}$$

where n is a normalization factor. (Strictly speaking, it is not a necessary requirement that the wavelets are orthogonal, but the use of orthogonal wavelets simplifies

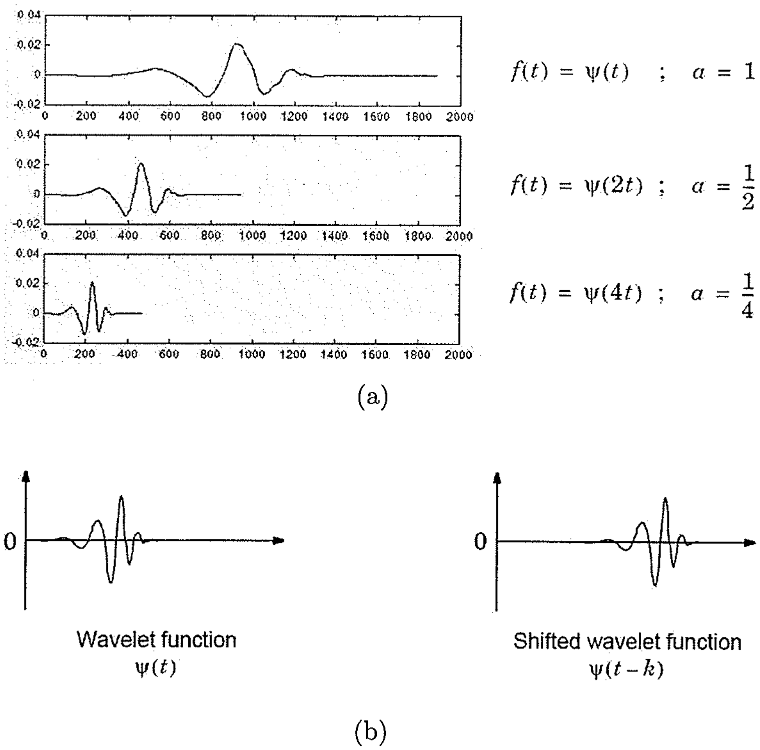

Figure 3.2: Basic operations on mother wavelet: (a) Dilation (b) Translation

computation.)

In the current research, the Daubechies family of wavelets, named after Ingrid Daubechies, were used. The first order Daubechies wavelet is also known as the Haar wavelet, which wavelet function resembles a step function. The wavelet functions for the Daubechies functions with order 1 up to 8 are shown in Fig. 3.3. The order of the Daubechies functions denotes the number of vanishing moments, or the number of zero moments of the wavelet function. This is weakly related to the number of oscillations of the wavelet function. The larger the number of vanishing moments, the better the frequency localization of the decomposition. The dependence between wavelet coefficients on different scales decays with increasing wavelet order. The order of the wavelet functions can be compared to the order of a linear filter. The Daubechies wavelets are compactly supported orthogonal wavelets [65].

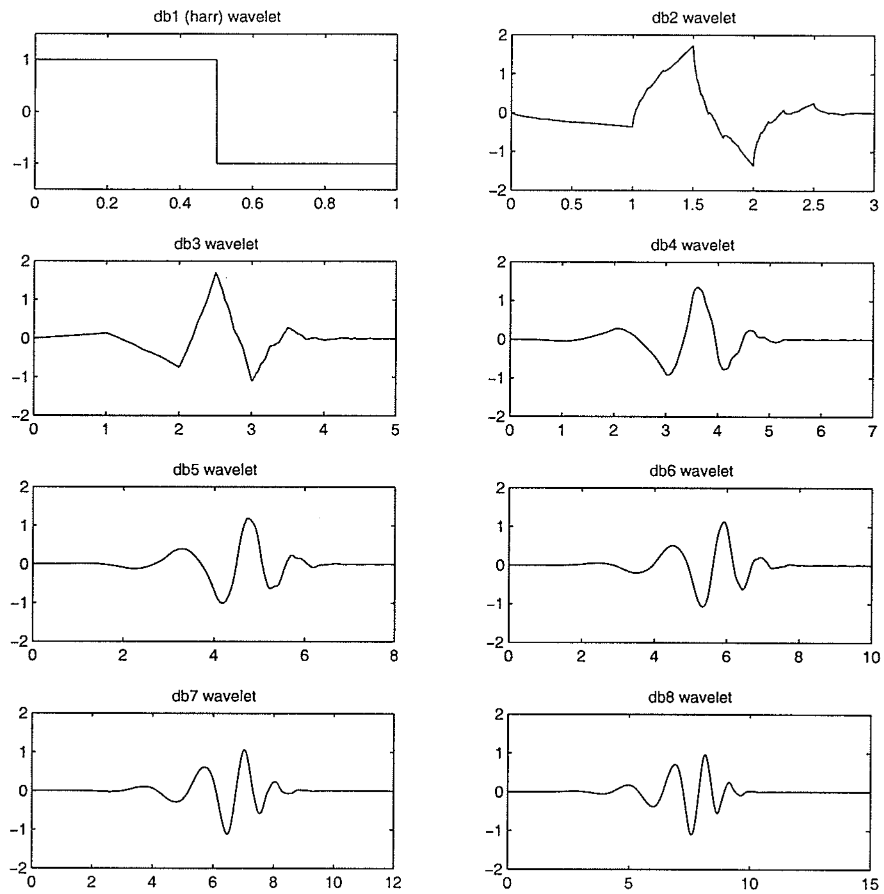

Figure 3.3: The wavelet functions for the Daubechies functions with order 1 up to 8.

Following explains the construction of the Daubechies 4-coefficient scaling function and wavelet (db2). Higher order Daubechies functions are not easy to describe with an analytical expression. In general, a scaling function is a solution to the dilation equation

$$\phi(t) = \sum_{k=-\infty}^{\infty} a_k \phi(St - k) \tag{3.16}$$

The dilation factor $S = 2$ is selected as a convenient choice. The constant coefficients a_k are known as filter coefficients and are obtained by imposing some conditions on the scaling function. In order for the wavelet to have compact support and some type of smoothness, three conditions must be imposed on the $\phi(t)$. First, the scaling function has a nonvanishing integral

$$\int_{-\infty}^{+\infty} \phi(t)\ dt = 1 \tag{3.17}$$

This leads to

$$\sum_{k=-\infty}^{\infty} a_k = 2 \tag{3.18}$$

Second, the scaling function is orthogonal to its translates, as in

$$\int_{-\infty}^{+\infty} \phi(t)\phi(t+m)\ dt = \delta_{0,m} \tag{3.19}$$

This orthogonality condition implies that

$$\sum_{k=-\infty}^{\infty} a_k\ a_{k+2m} = 2\delta_{0,m} \tag{3.20}$$

Third, the mother wavelet $\psi(t)$ must have vanishing moments (must satisfy the moment conditions)

$$\int_{-\infty}^{+\infty} \psi(t)\ t^p = 0, \qquad p = 0, 1. \tag{3.21}$$

This implies that

$$\sum_{k=-\infty}^{+\infty} a_k\ k^p = 0, \qquad p = 0, 1. \tag{3.22}$$

For the Daubuchies four-coefficient (db2) scaling function, (3.18), (3.20), and

(3.22) become

$$\begin{aligned} a_0 + a_1 + a_2 + a_3 &= 2 \\ a_0^2 + a_1^2 + a_2^2 + a_3^2 &= 2 \\ a_0 - a_1 + a_2 - a_3 &= 0 \\ -a_1 + 2a_2 - 3a_3 &= 0 \end{aligned} \tag{3.23}$$

leading to

$$\begin{aligned} a_0 &= \frac{1+\sqrt{3}}{4}, \qquad & a_1 &= \frac{3+\sqrt{3}}{4} \\ a_2 &= \frac{3-\sqrt{3}}{4}, \qquad & a_3 &= \frac{1-\sqrt{3}}{4} \end{aligned} \tag{3.24}$$

Thus, the scaling function becomes

$$\phi(t) = a_0\phi(2t) + a_1\phi(2t-1) + a_2\phi(2t-2) + a_3\phi(2t-3) \tag{3.25}$$

In general, it is not possible to solve this equation directly to find the scaling function $\phi(t)$. There are two methods that can be used:

Method 1: An iterative solution is possible when $\phi(t)$ is approximated as

$$\phi_j(t) = a_0\phi_{j-1}(2t) + a_1\phi_{j-1}(2t-1) + a_2\phi_{j-1}(2t-2) + a_3\phi_{j-1}(2t-3) \tag{3.26}$$

We start the iteration with $\phi_0(t)$. The iterative process is continued until $\phi_j(t)$ is indistinguishable from $\phi_{j-1}(t)$.

Method 2: Alternatively, we can substitute $t = 1$ and $t = 2$ to obtain

$$\phi(1) = \frac{1+\sqrt{3}}{2}, \qquad \phi(2) = \frac{1-\sqrt{3}}{2}$$

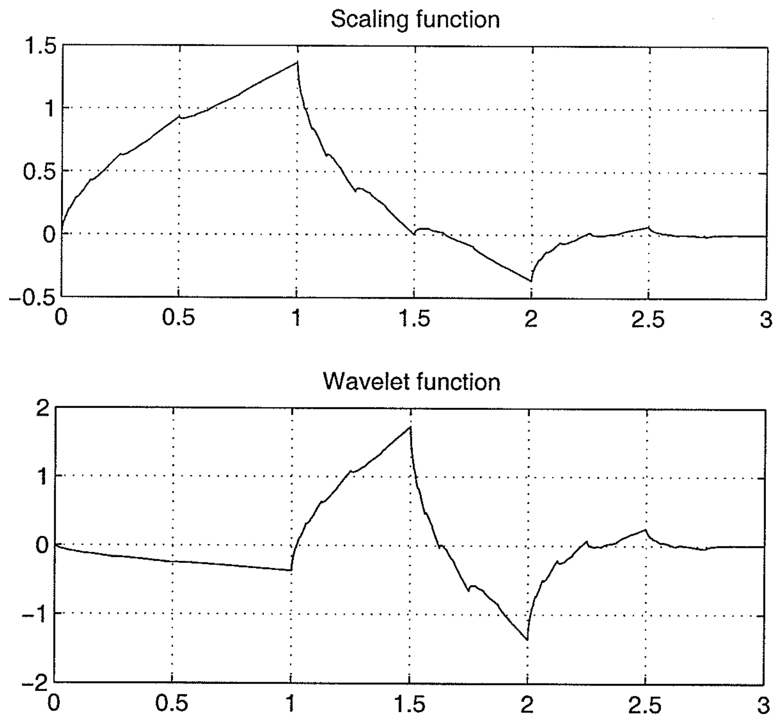

Figure 3.4: The Daubechies D4 (db2) (a) wavelet function, (b) Scale function.

We keep in mind that $\phi(t)$ is zero outside the interval $(0, 3)$, as in $\phi(0) = 0 = \phi(3)$. Then we use (3.25) to obtain $\phi(t)$ at $t = 1/2, 3/2, 5/2$, and $7/2$ because $2t$ on the right hand side is a whole number. From these half-integer times, we go to quarter-integer times. Eventually, we have enough values to plot $\phi(t)$ for $0 < t < 3$.

The corresponding wavelet function $\psi(t)$ is obtained from the scaling function $\phi(t)$ by reversing the order of the coefficients and changing the sign of the alternate terms:

$$\psi(t) = -a_3\phi(2t) + a_2\phi(2t-1) - a_1\phi(2t-2) + a_0\phi(2t-3) \qquad (3.27)$$

The scaling function and wavelet for Daubechies db2 are shown in Fig. 3.4.

3.4 Continuous Wavelet Transformation

Mathematically, the continuous wavelet transform is expressed as

$$CWT_x(\tau, a) = \frac{1}{\sqrt{|a|}} \int x(t)\ \psi(\frac{t-\tau}{a})\ dt \tag{3.28}$$

and we assume that ψ satisfies

$$\int \psi\ dt = 0 \tag{3.29}$$

where a is the scale factor and τ is the translation factor. One usually considers only positive factor $a > 0$. The wavelets are dilated when the scale $a > 1$ and are contracted when $a < 1$. The wavelet, $\psi_{a,\tau}(t)$, generated from the same basic wavelet have different scale, a, and location, τ, but all have the identical shape.

The CWT maps a one-dimensional time signal into a two-dimensional function of the scale, a, and the time shift, τ, that represents the signal in the time scale space and is referred to as joint time-scale representation. The time-scale wavelet representation is equivalent to the time-frequency joint representation, which is familiar in the analysis of non-stationary and fast transient signals.

3.5 Discrete Wavelet Transformation

The CWT maps a one-dimensional time signal to a twodimensional time-scale joint representation. The time bandwidth product of the CWT output is the square of that of the signal. For most applications, however, the goal of signal processing is to represent the signal efficiently with fewer parameters. The use of the discrete wavelet transform (DWT) can reduce the time bandwidth product of the WT output.

The term DWT means the continuous wavelets with the discrete scale and translation factors. The wavelet transform is then evaluated at discrete scales and translations. The discrete scale is expressed as $a = a_0^i$, where i is integer and $a_0 > 1$ is a fixed dilation step. The discrete translation factor is expressed as $\tau = k\tau_0 a_0^i$, where k is an integer. The translation depends on the dilation step, a_0^i . The corresponding discrete wavelets are written as:

$$DWT_x(\tau, a) = \frac{1}{\sqrt{|a|}} \sum x(k)\ \psi(\frac{k - na_0^m \tau_0}{a_0^m}) \tag{3.30}$$

By careful selection of a_0 and τ_0, the family of scaled and shifted mother wavelets constitutes an orthonormal basis. We can choose $a_0 = 2$ and $\tau_0 = 1$ to constitute the orthonormal basis to have the WT called a *dyadic orthonormal* WT. The implications of the dyadic orthonormal WT is that due to the orthonormal properties there will be no information redundancy in the decomposed signals. Also, with this choice of a_0 and τ_0, there exists a novel algorithm, known as *Multiresolution Signal Decomposition* [66] technique, to decompose a signal into scales with different time and frequency resolution.

3.6 Multiresolution Signal Decomposition

An efficient way to implement the DWT in the form of a *Multiresolution Signal Decomposition* (MSD) was developed by Mallat [66, 67]. The operational Mallat algorithm is in fact a classical scheme known *Subband Coding.* This filtering algorithm yields a Fast Wavelet Transform, similar to the FFT.

The faults between the turns or sections during impulse tests may results in the neutral current which has high frequency components for a short duration due the capacitance of the winding, and low frequency component for long duration due to the inductance of the winding. Mallat showed that one can completely decompose a signal $x(t)$ in terms of approximations (A), provided by scaling functions, $\phi(t)$, and details (D), provided by the wavelets, $\psi(t)$. The approximations are the high-scale, low-frequency components of the signal. The details are the low-scale, high-frequency components. Current research focus on the detection of the details (i.e. high-frequency component) of the signal to detect impulse test failures.

Mathematically, for the MSD of the signal $x(t)$, one needs two closely related basic functions. In addition to the wavelet, which provides the details, one needs a second basis function, the scaling function, which provides the low frequency approximation, e.g., like an average or mean. This scaling function and the wavelets are conjugated.

Therefore, a signal can be decomposed into approximate coefficients, $a_{j,k}$ through the inner product of the original signal at scale j and the scaling function.

$$a_{j,k} = \int_{-\infty}^{+\infty} x(t)_j \phi_{j,k}(t)\ dt \tag{3.31}$$

$$\phi_{j,k}(t) = 2^{-j/2}\phi(2^{-j}t - k)\ dt \tag{3.32}$$

Similarly, the detailed coefficients, $d_{j,k}$ can be obtained through the inner product of the original signal and the complex conjugate of the wavelet function.

$$d_{j,k} = \int_{-\infty}^{+\infty} x(t)_j \psi^*_{j,k}(t)\ dt \tag{3.33}$$

$$\psi_{j,k}(t) = 2^{-j/2}\psi(2^{-j}t - k)\ dt \tag{3.34}$$

The original signal can therefore be reconstructed by a single series of scaling coefficients and double series of the detailed coefficients.

$$x(t) = \sum_{j=-\infty}^{+\infty} a_{j0,k}\phi_{j0,k}(t) + \sum_{j=-\infty}^{j0} \sum_{k=-\infty}^{+\infty} d_{j,k}\ \psi_{j,k}(t) \tag{3.35}$$

$$= A + D \tag{3.36}$$

where the approximation (A) is provided by the one-dimensional linear combination of the scaling functions, which form the *low-pass* filters, and the details (D) by the two-dimensional linear combination of the dyadic wavelets, which form the *high-pass* filters.

A digitized signal can be decomposed at different scales as follows:

$$x(n) = \sum_{k=0}^{N-1} a_{(j+1),k}\phi_{(j+1),k}(t) + \sum_{k=0}^{N-1} d_{(j+1),k}\ \psi_{(j+1),k}(t) \tag{3.37}$$

This decomposition process can be iterated, with successive approximations being decomposed in turn, so that a signal $x(t)$ is broken down in many lower-resolution components. This is called the wavelet decomposition tree [67]. Since the decomposition process is iterative, in theory it can be continued indefinitely. In reality, the decomposition can proceed only until the individual details consist of a single observation.

The coefficients of the next decomposition level, $(j+1)$, can be expressed as

$$a_{(j+1),k} = \sum_{k=0}^{N} a_{j,k} \int \phi_{j,k}(t) \cdot \phi_{(j+1),k}(t)\ dt \tag{3.38}$$

$$= \sum_{k=0}^{N} a_{j,k} \cdot g[k] \tag{3.39}$$

$$d_{(j+1),k} = \sum_{k=0}^{N} a_{j,k} \int \phi_{j,k}(t) \cdot \psi_{(j+1),k}(t)\ dt \tag{3.40}$$

$$= \sum_{k=0}^{N} a_{j,k} \cdot h[k] \tag{3.41}$$

As discussed earlier, MSD technique decomposes the signal in the form of the smoothed version of the original signal, and the detailed version of the original signal. The decomposition process can be iterated, with successive approximations being decomposed in turn, so that a signal is broken down in many lower-resolution components.

Fig. 3.5 is a level-3 decomposition which produce WT coefficients for approximation at level 3 ($A3$), and coefficients for details at level 1, 2, and 3 ($D1$, $D2$, and $D3$). Let $x[n]$ be the digitized time signal, then $x[n]$ is decomposed simultaneously using a high-pass filter $h[n]$ and low-pass filter $g[n]$. The outputs giving the detailed coefficients ($D1$) from the high-pass filter, and approximation coefficients ($A1$) from the low-pass filter. Downsampling is done in the process of decomposition so that the resulting $A1$ and $D1$ are each $n/2$ point signals (Since half the frequencies of the signal have now been removed, half the samples can be discarded according to Nyquists rule). Thus, for the original n point signal $x[n]$, after the decomposition we have n point signal together with $A1$ and $D1$, not $2n$ point. The next higher scale

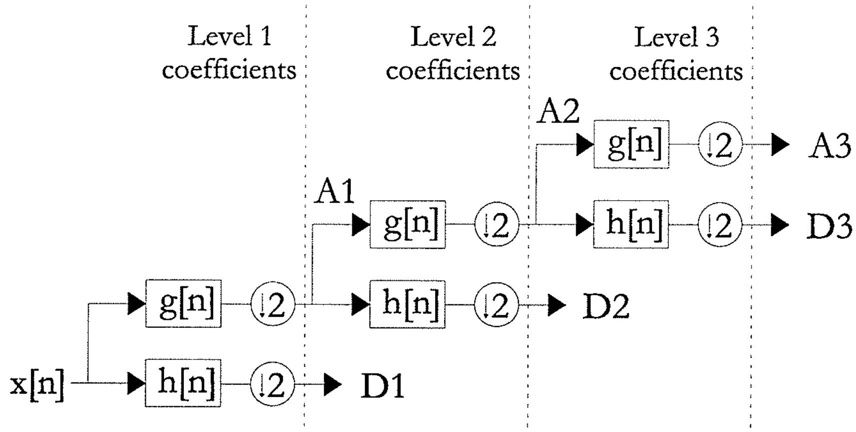

Figure 3.5: Flow chart of multiresolution algorithm

decomposition will be based on $A1$. Thus, the decomposition process can be iterated, with successive approximations being decomposed in turn, so that the original signal is broken down into many lower resolution components.

3.7 Wavelet Packet Decomposition

In the MSD, each level is calculated by passing the previous approximation coefficients though a high and low pass filters. However in the WPD, both the detailed and approximation coefficients are decomposed.

As shown in Fig. 3.6, the WPD can be viewed as a tree. The root of the tree is the original data set. The next level of the tree is the result of one step of the WT. Subsequent levels in the tree are constructed by recursively applying the WT step to the low and high pass filter results of the previous wavelet coefficients.

The numbers shown in Fig. 3.6 indicate the path of each packet. The path is a combination of the characters 0 and 1, where 0 represents low-pass filtering (approximate) followed by a decimation by a factor of two, and 1 represents high-pass

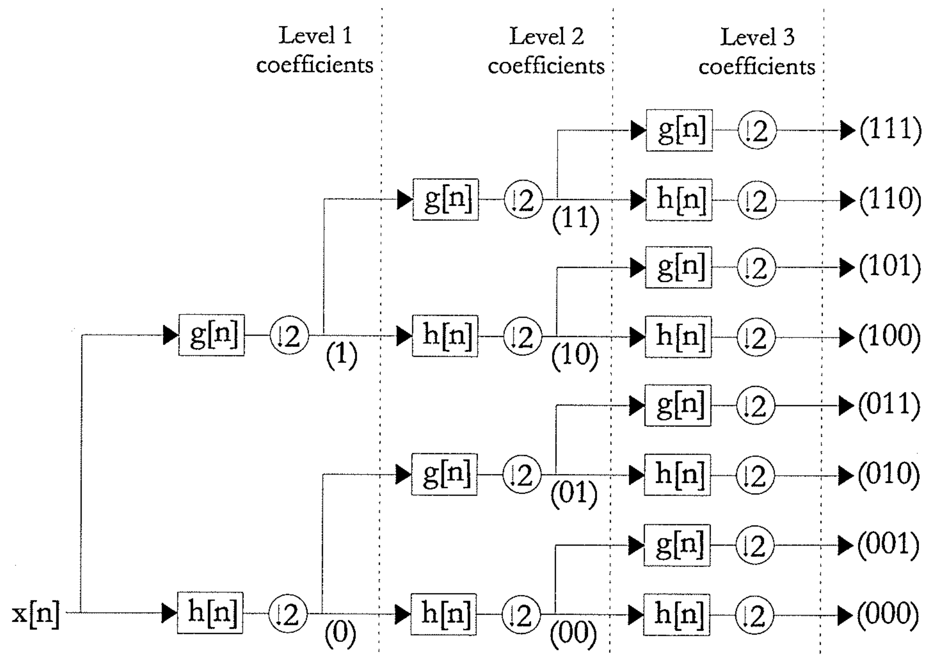

Figure 3.6: Wavelet Packet Decomposition over 3 levels.

filtering (detailed) followed by a decimation by a factor of two. Based on Fig. 3.6, the signal can be represented with different sets of sequences, or different decomposition schemes, such as (1, 01, 001, 000), (1, 00, 010, 011), or (000, 001, 010, 011, 100, 101, 110, 111). As the decomposition level increases, the number of different decomposition schemes also increases. In this thesis, decomposition scheme (1, 01, 10, 11, 100, 101, 110, 111) is proposed for detection of impulse test failures.

Chapter 4

Critical Review on Fault Detection using Signal Analysis

This chapter provides a literature survey of the research work on the application of time-frequency based methods to detect minor insulation failures during lightning impulse tests on power transformers. This is followed by a general discussion, which highlights the limitations of the published work, and provides a rationale for the motivation behind the research. This chapter also provides a brief review of the transfer-function method.

4.1 Fault Detection using Wavelets

This section reviews, in chronological order, published research work on the application of time-frequency based methods to detect minor insulation failures during impulse testing of power transformers.

Satish [12] proposed the application of time-frequency analysis, specifically the short time Fourier transform (STFT) and the continuous wavelet transform (CWT), to detect faults during impulse testing of power transformers. Time-frequency analysis of a non-stationery signal shows the time at which various frequencies of the signal are present. Advantage of such analysis is the possibility of accurate location in time of all local features, such as peaks, edges, and breakdown points, in the signal. It is this very application, i.e. to locate low magnitude abrupt changes in the neutral current waveforms, that created interest in the author of [12] to use time-frequency analysis to detect faults. In this context, the neutral current can be visualized as a nonstationary signal whose properties change or evolve in time, when a fault is present. This is particularly so when there is a momentary short-circuit between adjacent turns due to high electric stress. This short circuit lasts for only, say 1-2 μs, and can be considered to manifest itself as a fast decaying oscillation superimposed on neutral current.

Since the detection of major faults has never been an issue, the focus in [12] was to detect accurately smaller or minor type of faults, which according to the author, are hard to detect. Since the transfer-function method may not be able to detect minor faults [12], the author has proposed their method as an alternative to the transfer-function method. Satish has identified the following as possible sources leading to error and ambiguity in the transfer-function method:

- noise inherent in the acquired data, in spite of good shielding

- errors due to sampling, quantization, A/D errors, finite record length

- different signal processing methods being adopted: windowing, filtering etc.

In [12], the entire analysis is based on simulation work. The neutral current of transformers which have failed the impulse test was simulated by superposing a short-duration (exponentially decaying) oscillating transient onto the neutral current of a healthy transformer, starting at a time instant of 6.5 μs. Its frequency, decay time constant and amplitude are chosen as 2 MHz, 0.2 μs and about 6% of the neutral current peak, respectively. The neutral current of a healthy transformer was also simulated. The author in [12] has provided limited information on the method used for the simulations.

In [12] the ability of the transfer-function method to detect simulated faults has also been investigated. Inclusion of a fault, resulted in only a small variation in the transfer-function and it's effect was spread throughout the spectrum. Therefore, the author has concluded that neither the frequency content of fault nor the time of it's occurrence can be determined using the transfer-function method. To overcome the limitations of transfer-function method, STFT and CWT analysis were considered. Satish has used the Morlet wavelet as the mother wavelet.

Based on the preliminary simulation results, Satish has concluded that STFT and CWT have the potential and suitability as a possible future tool for fault detection since simulation results have highlighted advantages of the method proposed over the conventional transfer function approach. Furthermore, according to the author, the transfer-function method has not been included in relevant standards due to the limitations which they have highlighted in their paper. However, IEC Standards [6] on impulse testing includes the transfer function method as a fault detection method. This was published two years after [12] was published. IEEE is considering the transfer-function method in their next version [4].

As an improvement over the methods based on STFT and CWT analysis of neutral current waveforms, Panday and Satish [13] have proposed the use of multiresolution signal decomposition (MSD) [66]. According to this paper, the previously published work by Satish [12] has following disadvantages;

- some expertise is required in studying the scalogram and spectrogram plots to detect faults

- STFT & CWT involve close examination of signal information in the time-frequency plane instead of time domain

- since the transformation is achieved by dilating and translating the mother wavelet by very small steps, generation of scalogram is computationally not efficient and consumes considerable time. Additionally, it yields substantial redundant information as well.

MSD, as implied by its name, involves an analysis of the signal at different frequencies with different resolutions. Every spectrum component is not resolved equally as was the case in the STFT. MSD is designed to give good time resolution and poor frequency resolution at high frequencies, and good frequency resolution and poor time resolution at low frequencies. This approach makes sense especially when the signal at hand has high frequency components lasting for short duration and low frequency components for long durations. During impulse testing, when a fault occurs, relatively high frequency components are present for a short duration and relatively low frequency components are present through the entire signal (neutral current).
Following are the advantages of MSD technique over the method based on CWT.

- The MSD technique involves the close examination of only two or three detailed and one smoothed signal component in time domain.

- It is very easy to detect the presence of sudden changes in the signal from the decomposed signals.

- Since signal representation is done using an orthonormal basis function, information redundancy among the decomposed signals does not exist

- There exists an elegant algorithm (pyramidal algorithm) to implement the MSD technique. This makes the technique computationally very efficient

The authors in [13] have used the Daubechies wavelet as the mother wavelet, and have used the same approach as in [12] to generate neutral currents. However, in [13] more details are provided on the methodology used to simulate the faults. Neutral current of transformers which have failed the impulse test was simulated by superposing a short-duration (exponentially decaying) oscillating transient onto the neutral current of a healthy transformer. The decaying sinusoid used to simulate the fault which was generated using a mathematical model given by

$$I_f = I_m \sin(2\pi f t) e^{-\frac{t}{\tau}} \tag{4.1}$$

Its frequency (f), and decay time constant (τ), were chosen as 1.5 MHz and 0.2 μs respectively. The actual peak of the superposed transient signal was 7.5% of the neutral peak.

Fig. 4.1 shows the neutral current with and without fault. Fig. 4.1 plot (a) shows the neutral current waveform of a healthy transformer, i.e. without fault; plot (b) is the decaying sinusoid, which was superimposed onto the neutral waveform shown in plot (a); plot (c) is the resultant neutral current waveform with fault.

The authors have not provided any information on how they simulated the neutral current except providing a reference to a CIGRE internal working group document [74]. They have also not provided any experimental data or reference to published literature to support the validity of the simulated neutral waveforms in their paper.

The authors in [13] have applied MSD to decompose the neutral current with and without fault into detailed and approximate signals. Results of their work with 3 scale decomposed signals are shown in Fig. 4.2. Neutral current without and with

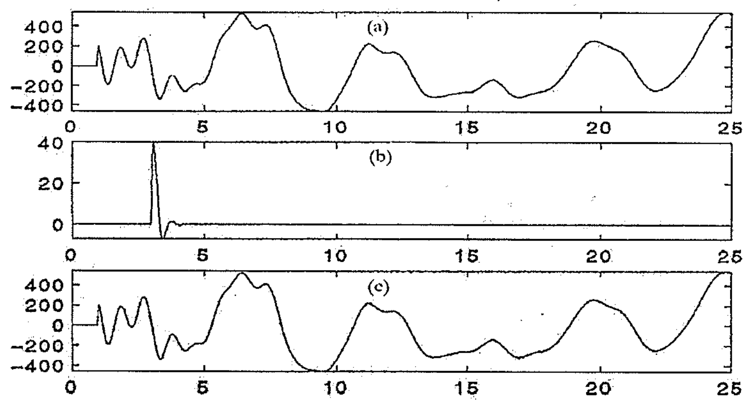

Figure 4.1: Simulated waveforms used by Panday et al. (a) neutral current without fault, (b) superimposed fault at 3 μs, (c) neutral current with fault.

fault are shown in Fig. 4.2(a) and Fig. 4.2(b) respectively.

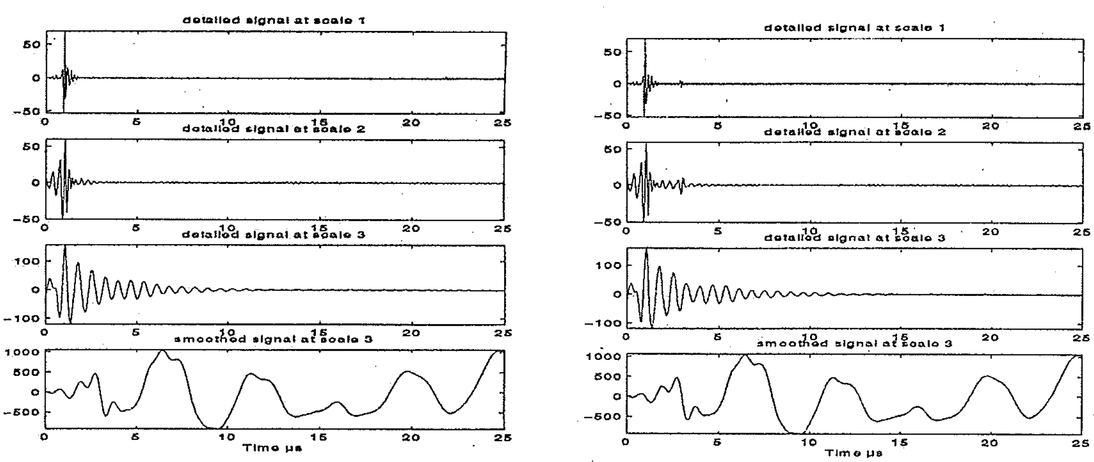

(a) (b)

Figure 4.2: Three scale decomposed neutral currents with and without fault.

Results of decomposed signal of a neutral current of healthy transformer is shown in Fig. 4.2(a). The plot shown at the bottom is the approximate (smooth) signal at scale 3 and the top 3 plots show detailed signals at scales 1 to 3. Plots shown in Fig. 4.2(b) have similar description to Fig. 4.2(a) except that the simulated neutral current belongs to a transformer, which failed during an impulse test.

Comparison of detailed signal of neutral current with and without fault at scales 1 and 2 shows a difference in the waveform at approximately 3 μs. Therefore, the proposed method has detected the superimposed sinusoid.

Panday et al have concluded that the proposed method is robust and far superior to other existing methods to detect minor faults. However, they have acknowledged a need for the proposed techniques to be evaluated "under real-world" conditions. Furthermore, they have identified that the selection of mother wavelet is critical for this application and more work needs to be done to select the best basis.

Karady et al [14] proposed a method based on power spectrum density (PSD) and wavelet analysis techniques. This method was suggested as a further improvement in the transfer-function method by using signal processing and signal analysis techniques which may enhance the differences between the transfer functions. Due to some limitations of FFT analysis, e.g. spectral leakage and degradation at spectral peaks, it was suggested in [14] to use parametric spectral estimation, and wavelet analysis techniques to enhance the sensitivity of fault detection.
Their method evidently consists of following steps:

- Calculation of wavelet transforms for both input and output signals using the Harr wavelet

- Calculation of the power spectrum density (PSD) of the wavelet transformed signal

- Calculation of the wavelet transfer functions (TF) using

$$TF_1 = \frac{PSD(WT(I_1))}{PSD(WT(V_1))} \tag{4.2}$$

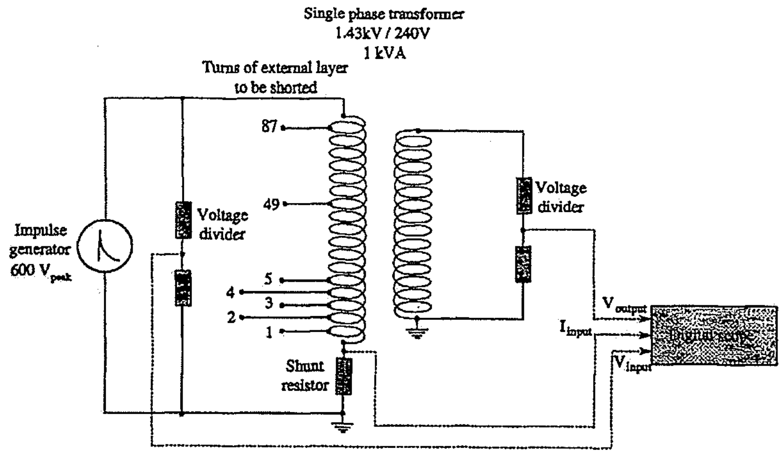

Figure 4.3: Experimental setup used by Karady et al.

$$TF_2 = \frac{PSD(WT(I_1))}{PSD(WT(V_2))} \tag{4.3}$$

where

I_1	Input current
V_1	Input voltage
V_2	Output voltage

To evaluate the sensitivity of the suggested technique, the author in [14] has performed impulse tests on a single phase transformer 1.43 kV/240 V, 1 kVA which is shown in Fig. 4.3. The primary winding has 7 layers containing 769 turns. The external layer, wound with 87 turns, was arranged in such a way that the leads from different turns were available outside the transformer for intentionally producing short circuit between turns.

The experimental work replicates a permanent fault within the transformer. However, in practice, faults during the impulse testing are more likely of the temporary variety which last a few microseconds. There are published works that show turn-to-turn failures can spark over and recover substantial dielectric strength from 2 to

5 μs. Immediately following the sparkover, the remainder of the wave matches an unfaulted, reduced-level reference wave flawlessly [75].

Rao et al [15] have used CWT analysis to detect and locate an inter-turn fault simulated at three different locations in a high voltage winding model. This paper does not provide new insight into application of wavelets to detect faults during impulse tests. The difference between the work reported in [15] and [12] lies in the use of a different type of mother wavelet and the method used to simulate fault currents. In this paper the author claims to be simulating minor faults during impulse tests. However there is no basis for this claim and the method proposed in this paper is similar to that in [12].

The schematic diagram and equivalent electric circuit of a 50 MVA 400/11.5 kV station transformer which was used in the simulation work in [15] is shown in Fig. 4.4. The tap, low-voltage (LV) and high-voltage (HV) windings are divided into eight, three and four sections respectively as shown in Fig. 4.4(a). For simulation work, the tap and LV windings of the transformer were grounded and the HV winding was divided into 12 sections. The HV winding is of the centre-entry type, with two identical parallel branches for increasing current carrying capacity. The ground point is node 1 and impulsed node is 7. The HV winding consists of both interleaved and disc type windings. It consists of 148 discs with 26.7 turns each, out of which 74 discs are placed in the upper half, and the remaining 74 in the lower half, symmetrically. Out of 74 discs (both upper & lower halves), 56 are of the plain disc type placed at the top and the remaining 18 are of the interleaved type placed below the plain type discs. These winding details were used to arrive at the values of the parameters of the model shown in Fig. 4.4(b). Three cases were considered because each one of them represents a fault at a different position of the HV winding and so the respective

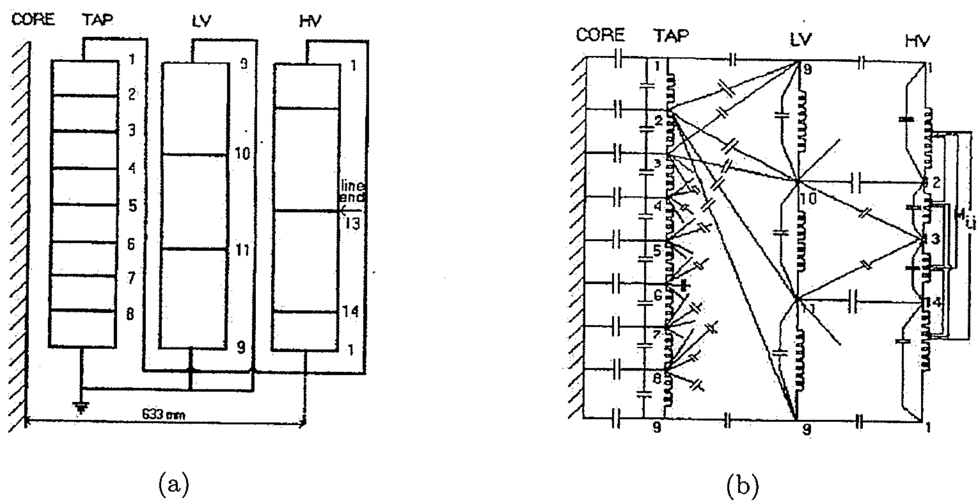

Figure 4.4: Schematic diagram and equivalent electric circuit of the station transformer used by Rao et al.

times of occurrence of the fault will also be different.

Neutral current of a transformer with "one-turn" fault have been simulated by shorting two turns in the transformer model. Fault has been detected by using CWT analysis on simulated neutral current. The authors have used the Mexican Hat wavelet as their mother wavelet.

Authors in [15] have also proposed a method for locating the fault. The distance travelled by the impulse wave before the fault, is calculated by the expression: $2\pi \times$ the average radius of the winding $\times$ the number of disks $\times$ the number of turns in each disk. Authors have considered the speed of propagation of the wave through a winding to be 80% of the speed of light. There is no explanation why this particular value has been selected. The speed of propagation of the wave through a winding is about 150 m/μs (i.e. 50% of the speed of light) [60].

The authors in [15] have concluded that their method is new and that it is capable of detecting minute faults and that it is superior to the transfer function based method. As a response to the claims made in [15], Gururaj et al have written a very critical discussion in [76].

The discussers in [76] were of the opinion that such a "one-turn" fault representation requires a more detailed circuit representation than that used in [15]. Even if it is assumed that the proposed model is capable of simulating faults between turns, shorting two turns does not represent the faults that wavelets based methods try to detect. Wavelets are suitable for locating faults that last for few μs and what the authors in [15] have simulated are permanent faults.

The authors in [15] have not published the waveforms of the neutral currents with and without fault for the various cases. Therefore it is difficult to judge whether the proposed method is any superior to the other techniques such as the transfer-function method or the neutral-current method, which examines the differences in neutral current waveforms.

Bhoomaiah et al in [16] have also used wavelet based methods to detect faults during impulse tests. Published work are based on experimental work which was conducted by applying a low voltage impulse from a recurrent surge generator and recording the voltage and neutral current on a digital oscilloscope. A coil of a generator transformer with power rating of 61 MVA, 11/230 kV has been used in their experimental work. The experimental set-up is shown in Fig. 4.5(a). Only the tapping winding was considered for the experimental work. The tapping winding comprises of 40 plain discs of 4 turns each. The high voltage winding is of a two-group construction with centre-entry type having a total of 112 discs and has been kept opened during the experimental work. A schematic diagram of the coil used in this work is shown in Fig. 4.5(b). The leads from different turns of the tapping winding have been brought out and the paper insulation of the outer most turn at specific locations have been removed so that bare copper has been available for creating permanent faults

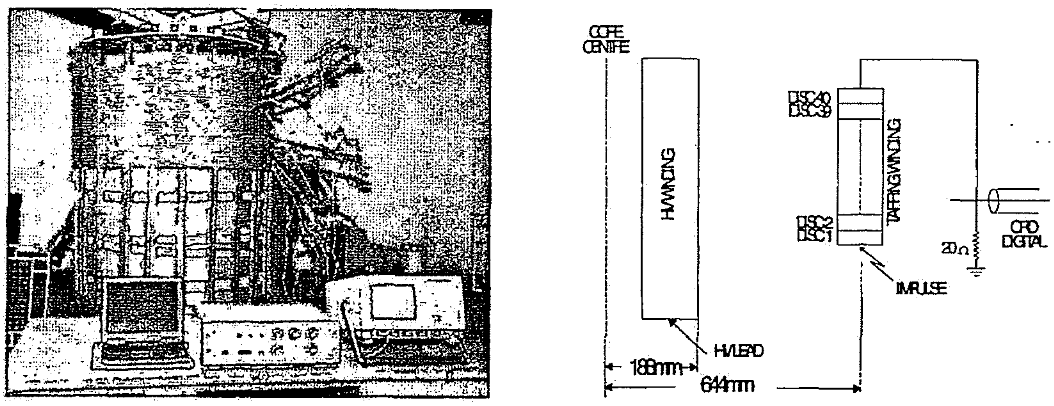

(a) (b)

Figure 4.5: Transformer coil and schematic diagram of a generator transformer used by Bhoomaiah et al.

between different discs and between adjacent turns. The exposed copper conductors of each turn are shorted to create turn-to-turn fault, creating a permanent fault in the transformer. Conclusions drawn by Bhoomaiah are well known and very general.

Kumar et al in [17] derive the neutral current waveforms from an experimental transformer coil. The waveforms were analyzed using MATLAB Wavelet tool box. The authors have used discrete wavelet transform (DWT) for analysis and Daubechies wavelet as choice of the mother wavelet. Method of creating the internal faults and the coils used to generate neutral currents are the same as that in [16]. The authors claim that minute faults in power transformers can be located, is not supported by published results in [17].

4.2 Discussion on Wavelets for Fault Detection

Following is a general discussion, which highlights the limitations of the published work on detection of minor insulation failures during impulse tests using wavelet-based techniques. This also provides a rationale for the motivation behind the research.

4.2.1 Selection of Methods for Time-frequency Analysis

In the published work researchers have used STFT, CWT, DWT and MSD analysis of neutral current waveforms to detect faults during impulse tests on power transformers.

The main problem with the method based on STFT as proposed by the author in [12] is that once a window has been chosen for the STFT, the time-frequency resolution is fixed over the entire time-frequency plane (since the same window is used at all frequencies). Therefore, when analyzing neutral current waveforms which have very high short duration frequency components corresponding to a fault then the signal can be analyzed with good time resolution or frequency resolution, but not both. However, the use of wavelets allows time resolution and frequency resolution to vary in time-frequency plane which allows multi-resolution analysis.

One of the wavelet-based techniques that has been proposed is CWT, which requires some expertise to interpret the scalogram, and generation of scalogram consumes lot of time and yields substantial redundant information as well. Most of the disadvantages of CWT analysis can be overcome by using MSD.

Since MSD analysis of neutral current waveforms involves close examination of only two or three detailed and one smoothed signal component in the time domain, it is very easy to detect the presence of sudden changes in the signal from the decomposed signals. Since signal representation is done using an orthonormal basis function, information redundancy among the decomposed signals does not exist. MSD analysis is based on a pyramidal algorithm which makes the technique computationally very efficient.

The WPD has not been considered in the reviewed published literature. In the MSD, each level is calculated by passing the previous approximation coefficients through high and low pass filters. However in the WPD, both the detailed and approximation coefficients are decomposed, and may have some advantages over the other techniques. Therefore, WPD will be considered in the current research.

4.2.2 Selection of Wavelets

Different wavelet families have been proposed in the published work, such as the Daubechies, Mexican Hat, Morlet and Harr wavelets. It appears that they were selected based on qualitative considerations. i.e. selection primarily based on how the results look on the plot.

The wavelet analysis is a measure of similarity between the basis function (wavelets) and the signal itself. Hence the similarity is in the sense having similar frequency content. So in this case, the mother wavelet must be highly localized in time and frequency as well in order to have good detecting properties. Selection of the wavelet function based on a quantitative method needs to be explored.

4.2.3 Simulation of Waveforms for Time-frequency Analysis

Some of the works [12, 13] are based on simulation of neutral current with minor fault, superimposed on a neutral current waveform. This is similar to superimposing a wavelet on a smooth waveform and using wavelet analysis to detect it, which does not expose the proposed methods to practical conditions. Therefore, further work is required to investigate the suitability of wavelets using valid experimental methods. Experimental work may also be used to investigate the suitability of decaying sinusoid given by (4.1) to simulate internal faults during impulse tests on power transformers.

Some work [15] has used a transformer model (LC ladder type model with some modifications) to generate faults currents. There are two problems with this approach. First the validity of model is in question since it is extremely difficult to simulate the impulse response of a transformer using a simple transformer model. Secondly the shorting of a disc does not represent the actual temporary faults that occur in practice. Perturbation caused by permanent faults are large and may not require wavelets to detect them.

Finally, there are published works [14, 16, 17] that have used experimental work to demonstrate the suitability of wavelet-based techniques to detect faults. However they have used permanent faults to create neutral currents, i.e. faults are created by shorting the turns of disc using a copper wire. As discussed in previous item, this approach in not correct.

4.3 Short Review of the Transfer-function Method

In the *transfer-function* method [10], the frequency domain graphs deconvoluted from the test-voltage and neutral current records obtained respectively at full and reduced test levels are compared. The transfer-function is calculated by first recoding the digital waveforms of the impulse voltage and neutral current simultaneously. Fast Fourier transform (FFT) software is then applied to convert these records into their frequency spectra in polar coordinates, and the module of the neutral current spectral characteristic is divided by the respective module of the test-voltage spectrum. The quotient can be perceived as a transadmittance of the transformer under test but, for brevity, has been labelled the *transfer-function.*

The *transfer-function* method was proposed to address the following limitations of the conventional method of comparing the transformer neutral currents produced when a standard lightning impulse is applied to the HV winding terminal at the BIL and at a reduced level [10].

- A malfunction of the impulse generator, which produces a slightly different impulse form at the full and reduced test levels, will cause a difference between the compared neutral current oscillograms. This may be interpreted as an impulse test failure.

- Rather crude evaluation of the chopped impulse test. Neutral current comparison is not applicable here, since the time to chop cannot be accurately controlled. Consequently, successive oscillograms of the neutral current may show a considerable difference due to the scatter in the chopped-impulse duration.

- Subjective manner of interpreting the differences observed in the oscillograms. An experienced inspector can supposedly tell the nature of the fault from the form of the observed deviation but in practice this often results in controversy between the inspectors representing the buyer and the seller, since there are no generally recognized evaluation criteria.

The transfer-function of a transformer is a characteristic feature and, is in theory, independent of the shape of the applied voltage impulse. The difference between the transfer functions recorded at BIL and at the reduced test level is observable as either a frequency shift or pole-height attenuation.
Following explanation is provided in [11] to explain frequency shift or pole-height attenuation in transfer functions.

- As a first approximation a HV transformer winding can be represented by a ladder network with the series inductance and capacitance as well as parallel capacitance to ground. The transfer-function of such network shows a number of poles at the resonance frequency of the local L and C circuits. A breakdown between the turns or coils of the transformer under test corresponds to a short circuit of the local LC network. This will result in shifting the resonant pole to another frequency or creation of a new pole.

- A partial discharge (PD) may be perceived as an escape of a certain charge from the discharge site in the winding to the core, tank or other windings. This charge will not pass through the neutral current measuring shunt. Hence, from the point of view of input and output terminal measurements, it would appear as if the PD pulse energy were lost or irreversible dissipated. Such loss of PD pulse can be simulated in the equivalent circuit by insertion of a (high ohmic) resistor, which dissipates this energy converting it to heat. An effect of this resistor on the transfer function can be easily predicted, the resonant frequency of the effected pole will not change significantly, but the pole height, i.e. its Q factor, will be reduced.

Consequently, a change of resonant pole frequency indicates a breakdown in the winding insulation, whereas a reduction of the pole height reveals PD activity. The distinction between a local breakdown and a PD constitutes the main advantage of the transfer-function method used as a tool for interpretation of the impulse test results [11].

Fig. 4.6 shows the experimental set-up, which Malewski used to demonstrate the suitability of the transfer-function method to detect faults during impulse tests on power transformers. Malewski applied low-voltage standard full and chopped lightning impulses to a real-scale winding model (section of a 735-kV transformer winding) using a low-voltage Haefely impulse generator. The test voltage and winding neutral terminal current were recorded by a 10-bit digitizer, which was used for monitoring real impulse tests, and the fault was simulated by connecting a back-to-back diode (diac) between the winding turns. The winding consisted of 42 turns numbered from

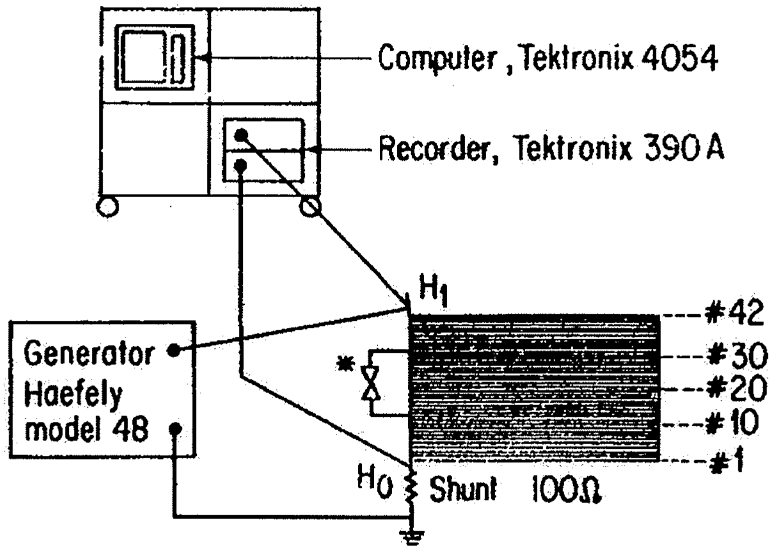

Figure 4.6: Sketch of the experimental setup used by Malewski.

HV terminal to ground, as shown in Fig. 4.6.

For impulse test results to be reliable and accurate, correct transfer function needs to be calculated. Although in theory transfer-function method is an excellent technique, in practice there are several problems. These problems were caused by the commercially available digitizers which frequently have limitations in their accuracy and in their memory length. Koremann [77] has described some methods to overcome some of the problems discussed above.

One of the consequence of limited memory size is that the measured signals are not zero when recording stops. However FFT works as if the data were periodic for all time. When the FFT assumes the signal repeats, the end of one signal segment does not connect smoothly with the beginning of the next. The assumed signal is similar to the actual signal, but has little glitches at regular intervals. Transforming this signal into frequency domain gives the wrong signal. In order to overcome this problem the measured data has to be processed in the time domain. This technique is called windowing. A survey of different windowing types and their effect in the frequency domain are given by Harris in [78].

During a panel discussion at CIGRE, Maier and Fellmann presented four transfer functions obtained from four tests (Full 90%, chopped 70%, full 115% and chopped 100%) for the same transformer. These transfer-functions were not consistent with the theory. i.e. transfer-function of a healthy transformer should be unique. After analyzing these data, Malewski argued that the lack of consistency of the four transfer-function plots implies an ingress of interference in the measuring system, which result in a corrupted record of the measured transients. To check the four sets of records for coherence, the author proposed to calculate their auto-correlation and cross-correlation, and then to determine the coherence-function [11].

The coherence-function δ is calculated as a quotient of the cross-correlation $|G_{xy}|^2$ and auto-correlation of the applied voltage $|G_{xx}|^2$ times auto-correlation of the neutral terminal current $|G_{yy}|^2$.

$$\delta^2 = \frac{|G_{xy}|^2}{|G_{xx}|^2 \times |G_{yy}|^2} \tag{4.4}$$

where

$$|G_{xx}|^2 = \sum_{i=1}^{n} \frac{|V|}{n}$$
$$|G_{yy}|^2 = \sum_{i=1}^{n} \frac{|I|}{n}$$
$$|G_{xy}|^2 = \sum_{i=1}^{n} \frac{|V \times I|}{n}$$

In this expression V denotes the frequency spectrum of the recorded voltage, I is the neutral terminal current spectrum and n is the number of sets.

The coherence-function attains unity when the set of voltages and currents are recorded on the same winding which has not changed during the impulse test, and the records are free from interference. An interference imposed on the test records decreases the coherence, attaining zero when the signals are completely masked by noise. The coherence-function provides an effective test of the significance of the transfer-function. A low coherence region should not be considered as reliable information for detection of the faults in the winding under examination.

Most of the commercially available impulse test systems allow transfer-function and coherence-function analysis of waveforms to permit frequency domain display and analysis.

Chapter 5

Experimental Work using RSG: Wavelet-based Fault Detection

The main objective of this research work was to investigate the application of WT to detect minor insulation failures during impulse tests on power transformers, by considering experimentally generated waveforms. This chapter describes an investigative study at reduced voltage using a recurrent surge generator (RSG) and a model transformer. The neutral currents were analyzed using wavelet-based techniques to detect artificially created minor insulation failures, and the results are reported. Application of WT for fault detection requires the determination of the particular wavelet function. A quantitative method to select the optimum wavelet function for this particular application is proposed. Since the captured neutral current waveforms are contaminated with noise, sometimes, signal processing is required prior to the application of WT for fault detection. A wavelet-based method, which is suitable for reducing noise in the neutral current waveforms is also reported.

5.1 Experimental Work using RSG

5.1.1 Introduction

The main limitation of the published work in literature is either they are based on simulated waveforms or based on experimental data that do not represent a realistic method to simulate minor insulation failures during impulse tests. In this section, an experimental method at reduced voltage is proposed to generate neutral currents with faults that last for a short time, and which result in a disturbance in the neutral current for a few microseconds. The main objectives of the work are to (a) generate neutral current waveforms with faults by using a suitable method to create an artificial fault between sections of the winding, and (b) demonstrate that the experimental methods used by other researchers [14, 16, 17] are not suitable for studies that investigate wavelet-based techniques for detection of impulse test failures.

Motivation for the initial experimental work using a LV RSG was based on the work reported by Malewski [10]. Malewski used a low-voltage impulse generator to apply standard full and chopped lightning impulses to a real-scale winding model (section of a 735 kV transformer winding). The test voltage and winding neutral terminal current were recorded by a 10-bit digitizer, which had been used for monitoring real impulse tests, and the faults were simulated by connecting a back-to-back diode (diac) between winding sections. The experimental setup used in the current research work is described in the following section.

5.1.2 Test Set-up using RSG

The test setup consisted of a 1000 V recurrent surge generator, a single phase model-transformer, and a measuring system to measure voltages and currents. A schematic

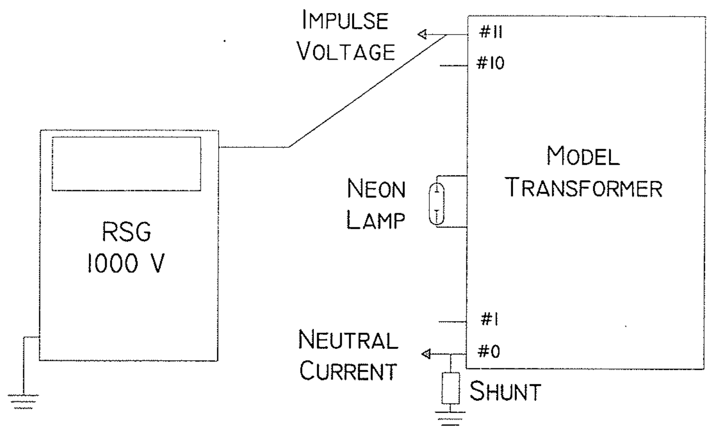

Figure 5.1: Sketch of experimental set-up using RSG.

diagram of the test setup is shown in Fig. 5.1.

The single phase model-transformer, shown in Fig. 5.2(a), is rated 80 V/2.2 kV. The 2.2 kV winding has 12 winding sections and the leads from different winding sections are brought out for intentionally producing faults between winding sections. These leads are numbered from #11 to #0 i.e. the top most lead is numbered #11 and the one closest to the ground is labelled #0. Two types of faults were created:

- Permanent faults - faults were artificially created by shorting the leads
- Temporary faults - faults were artificially created by connecting a neon lamp between the leads

The applied impulse voltage was measured using a voltage probe, and the neutral current was measured using a noninductive shunt as shown in Fig. 5.1. Waveforms, shown in Fig. 5.2(b), were simultaneously recorded using a digital oscilloscope with 9-bit resolution (separate digitizer for each channel) and sampling rate of 100 Ms/s. The neutral current and voltage waveforms in Fig. 5.2(b) are those obtained without introduction of a fault. The impulse waveform shown has a wave shape of 1.0/40.0 μs.

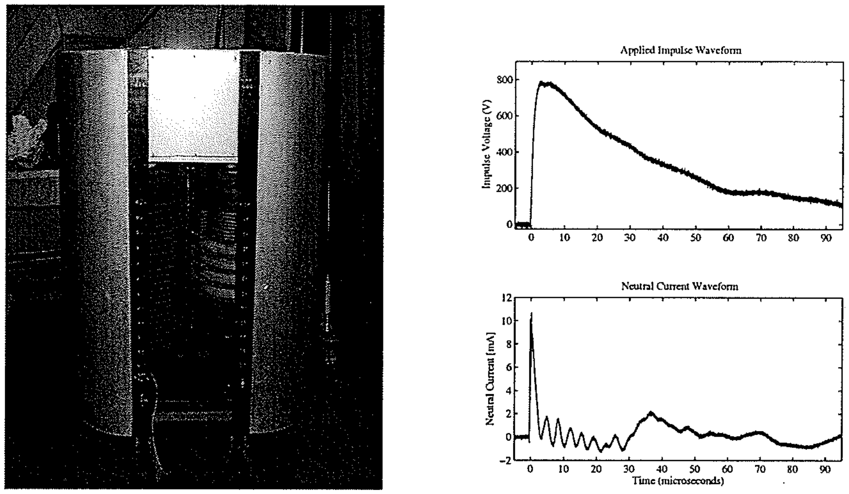

(a) (b)

Figure 5.2: Model transformer and experimental waveforms.

The main objective of introducing *permanent faults* was to demonstrate that experimental methods used by other researchers [14, 16, 17] to investigate the use of wavelet-based methods for fault detection, is not the correct approach to realistically model the dielectric failures in a transformer. Permanent faults were created by connecting a copper wire across adjacent leads.

The neutral current waveforms with *temporary faults* were used in the current research to investigate the suitability of wavelet-based method for detection of minor faults during impulse tests. Neon lamps, rated for 120 V, were used. Such lamps are typically used as indicator lamps in switchgear applications. The duration of the fault, which has an effect on the inductive portion of the neutral current, was controlled by connecting a resistor in series with the neon lamp.

5.1.3 Results and Discussion

During the experimental work, faults were created between different sections of the model transformer. Faults between the top three sections (i.e. between #11-#10,

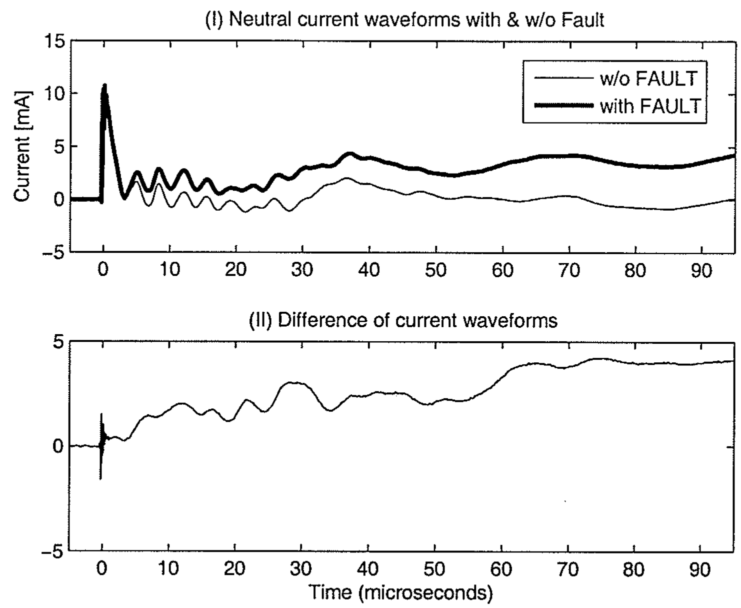

Figure 5.3: Neutral current waveforms obtained with and without a permanent fault.

#10-#9 and #9-#8) resulted in changes in the neutral current that can be detected using both CWT and the neutral-current method. Fault between sections #9-#8 was the least sensitive to the neutral-current method. Temporary faults created between sections beyond the top three sections could not be detected using either CWT or the neutral-current method. In this section, waveforms resulting from permanent and temporary faults between sections #9 and #8 are presented.

Permanent Faults

Waveforms of neutral currents with and without a permanent fault are shown in Fig. 5.3. The permanent fault was created between sections #9 and #8 of the single phase model-transformer. Neutral current waveforms with and without fault are shown in plot (I). The difference in the neutral currents are shown in plot (II). The waveforms were measured using a 500 Ω noninductive shunt. It is seen that these faults can be detected by simple comparison of waveforms.

The main purpose in using wavelet-based techniques for fault detection is that wavelets can capture the transient features of the neutral current, and enable signal analysis at multiple resolutions. The fine frequency resolution of large-scale wavelets provide an opportunity to measure the frequency of the slow variation component in the signal. The fine time resolution of small-scale wavelets provide an opportunity to detect the fast variations in component in the signal. Therefore, wavelets are suitable for analyzing signals that last for a few microseconds and have relatively high-frequency components. Results obtained with employing permanent faults show that experimental methods used in [14, 16, 17] to create neutral currents with permanent faults, are not valid for work that investigates the suitability of wavelet-based techniques to detect impulse test failures.

Temporary Faults

Waveforms of neutral currents with and without a temporary fault are shown in Fig. 5.4 and Fig. 5.5. The temporary fault was created by connecting a neon lamp between sections #9 and #8 of the single phase model transformer. The waveforms obtained with and without fault are shown in plot (I). The difference in the neutral currents are shown in plot (II).

In Fig. 5.4, plot (II) the spike at approximately 8 μs indicates the change in the neutral current due to the temporary fault. The fault was verified by visual confirmation of the discharge between the electrodes of the neon lamp. Using the conventional method, it is possible that this type of fault (temporary faults) may not be detectable.

In order to examine the sensitivity of wavelet-based techniques, a few faults were created by connecting a 30 kΩ resistor in series with the neon-lamp. These temporary faults lasted for a very short time compared to the duration of the applied impulse

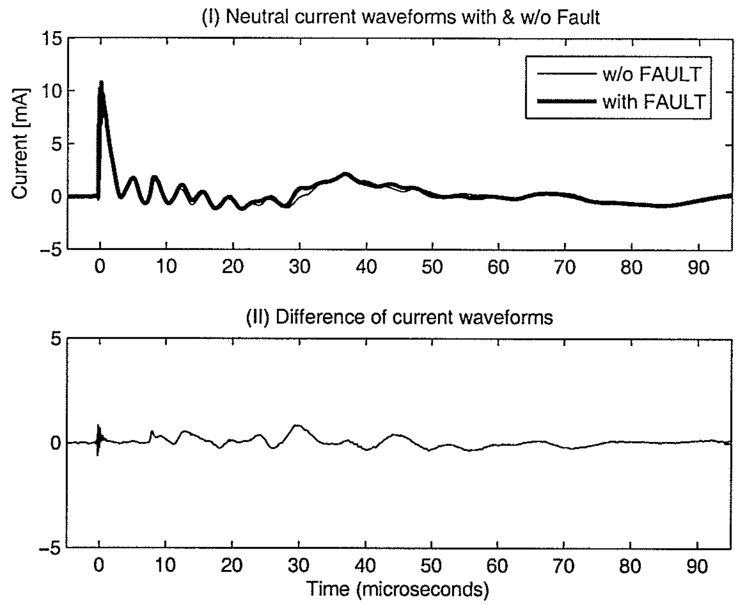

Figure 5.4: Neutral current waveforms obtained with and without a temporary fault.

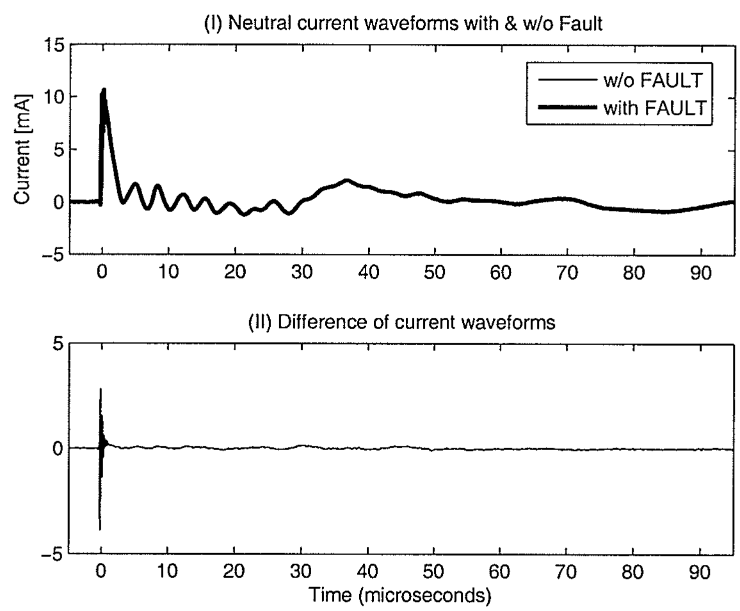

Figure 5.5: Neutral current waveforms obtained with and without a temporary fault. A resistor was connected in series with the neon lamp.

voltage. Waveforms of neutral currents obtained with and without a temporary fault (with short time) are shown in Fig. 5.5. The temporary fault was created between sections #9 and #8 of the single phase model transformer.

There are no visible changes in the waveforms due to the fault. As mentioned earlier, for each case, the occurrence of the fault was verified by observing the discharge between the electrodes of the neon lamp. In this particular case, the neutral currents - if first few μs are ignore - are a perfect match, and the neutral-current method would not have detected the fault.

5.1.4 Summary

In this section an experimental setup using a RSG has been used to create minor faults using a model transformer. Two types of faults were created: permanent faults and temporary faults.

When the faults are of the permanent variety, the conventional neutral-current method is capable of locating the fault. The use of neutral currents resulting from permanent faults in transformer winding, is not the correct approach for investigative work that evaluate the application of wavelets for fault detection; permanent faults do not create features such as peaks, edges and breakdown points which are especially suitable for detection by employing wavelet-based techniques.

Temporary faults were created using neon lamps. These temporary faults lasted for a short time relative to the duration of the applied impulse voltage wave. It is possible that temporary faults may not be detected as an impulse test failure by the use of the conventional neutral-current method. The use of temporary faults to create faulted neutral current waveforms is an acceptable approach for work investigating the application of wavelets to detect minor faults.

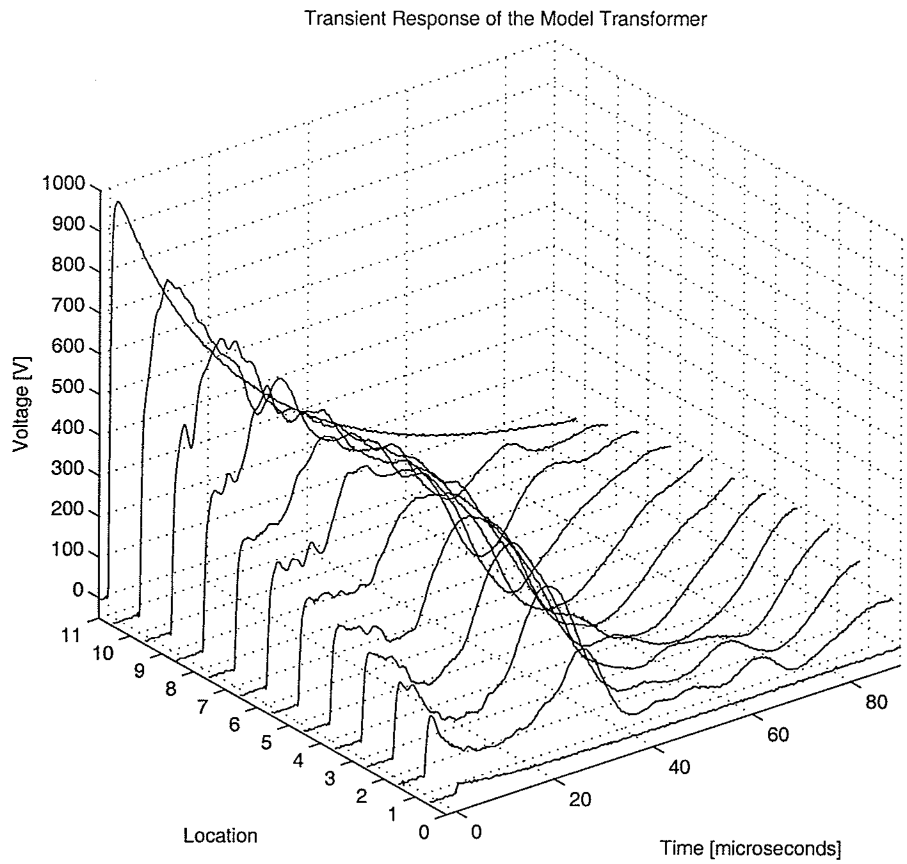

Figure 5.6: Transient behaviour of the model transformer.

In the current research work, recorded neutral currents were analyzed using CWT and MSD, and the results are reported in Section 5.5.

5.2 Transient Response of Model Transformer

To understand the behaviour of the model transformer when subjected to lightning impulse voltage, the voltage response at different locations along the winding was measured due to a 1000 V impulse applied at the terminal. Fig. 5.6 shows the applied voltage and measured voltages at different locations of the winding.

As discussed in Chapter 2, during impulse tests, the initial distribution in the

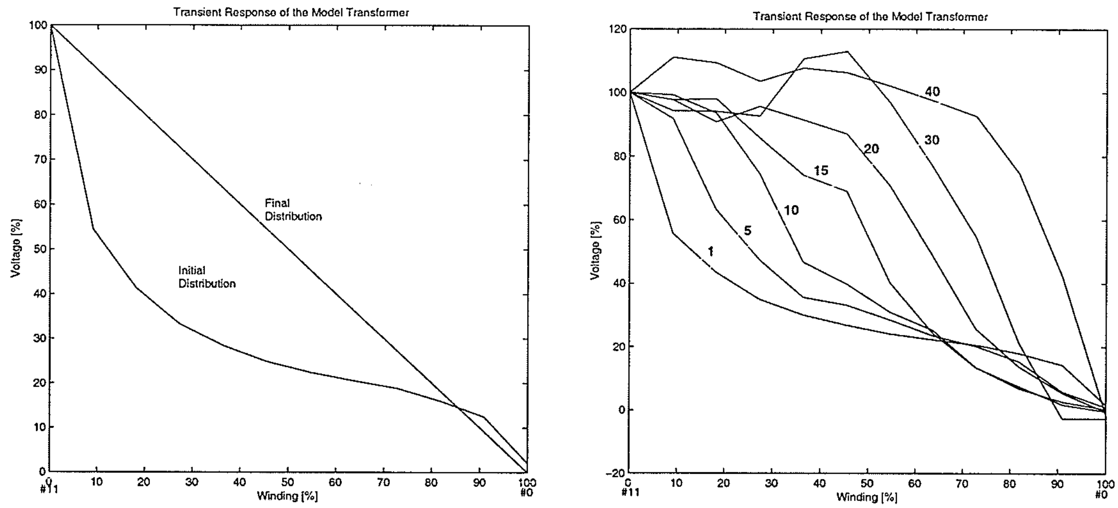

(a) (b)

Figure 5.7: Initial and final distribution of impulse voltage.

winding depends on the capacitances between turns, between windings, and those between windings and ground. The winding inductances have no effect on the initial voltage distribution since the magnetic field requires a finite time to build up. When the applied voltage is maintained for a sufficient time, appreciable currents begin to flow in the inductances eventually leading to a uniform voltage distribution. Since there is a difference between the initial and final voltage distributions, as shown in Fig. 5.7, a transient phenomenon takes place during which the voltage distribution readjusts itself from the initial to final value.

The initial voltage distribution along the model transformer is shown in Fig. 5.7(a). One end of the winding (#0) was grounded through a 500 Ω resistor. These values were examined at 0.5 μs and it was observed that the voltage distribution is highly nonuniform. For example, the first 10% of the winding supports 47% of the applied voltage rather than the anticipated 10%. Depending on the termination, there will be reflections at the far end of the winding. If the termination is a short circuit at the lowest point, the voltage wave whose amplitude is same as the original wave but of opposite polarity is reflected. For a line which is open circuited, the reflected wave would be of the same magnitude and of the same sign.

The transitional behaviour between the initial and final voltage distribution takes a form of complex oscillations and these are shown in Fig. 5.7(b). These curves corresponds to different time instances (i.e. 1, 5, 10 μs etc.) Experimental results show that all parts of the winding were severely stressed at different instants of time; initially, concentrations of voltage appeared at the line end of the winding; during the transitional period, concentrations appeared at the neutral end while voltages to earth considerably in excess of the incident impulse developed in the main body of the winding.

The applied impulse voltage and measured voltages at sections #10 to #7, and voltage across first four sections are shown in Fig. 5.8. Plots (I) to (IV) show voltages at different locations along the winding. As the impulse travels along the winding, it's magnitude attenuates. Plots (V) to (VIII) shows the voltage as appeared across the first four individual sections of the winding. Highest peak voltage appears across the top-most sections. If there are no reflections, voltage across the sections are lower for the lower portion of the winding. The different time of occurrence of the peak voltage is significant, since this information may be used to find the physical location of the fault.

The voltage across the first 5 sections are shown in Fig. 5.9. Due to the sharp rise of the impulse voltage, there is a large difference of voltage caused in the winding as the wave front travels along the winding. Thus there would be an overvoltage across adjacent windings. For the first few sections, the time of occurrence of the peak voltage across the sections were different, and they were a few microseconds apart. For example, between sections #10 and #9 the maximum voltage appeared

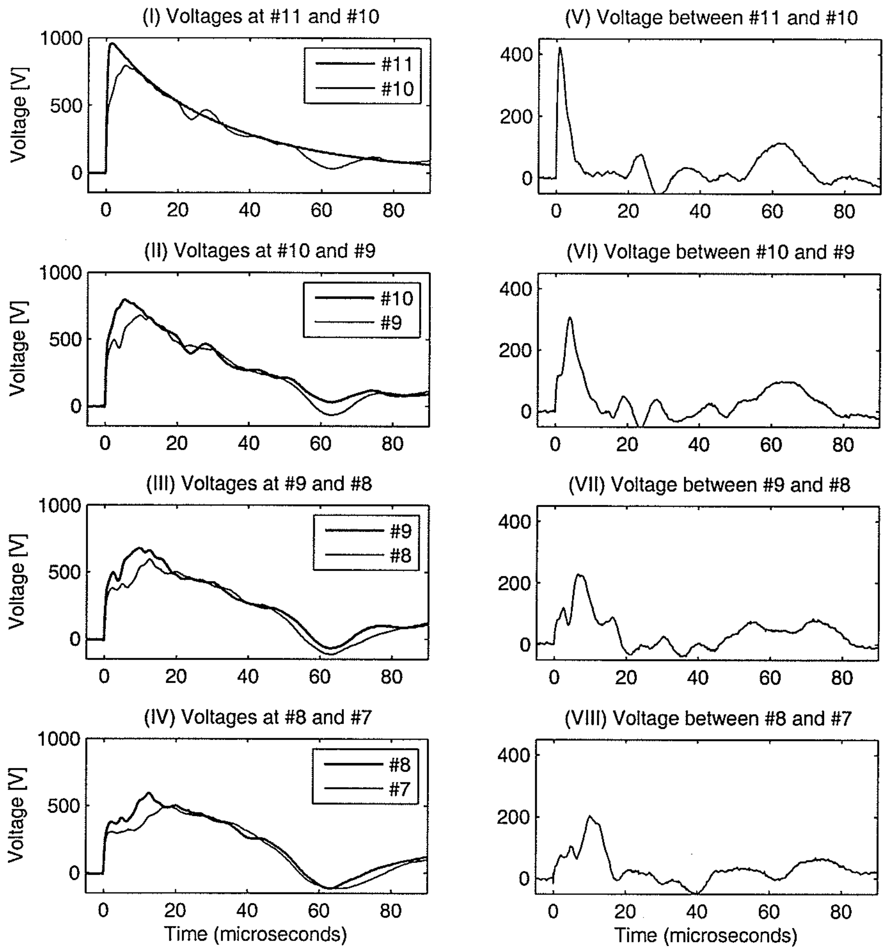

Figure 5.8: Voltage at different points of the winding and voltage across top five sections. Note the voltage scale change for plots (V) to (VIII).

at approximately 4 μs, whereas for #9 and #8, maximum voltage occurred at 6.5 μs.

Table 5.1 shows maximum voltage across each section of the model transformer winding and the time of occurrence of the peak voltage. As stated earlier, these times are a few microseconds apart. Therefore, position of the dielectric failure between sections due to a lightning impulse may be approximated, provided one knows the time instance of the impulse test failure.

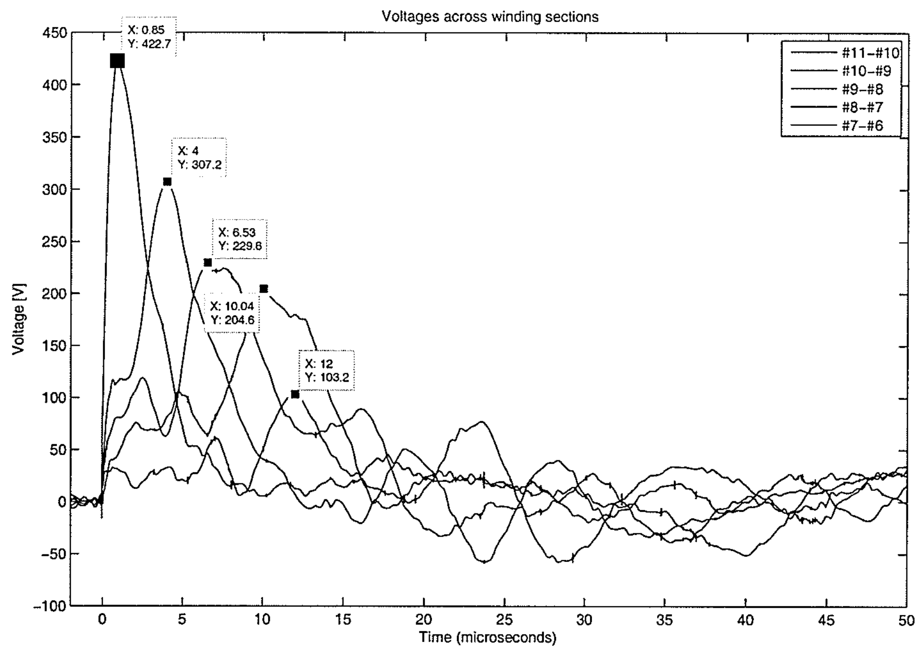

Figure 5.9: Voltage across winding sections.

Table 5.1: Time instance of the peak voltage across adjacent sections of the winding.

Location	Voltage across Sections (V)	Time instance of Vp (μs)
11-10	423	0.8
10-9	307	4.0
9-8	230	6.5
8-7	204	10.0
7-6	103	12.0
6-5	176	18.1
5-4	148	20.8
4-3	132	24.7
3-2	125	28.0
2-1	141	31.5

5.3 Selection of Wavelet Function

Wavelet analysis is a measure of similarity between the basis function (wavelets) and the signal itself. Hence the similarity is in the sense having similar frequency content. So in this case, the mother wavelet must be highly localized in time and frequency as well in order to have good detecting properties. This section proposes a quantitative method to select the best basis function for wavelet-based techniques for impulse test failures.

5.3.1 Introduction

The choice of the wavelet plays a significant role in detecting and localizing perturbations due to impulse test failures. For impulse failure detection, different wavelet families have been proposed in published work such as the Daubechies, Mexican Hat, Morlet and Harr wavelets. It appears that these choices were based on a trial and error basis. The selection of the wavelet function without knowing the shape of the perturbation due to the fault is a very difficult task. Furthermore, there are no methods available in literature for selection of the wavelet function when the shape of the signal of interest is unknown. In this thesis, a quantitative method is proposed to select the wavelet function for the particular application considered. This technique assumes that the perturbation due to the fault can be modelled as a decaying sinusoid as given in (4.1).

In theory, selection of the particular mother wavelet is possible from an infinite number of wavelets. A detailed comparative study of all wavelets is not reported, as this was not within the identified scope of the thesis. Therefore current research work on the selection of the wavelet function for fault detection was limited to Daubechies and Symmlet wavelet families. This choice was based on the experience with different wavelets considered and published in literature on similar type of work [79–82].

5.3.2 Methodology

Wavelet basis functions are short waves: on one hand, localized in time or space, depending on the nature of the signal. On the other hand, all basis functions are scaled versions of a mother function. Each basis function therefore corresponds to a unique combination of position and scale. A wavelet coefficient is indicative of how much of the corresponding wavelet basis function "is present" in the total signal: a high coefficient means that at the given location and scale there is an important contribution of singularity (or transient in signals). This information is local in space (or time) and frequency (frequency is approximately the inverse of scale): it yields information about the location of the singularity (perturbation in the neutral current) and how far it ranges, i.e. how large the scale is [83]. Therefore, the shape of the optimum wavelet basis function should be similar to the changes in the neutral current due to the fault during impulse test, i.e. the shape of the perturbation due to impulse test failure.

The optimum wavelet maximizes the cross correlation between the signal of interest and the wavelet, i.e. maximizes $\gamma(X,Y)$ (5.1), where X represents the fault current data set and Y is the wavelet data set [84].

$$\gamma(X,Y) = \frac{\sum_{i=1}^{n}(x_i-\overline{x})(y_i-\overline{y})}{\left[\sum_{i=1}^{n}(x_i-\overline{x})^2\sum_{i=1}^{n}(y_i-\overline{y})^2\right]^{1/2}} \tag{5.1}$$

The draw back of this technique is that one needs to know the shape of the fault current. In this thesis, in order to choose a suitable basis function, fault current data was generated using (4.1), with frequency (f) and decay time constant (τ) chosen as 1.5 MHz and 0.2 μs respectively. This method can be justified since (a) use of WT is suggested for minor insulation failures that last for 1 to 2 μs, and (b) breakdown between adjacent turns in an EHV transformer usually excites an oscillation at approximately 2.5 MHz, whereas an inter-disc breakdown causes an oscillation at about 0.8-1.2 MHz [10].

5.3.3 Results and Discussion

Table 5.2: Selection of wavelet.

Wavelet	Xcorr
db2	0.525
db3	0.713
db4	0.766
db5	0.716
db6	0.604
db7	0.483
db8	0.379
db9	0.295
db10	0.277
db11	0.298
db12	0.219
sym4	0.798
sym10	0.385

Results of similarity between the wavelet data and fault current data are given in Table 5.2. The first column shows different wavelets considered in this thesis. For Symmlet wavelet family 'sym4' and 'sym10' are shown. The second column shows the value of γ which is an indication of the similarity between a particular wavelet and the simulated fault current.

In Fig. 5.10, the fault current data set and the wavelet data set are shown on the

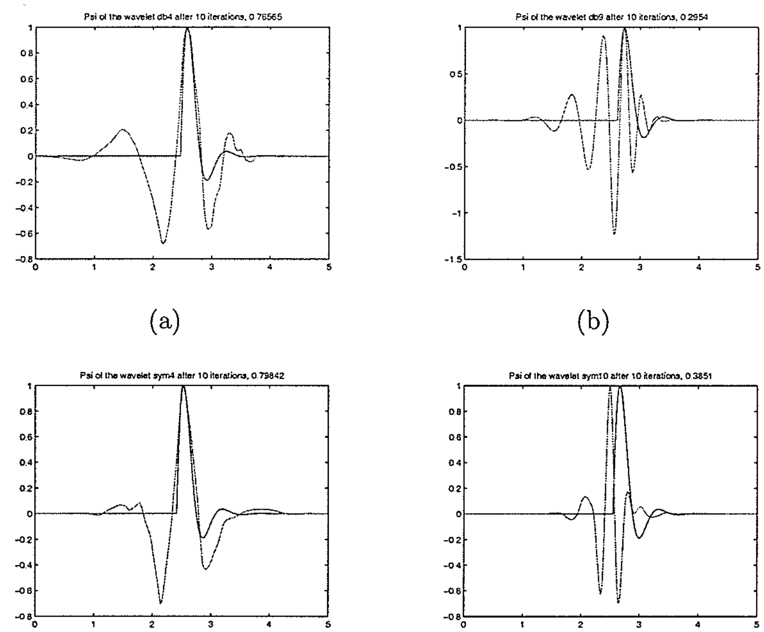

(a) (b) (c) (d)

Figure 5.10: Simulated fault current and wavelet functions for (a) 'db4' (b) 'db9' (c) 'sym4' (d) 'sym10'

same plot for 'db4', 'db9', 'sym4' and 'sym10'.

Based on the value of γ, the wavelets 'db3', 'db4', 'db5', and 'sym4' have the higher values suggesting that those wavelets are suitable over the other wavelets for fault detection wavelets. Similarity between the wavelet data and fault current for 'db4' and 'sym4' are shown in Fig. 5.10(a) and Fig. 5.10(c). The wavelet functions that have lower value of γ are shown in Fig. 5.10(b) and Fig. 5.10(d).

5.3.4 Summary

One of the most important aspects of the wavelet-based methods is that the selection of the "optimum" basis function (or the wavelet function). A quantitative method to select the wavelet function for this particular application is proposed. This technique is used in the present work resulting in the choice of 'db4' as a suitable basis function.

5.4 Noise Reduction

5.4.1 Introduction

One of the most effective applications of wavelets in signal processing is denoising, or reducing noise in a signal. The wavelet-based method retains the detail of the signal after denoising. Fig. 5.11 shows actual impulse test records with noise and the denoised test records using the wavelet-based method proposed in the current research work. With the WT, the noise in the waveforms, shown in Fig. 5.11(a), can be reduced. The reconstructed signal after wavelet denoising, shown in Fig. 5.11(b), contains less noise, and retains the details of the original waveforms.

With regard to the applications of wavelets in signal processing to reduce noise in a signal, the theoretical justifications and arguments in its favour remain highly compelling. Denoising does not require any assumptions about the nature of the signal, permits discontinuities and spatial variation in the signal, and exploits the spatially adaptive multiresolution features essential to the wavelet transform. Furthermore, the procedure exploits the fact that the wavelet transform maps white noise in the signal domain to white noise in the transform domain. Thus, while signal energy becomes more concentrated into fewer coefficient in the transform domain, noise energy does not. It is this important principle that enables the separation of signal from noise. Wavelet shrinkage denoising has been theoretically proven to be nearly optimal from the following perspectives: estimation when local smoothness is unknown, and estimation when global smoothness is unknown. In effect, no alternative procedure can perform better without knowing a priori the smoothness class of the signal [85].

The denoising method involves the calculation of the WT coefficients for a given signal, application of a threshold method, followed by reconstruction of the signal by

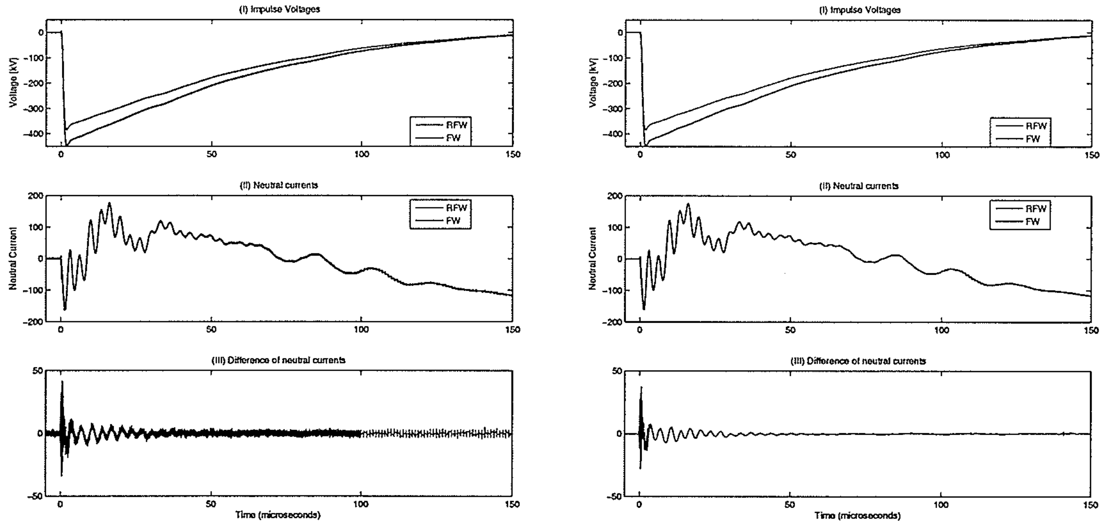

(a) (b)

Figure 5.11: Noise reduction. (a) Noisy waveforms (b) Denoised waveforms.

taking the inverse WT of the modified WT coefficients. When a signal is decomposed using the WT, it results in a set of wavelet coefficients that correlates to the high frequency subbands. These high frequency subbands consist of the details in the data set. If these details are small enough, they might be omitted without substantially affecting the main features of the data set. Additionally, these small details are often those associated with noise; therefore, by setting these coefficients to zero, the noise can be reduced very effectively. Denoising methods require the determination of choice of the wavelet function, number of levels of decomposition, and the threshold techniques. These determinations are based on empirical results and published literature on wavelet-based methods for denoising PD signals [81, 82].

5.4.2 Denoising

For simplicity, we concentrate on the case of a regularly sampled signal in the presence of near white Gaussian noise [86]. Thus, suppose (after a rescaling of the time interval) that the data consist of $n = 2^{J+1}$ pairs $(i/n, y_i)$, $1 \leq i \leq n$, with

$$y_i = f(i/n) + z_i \tag{5.2}$$

The aim is to recover the signal f. For the derivations of the methods below, the noise $\{z_i\}$ is assumed to be independent and identically distributed Gaussian with mean zero and (known) variance σ^2: in practice the methods tolerate at least small departures from these assumptions.

The denoising procedure is as follows:

1. Apply an empirical wavelet transform using a suitable **wavelet function**, yielding coarse level scaling coefficients (approximate coefficients) $\{v_k, k = 1, \ldots, 2^N\}$ at a pre-chosen **level** N, and wavelet coefficients (detailed coefficients) $\{\omega_{j,k}, k = 1, \ldots, 2^j, j = N, \ldots, J\}$, for a total of n transform coefficients in all.

2. To each individual wavelet coefficient, apply a **threshold rule**, either *soft* (a continuous function of the data which shrinks each observation) or *hard* (which retains unchanged only large observations) :

$$\eta_S(\omega, t) = \begin{cases} \omega - t, & \omega \geq t \\ 0, & |\, \omega \,| < t \\ \omega + t, & \omega \leq -t \end{cases} \tag{5.3}$$

$$\eta_H(\omega, t) = \begin{cases} \omega, & |\, \omega \,| \geq t \\ 0, & |\, \omega \,| < t \end{cases} \tag{5.4}$$

Form

$$\tilde{\omega}_{j,k} = \eta(\omega_{j,k}, \sigma n^{-1/2} t_j)$$

The scaling coefficients $\{v_k, k = 1, \ldots, 2^N\}$ are left unchanged in order that gross structure is not lost.

3. Invert the empirical wavelet transform on $\{v_k, \tilde{\omega}_{j,k}\}$ to obtain an estimated curve $\tilde{y}_i = f(i/n)$.

The following section discusses the selection of the wavelet function, number of levels of decomposition, and the threshold rule for wavelet-based noise reduction technique.

Wavelet Function

Donoho and Johnstone [86, 87] have shown that small wavelet coefficients can be replaced with zero, because those coefficients are dominated by noise and carry only small amount of information about the signal. Thus, by ignoring these coefficients when reconstructing the original signal from the rest of the coefficients, one obtains a denoised version of the signal. Therefore it is very important that the selected wavelet function yield high wavelet coefficients when analyzing a neutral current waveform with perturbation due to an impulse test failure.

As discussed in Section 5.3, wavelet basis functions are localized in time, and all basis functions are scaled versions of a mother function. Each basis function therefore corresponds to a unique combination of position and scale. A wavelet coefficient is indicative of how much of the corresponding wavelet basis function "is present" in the total signal: a high coefficient means that at the given location and scale there is an important contribution of singularity.

Therefore, the method, proposed in Section 5.3, can be used to select the wavelet function for denoising.

Threshold Rule

According to the noise model, there are four threshold rules as described below [88]. They are based on the work by Donoho [86, 87].

RigrSure uses for the soft threshold estimator a threshold selection rule based on Stein's Unbiased Estimate of Risk (quadratic loss function). In this method, the risk for a particular threshold value t is estimated. Minimizing the risks in t gives a selection of the threshold value.

Sort the absolute of the vector to be estimated minimum to maximum, then extract the root of the sorted vector and a new vector NV is obtained. And the algorithm of risk at the index k is

$$Risk(k) = \frac{n - 2k + \sum_{j=1}^{k} NV(j) + NV(n-k)}{n}$$

The corresponding threshold is

$$t = \sqrt{NV(k)}$$

Sqtwolog uses a fixed form threshold yielding minimax performance multiplied by a small factor proportional to log(length(x)). The fixed form threshold is

$$t = \sqrt{log(2n)}$$

Heursure is a mixture of the two previous options. As a result, if the signal-to-noise ratio is very small, the SURE estimate is very noisy. So if such a situation is detected, the fixed form threshold is used.

First, calculate the variables A and B and judge which is larger, then fixed form threshold is used when A is less than B, else threshold selection rule based on Steins unbiased estimate of risk is adopted. A and B is defined by

$$A = \frac{\sum_{i=1}^{n} |f_i| - n}{n}$$

$$B = \sqrt{\frac{1}{n}\left(\frac{log(n)}{log(2)}\right)^3}$$

Minimax uses a fixed threshold chosen to yield minimax performance for mean square error against an ideal procedure. The minimax principle is used in statistics to design estimators. Since the de-noised signal can be assimilated to the estimator of the unknown regression function, the minimax estimator is the option that realizes the minimum, over a given set of functions, of the maximum mean square error. The algorithm of the threshold selection is

$$t = 0.3936 + 0.1829 \times \frac{log(n)}{log(2)}$$

Fig. 5.12 demonstrates the performance of different threshold rules. In this example, the 'db4' wavelet was chosen and used to perform level 5 wavelet decomposition and compare the performance of the different threshold selection rules. The method of threshold processing was according to the detailed coefficients at the first level.

Fig. 5.12(a) shows a neutral current waveform with a fault known to occur at approximately 2 μs. The original neutral current without any signal processing is shown

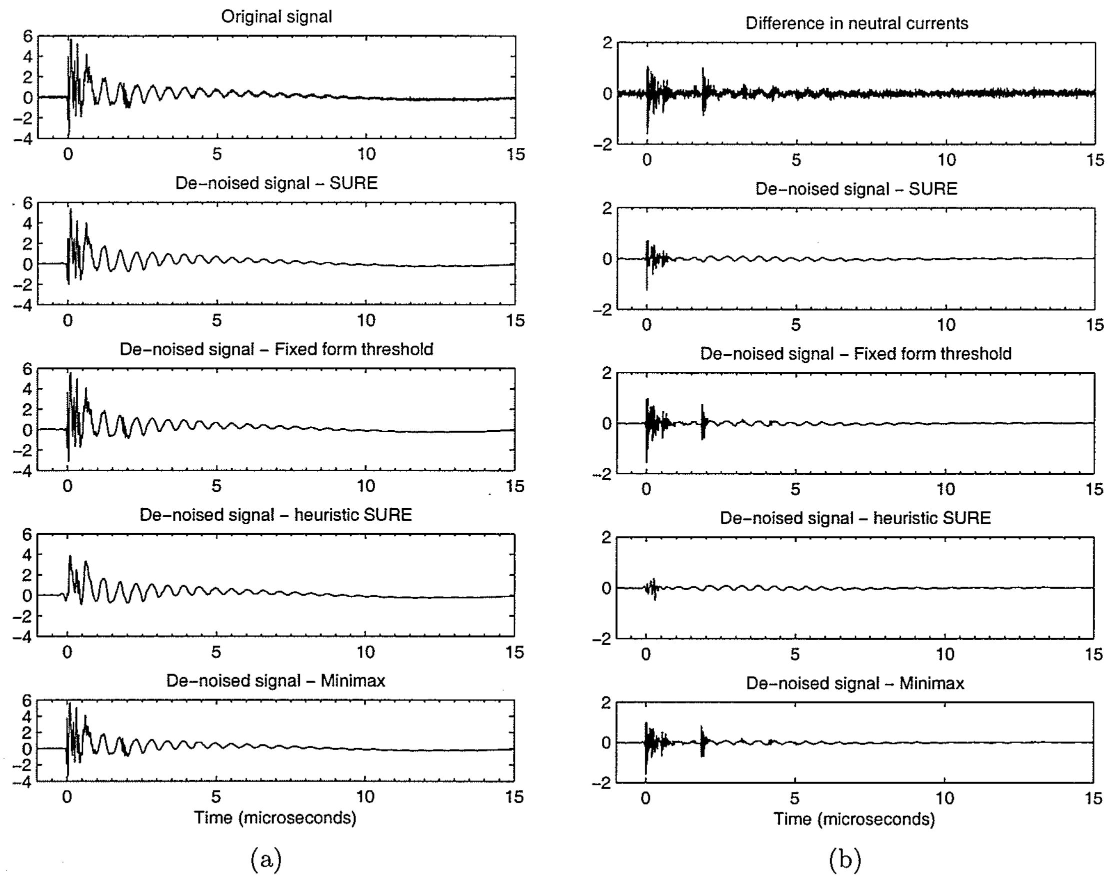

Figure 5.12: Results from denoising using different threshold rules.

in the first plot of the Fig. 5.12(a). The experimental waveforms were recorded during HV experimental work. The remaining plots in the Fig. 5.12(a) stand for threshold selection based on Steins unbiased estimate of risk (RigrSure), fixed form threshold (Sqtwolog), mixed threshold selection rule (Heursure) and minimax-performance threshold selection rule (Minimax) respectively.

Fig. 5.12(b) shows the difference between the neutral currents with and without temporary fault. In Fig. 5.12(a), the first plot corresponds to waveforms with noise. Other four plots stand for threshold selection based on RigrSure, Sqtwolog, Heursure, and Minimax respectively. The threshold selection based on RigrSure and Heursure were the worst, because during the denoising process, perturbations due to the fault was completely removed. Results show that Sqtwolog and Minimax threshold selection rules were able to retain the information relevant to the fault after denoising.

Decomposition Levels

The selected decomposition level should be such that it has sufficient resolution in frequency bands at lower frequencies, as low frequency pulsive interferences were also to be eliminated. If lesser levels are used, then perturbation due to the fault and the low frequency interferences would be clubbed together, and hence difficult to segregate [81]. In this thesis, as a compromise, five decomposition-reconstruction levels were chosen, and found to be sufficient in most of the cases.

Fig. 5.13 demonstrates the performance of different decomposition levels. In this example, the 'db4' wavelet was chosen, 'Minimax' was chosen as the threshold selection rule to compare the performance of different levels of wavelet decomposition. The first plot shows the difference between the neutral currents with and without temporary fault, which corresponds to the waveforms with noise. The remaining plots stand for different levels of wavelet decompositions. Results show that even after level 5 of decomposition, the signal was able to retain the information relevant to the fault after denoising.

5.4.3 Summary

The noise present in the neutral current with faults, which were recorded during HV experimental work were reduced by application of signal denoising. The proposed denoising algorithm recovers a close approximation of the original signal and the details (corresponds to the fault) of the denoised signal is very similar to that of the

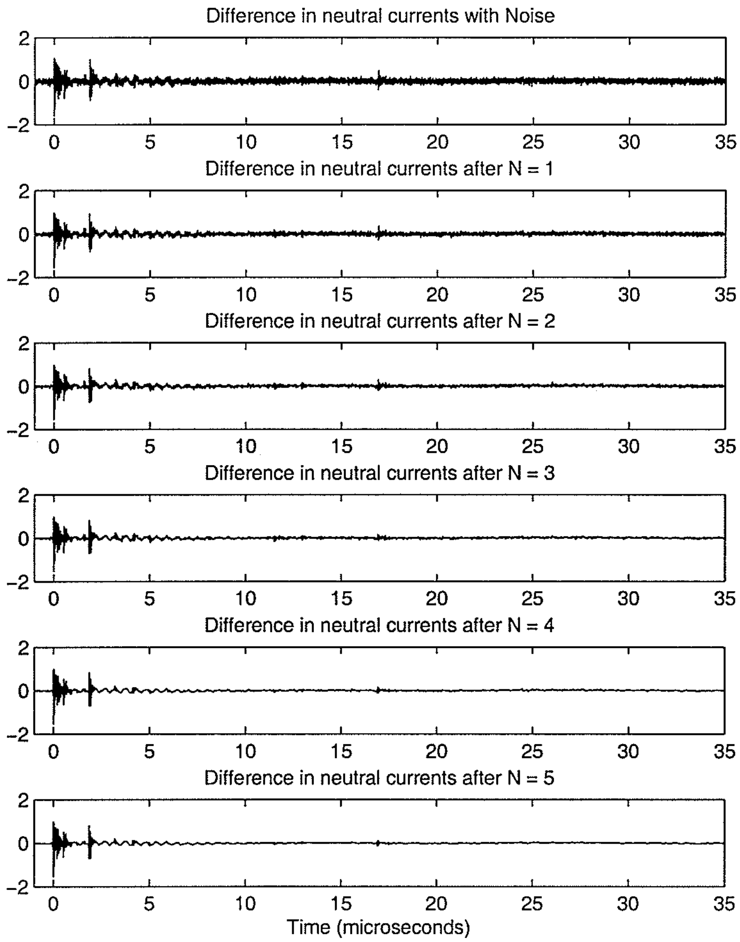

Figure 5.13: Results from denoising procedure for level 1 to 5.

original signal.

To select a threshold rule, four kinds of threshold selection rules were studied. Results show that Sqtwolog and minimax threshold selection rule are better than the other two thresholds.

Following procedure, which was implemented in the current research work is proposed for denoising:

- Compute the wavelet decomposition of the signal at level 5 using the wavelet 'db4'

- For each level from 1 to 5, select the threshold and apply to the detailed coefficients. The threshold rule is based on minimax algorithm. Minimax is a method used in decision theory for minimizing the maximum possible loss. The method of threshold processing is according to the detailed coefficients at the first level.

- Compute wavelet reconstruction using the original approximation coefficients of level 5 and the modified detailed coefficients of levels from 1 to 5.

5.5 Fault Detection via Wavelet-based Techniques

Fig. 5.14 shows the analysis of neutral currents with faults between sections, which was obtained using CWT. In these plots, the x-axis represents time, y-axis represents scale, and the colour at each x-y point represents the magnitude of the wavelet coefficient. The lighter shades represent relatively high wavelet coefficients.

The scalogram in Fig. 5.14, plot (I) corresponds to a neutral current without a fault. Plots (II) to (IV) correspond to neutral current with fault between sections #11 & #10, #10 & #9, and #9 & #8 respectively. Faults created below section #8 could not be detected with either the neutral-current method or with the CWT, because perturbation due to the fault may have been masked by the noise present in the neutral current. Other wavelet-based techniques, such as MSD and WPD, were not able to detect the temporary fault created as described in Section 5.1.

Table 5.3 shows a good correlation between the time instance of the fault as detected by CWT, and time instance of the peak of the voltage across the section (Fig. 5.9). Therefore, the physical location of the fault may be estimated provided that the transient behaviour of the winding is known.

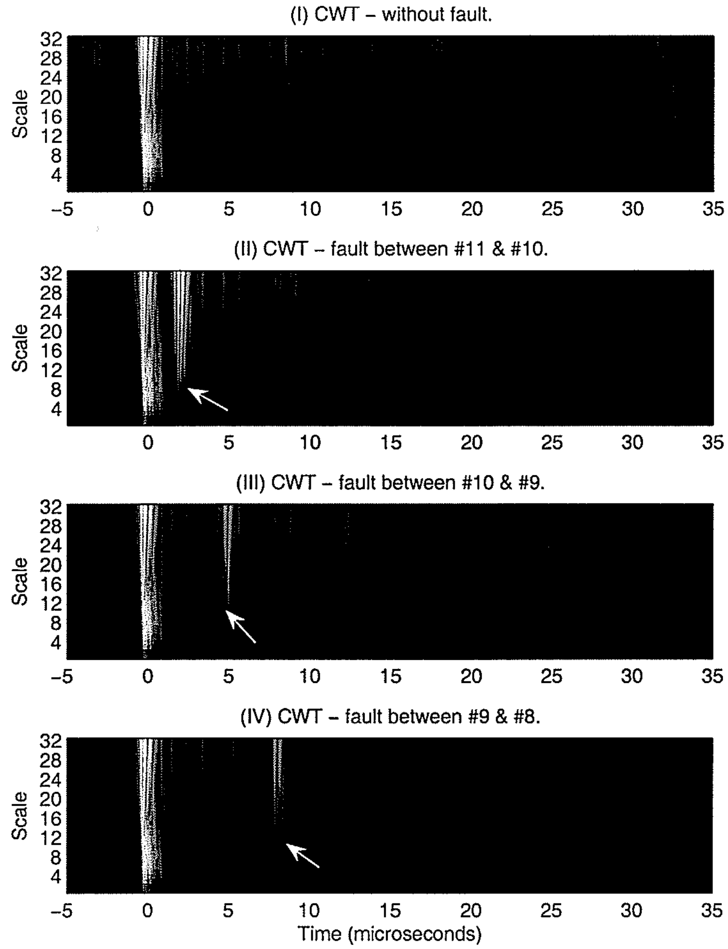

Figure 5.14: Scalogram of neutral current with and without faults.

5.6 Summary

In this chapter an experimental setup, which utilized a RSG has been used to create temporary and permanent faults with a model transformer and neon lamps. The temporary faults lasted for a short time relative to the duration of the applied impulse voltage wave.

It is shown that the use of permanent faults to create faulted neutral currents in transformer windings is not the correct approach for investigative work that involves

Table 5.3: Location of the fault.

Location	Time instance of fault based on CWT (μs)	Time instance of Vp (μs)
11-10	1.0	0.8
10-9	5.0	4.0
9-8	7.0	6.5

use of wavelets.

Application of WT to detect minor faults requires the determination of the particular wavelet function. A quantitative method to select the optimum wavelet function for this particular application is proposed. The technique suggested by (5.1) resulted in the choice of 'db4' as a suitable basis function. Although faults created by neon lamps do not replicate actual conditions, and the shape of the perturbation may not be the same as one would expect in practice, the results presented in this chapter suggest that 'db4' to be acceptable for fault detection.

Since the captured neutral current waveforms are contaminated with noise, signal processing is required prior to the application of WT for fault detection. A wavelet-based method, which is suitable for reducing noise in the neutral current waveforms has been suggested.

The recorded neutral currents were analyzed using the CWT, MSD, and WPD techniques. The results show that the CWT could detect temporary faults with adequate sensitivity. The MSD and WPD techniques were not able to detect such faults. This highlights one of the limitation of the wavelet based techniques, i.e., selection of the wavelet function is crucial for the wavelet based method to detect minor insulation failures during impulse tests.

The CWT analysis of neutral current with minor faults demonstrate that the physical location of the fault in the winding may be estimated provided that the transient behaviour of the winding is known.

The main limitation of the experimental work as proposed in this chapter, is that the magnitude of the neutral current is low compared to noise present in the signal (i.e. low signal-to-noise ratio). Wavelet-based techniques were not able to detect certain faults that resulted in small perturbations on the neutral current. To overcome this limitation, it was decided to conduct experiments on an actual coil removed from a transformer with a HV impulse generator. The next chapter describes the HV experimental work, which was conducted to generate neutral currents with minor insulation failures to investigate the application of wavelets to detect minor faults.

Chapter 6

Experimental Work using IG: Wavelet-based Fault Detection

This chapter describes lightning impulse tests on an actual transformer coil using an impulse generator (IG). Minor insulation failures between sections and turns were artificially created by using small sphere gaps and a neon lamp respectively. Neutral current waveforms, which were recorded during the experimental work were analyzed by using wavelet-based techniques. Effectiveness of the wavelet-based techniques is compared to other methods, which are based on time-domain and frequency-domain analysis. Finally, sensitivity of wavelet-based method for fault detection is investigated and reported.

6.1 High Voltage Experimental Work

6.1.1 Introduction

The high-voltage (HV) experimental work was undertaken because the results of the experimental work at reduced voltage were not conclusive enough to justify the use of wavelet-based techniques for fault detection. The main objective of the HV experimental work was to generate neutral current waveforms with short duration faults using a suitable method to create an artificial fault between adjacent sections of an actual transformer coil.

The ideal way to demonstrate the suitability of wavelets to detect minor faults during impulse testing would be to conduct the experiments on an actual power transformer. It would not be realistic to do such experiments for practical reasons. Therefore, it was decided to conduct experiments on an actual coil removed from a transformer.

6.1.2 High Voltage Test Set-up

The high voltage test setup, which consists of a 50 kV impulse generator, a transformer coil, sphere gap arrangement to create faults, and measuring system to measure voltages and currents is shown in Fig. 6.1.

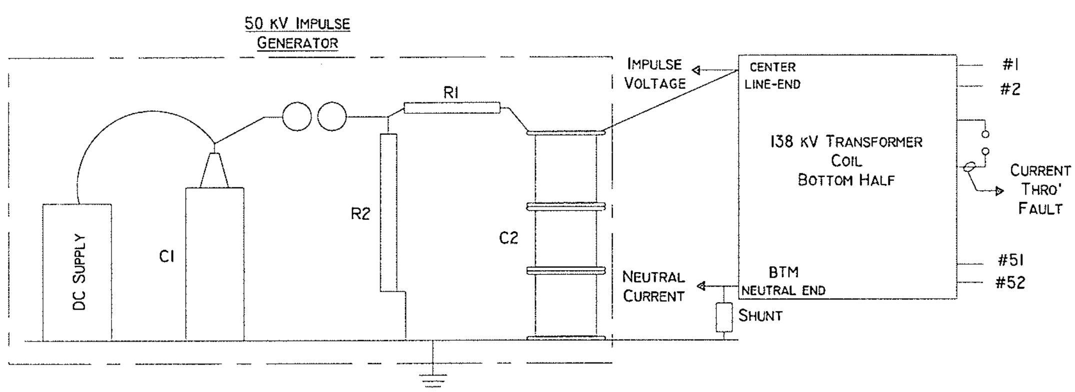

Figure 6.1: Sketch of high voltage experimental set-up used in the experimental work.

The transformer coil, shown in Fig. 6.2(a), was a high voltage coil of a three phase 150 MVA, 138/13.8 kV power transformer. The type of the coil used in the

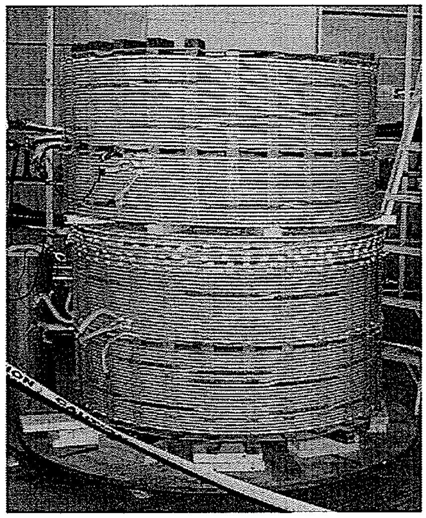

(a)

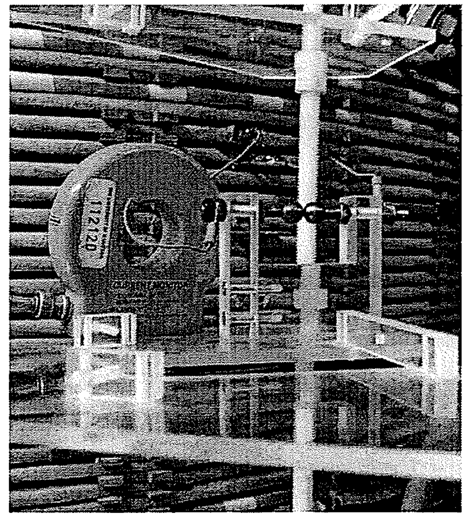

(b)

Figure 6.2: High voltage transformer coil and sphere gap used in the experimental work.

experiments is Disc-Spiral, Centre Fed and has 376 turns per half. Each half has 52 sections and they are numbered #1 to #52. The one closest to the line-end (at the centre of the winding) is numbered #1 as shown in Fig. 6.1, in which only the bottom half of the coil is shown. During the experimental work, the neutral end of the both coils, i.e. top and bottom, were connected together, and grounded through a noninductive resistor. More details on the HV coil is given in Appendix A.

The sections of the HV coil are placed in axial direction, Fig. 6.3, with ducts between them. Each section is a flat coil, having more than one turn. The number of turns per section depends on the physical location of the sections. Sections close to the line-end (#1 to #19) and neutral-end (#31 to #52) have 7 25/28 turns per section, while sections close to the taps have 4 14/28 turns per section. The winding is continuously wound with a winding conductor, so that the winding sections are connected in series without any additional joins between them. When faults are created, for example, between #3 and #4, the fault sees a higher voltage due to the fact that the number of turns between these two sections are approximately 15 turns. Whereas, a fault between #4 and #5 sees a lower voltage since the fault is created between approximately one turn.

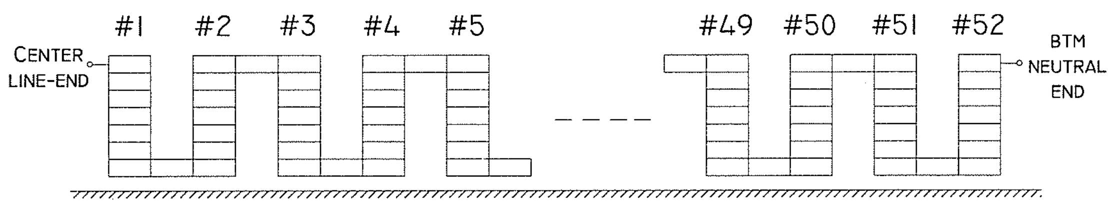

Figure 6.3: Disk winding.

During actual impulse tests in practice on power transformers, impulses are applied to the HV winding while the LV winding and the core are grounded. However, for experimental work only the HV winding was available. A grounded metal cylinder was inserted into the HV winding to simulate the LV winding and core.

When an impulse voltage test is conducted on a transformer, the main flux in the iron core will be cancelled by the flux caused from a short-circuited non-impulsed winding, so that only leakage flux contributes to impulse voltage response in the windings. As a result, it can be assumed that the inductance of a transformer winding with an iron core is approximately similar to that of a winding without an iron core,and that the impulse voltage distribution in transformer windings may be analyzed using the inductance values of a winding without an iron core. The impulse voltage response in transformer windings can be analyzed by using the inductances of a winding without an iron core [89].

When an inner winding, such as a LV winding, is provided and is short-circuited, the voltage response in an impulsed HV winding with an iron core is similar to that in the winding without an iron core, even when the neutral terminal of the impulsed winding is isolated. Since the capacitance distributions in both cases, either with or without iron cores, are approximately same, the similarity of voltage responses indicates that the magnetic flux in an iron core is cancelled by the short-circuited winding and the impulse voltage distribution is affected by leakage flux through air [89].

The difference between the measured waveshapes of the impulse voltage response in a single winding with the neutral terminal grounded, and with and without an iron core is negligible. On the other hand, if the neutral terminal is isolated, the voltage response in the winding with an iron core is different from that in the winding without an iron core. This seems to indicate that magnetic flux exists in the iron core when the neutral terminal is isolated. The damping effect caused by iron loss keeps the peak value of the voltage response in the winding with the iron core lower than that in the winding without the iron core.

The high voltage coil used in the present experimental work, had an original basic insulation level (BIL) of 650 kV. Since the experiments were conducted on the unimpregnated coil, it was assumed that it would be safe to apply 100 kV impulses without causing any damage to the coil. The author decided to limit the maximum voltage to 30 kV to ensure that the coil would not fail during the testing except where faults are intentionally created. To generate the required impulse voltage, a 50 kV impulse voltage generator was designed. Details of the circuit are given in Appendix B.

A typical impulse voltage waveform generated using 50 kV impulse generator, and the resulting neutral current waveforms, without introduction of a fault, is shown in Fig. 6.4. Rise time of the impulse is approximately 1 μs and tail time is approximately

30 μs. Plot (III) shows the current through the sphere gap. In this case, the gap did not sparkover. The current was measured using a current monitor.

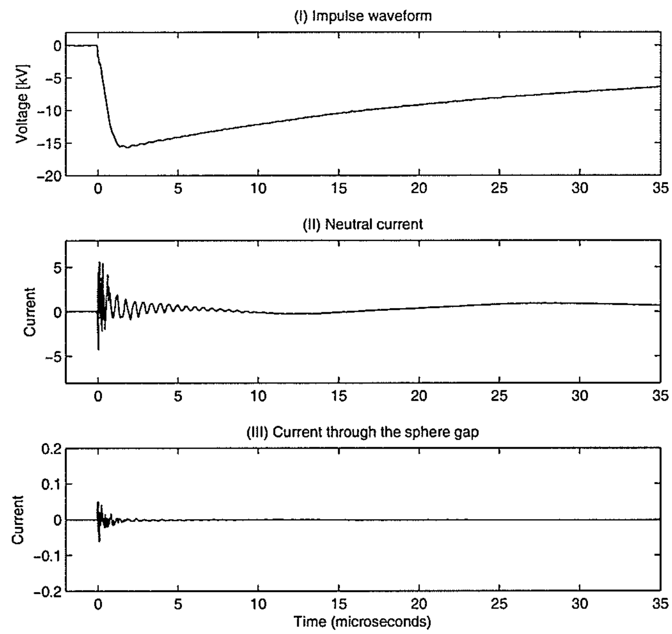

Figure 6.4: Impulse voltage and neutral current observed in HV experiments without a temporary fault.

The applied impulse voltage, neutral terminal current, and current through the gap were simultaneously recorded using a digital oscilloscope with a sampling rate of 100 Ms/s. Applied voltage was measured using a high voltage probe rated for 40 kV impulse. Electrical specifications of HV probe and current monitor are provided in Appendix B. The neutral current was measured by measuring the voltage drop across a non-inductive resistor (1.857 Ω), which was used to ground the neutral-end of the transformer.

6.1.3 Transient Response of HV Coil

The behaviour of the HV coil was studied by applying a 19.5 kV impulse to its line-end terminal and measuring the voltage at several locations along the winding. Fig. 6.5 shows the transient behaviour of the HV coil.

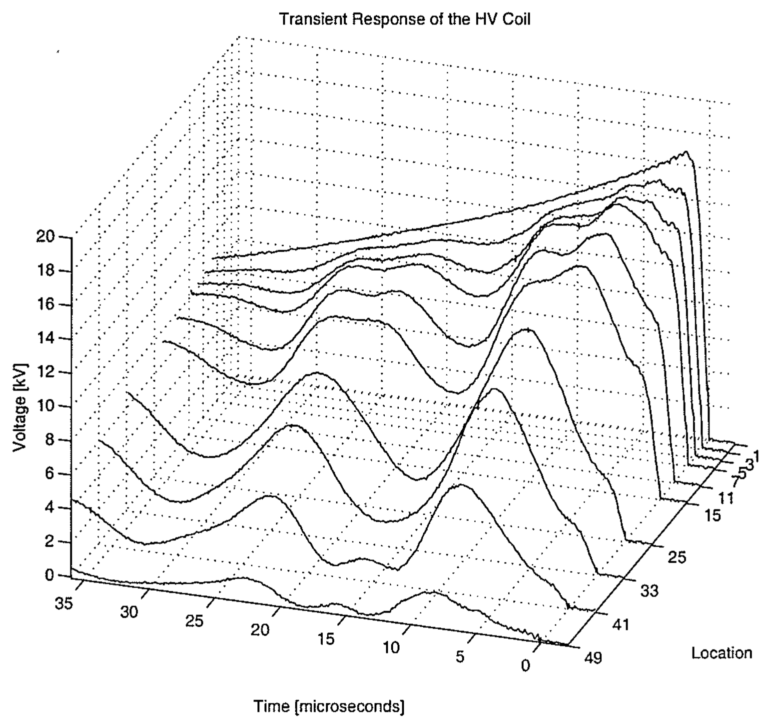

Figure 6.5: Transient behaviour of the HV coil.

The applied impulse voltage and measured voltages at different sections (up to #8), and voltage across five sections are shown in Fig. 6.6. Plots (I) to (V) show voltages at different locations along the winding. As the impulse travels along the winding, it's magnitude attenuates. Plots (VI) to (X) shows the voltage as appeared across the different sections of the winding. Voltage difference between sections #4 and #5 (plot VIII) was low due to the fact that this voltage was due to approximately one turn (Fig. 6.3). The difference voltage in the other plots are due to approximately

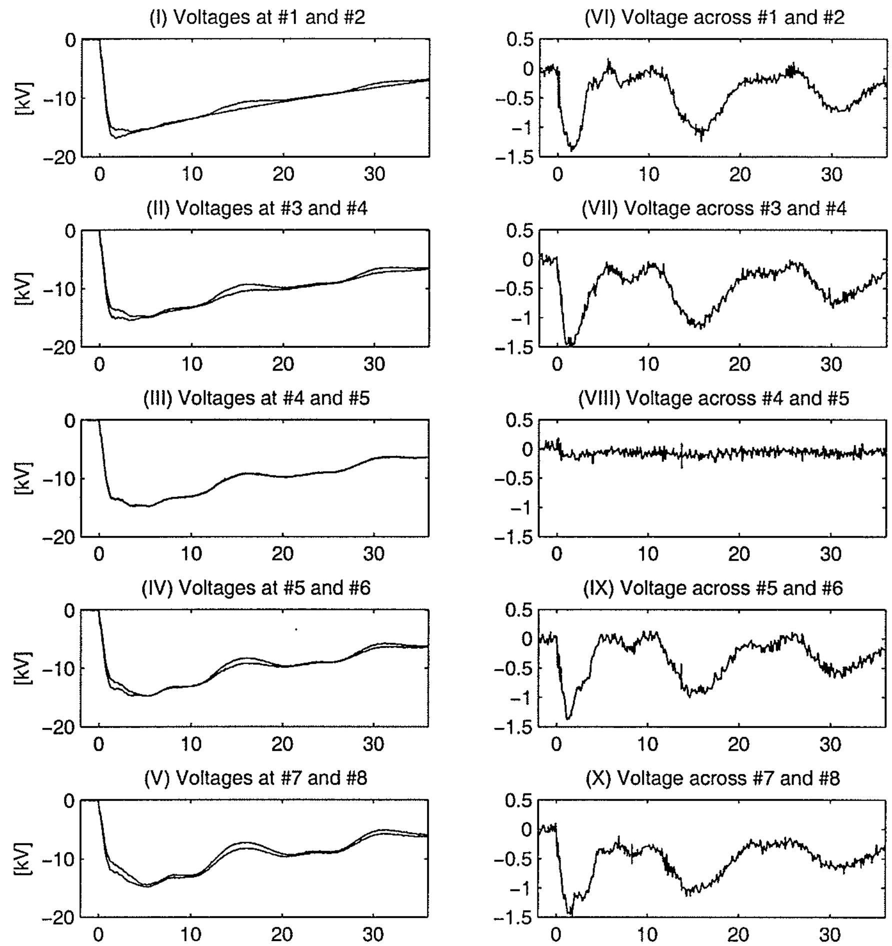

Figure 6.6: Voltage at different sections of the winding close to line-end and voltage across those sections.

15 turns. Highest peak voltage appears across the top most sections. If there are no reflections, voltage across the sections are lower for the lower portion of the winding. The different time occurrence of the peak voltage is significant, since this information may be used for fault location.

The measured voltages at different sections below section #15, and voltage across five sections are shown in Fig. 6.7. Plots (I) to (V) show voltages at different locations along the winding. Plots (VI) to (X) shows the voltage as appeared across the different

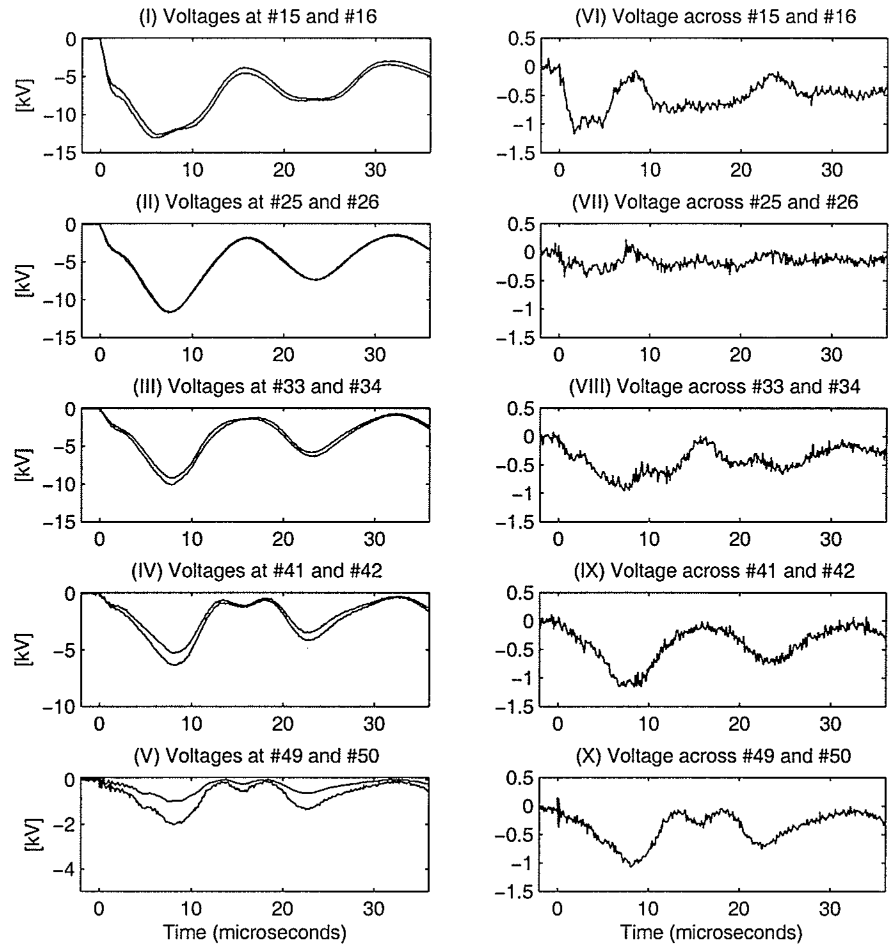

Figure 6.7: Voltage at different sections of the winding close to neutral-end and voltage across those sections.

sections of the winding. Voltage difference between sections #25 and #26 (plot VII) was lower than the rest. This location is close to the voltage taps and the voltage difference is due to approximately four turns.

6.1.4 Minor Insulation Failures using Sphere Gaps

The temporary faults were created by connecting a small sphere gap with spheres of diameter 12.5 mm between the sections which are adjacent to each other, as shown in Fig. 6.2(b). Insulation between the strands were removed and sphere gap was connected to bare copper using crocodile clips. Faults were created at several locations. Some of these locations were used to identify the transient response of the coils as shown in Figs. 6.6 and 6.7.

In the 1950's, CIGRE published several reports [38, 54, 55, 58, 90–92] that investigated impulse test procedures and impulse fault detection methods based on comparison of waveforms. Artificial faults between sections were created using sphere gaps [58, 90]. Preston [90] reports that although faults created by a spark gap in air do not replicate actual conditions, they provide a useful indication of results which might be obtained in practice.

When faults were created with sphere gaps, the faults lasted for a long time compared to the duration of the applied impulse voltage, and resulted in an increased current and a displacement of the current curve with respect to the zero line. Under these conditions the neutral-current method was easily capable of locating the fault. In the work reported in this chapter, a resistor was connected in series with the gap, which results in minor faults that last for a short time compared to the duration of an impulse voltage wave shape.

The breakdown in the spark gap is assumed to simulate the internal breakdown of the oil during the impulse failure of power transformer. This assumption was based on the results published in [93] which compares the propagation mechanism of the impulse breakdown of oil and breakdown in air gaps. This publication concludes that the streamer propagation process in oil is similar to the propagation process in lightning and sparks in air. During an insulation breakdown of oil, hydrogen bubbles are formed before the final discharge. Although the characteristics of the arc is different in hydrogen and air, however, for the current work these differences are not significant [94]. The velocity of a streamer in air is grater than that of a streamer developing in oil. However, one may compensate for this difference by adjusting the spacing of a spark gap. Furthermore, due to the short duration of the breakdown in air gap, as well as in oil gap, the duration of the streamer development does not play significant role in the time-scale used to analyze the failure of a transformer.

6.1.5 Results and Discussion

Figures 6.8 and 6.9 show recorded neutral currents and current through the sphere gap for (a) without a series resistor, (b) 120 Ω resistor in series, (c) 340 Ω resistor in series, and (d) 827 Ω resistor in series.

If the fault lasts for a short time compared to the duration of an impulse voltage wave, the shape of the neutral current wave is dominated by the change of capacitance. If, however, the fault lasts for a longer time, then the effect of the change of inductance is also present. Therefore, a fault of short duration will cause minor distortion in the shape of the neutral current, and a longer fault will result in an increased current and displacement of the current curve with respect to zero line.

Fig. 6.8(a) shows waveforms of a fault that lasted for a longer time compared to the duration of the applied impulse voltage. The fault was created by connecting only a sphere gap between sections #7 and #8. Plot(I) shows the neutral current with and without a fault. To compensate any small differences in the applied voltage, waveforms have been normalized. Plot (II) shows the difference between the neutral currents. Plot (III) shows the fault current through the sphere gap. In this particular case the neutral-current method is capable of locating the fault. However, since the fault occurred during the first 2 μs of the neutral current trace, the exact time of occurrence of the fault cannot be inferred from a comparison of the neutral currents.

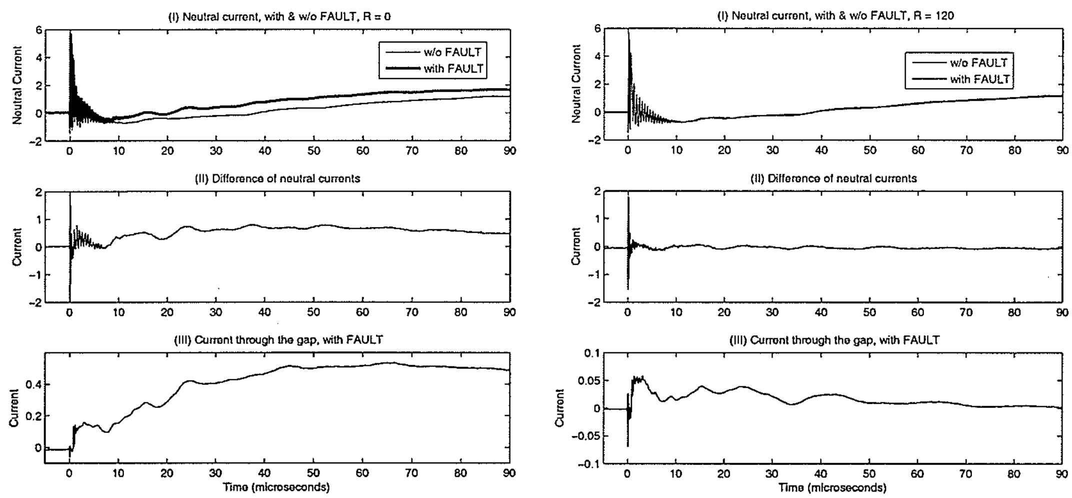

(a) (b)

Figure 6.8: Neutral current waveforms, without and with a fault; (a) w/o resistor, (b) 120 Ω resistor in series.

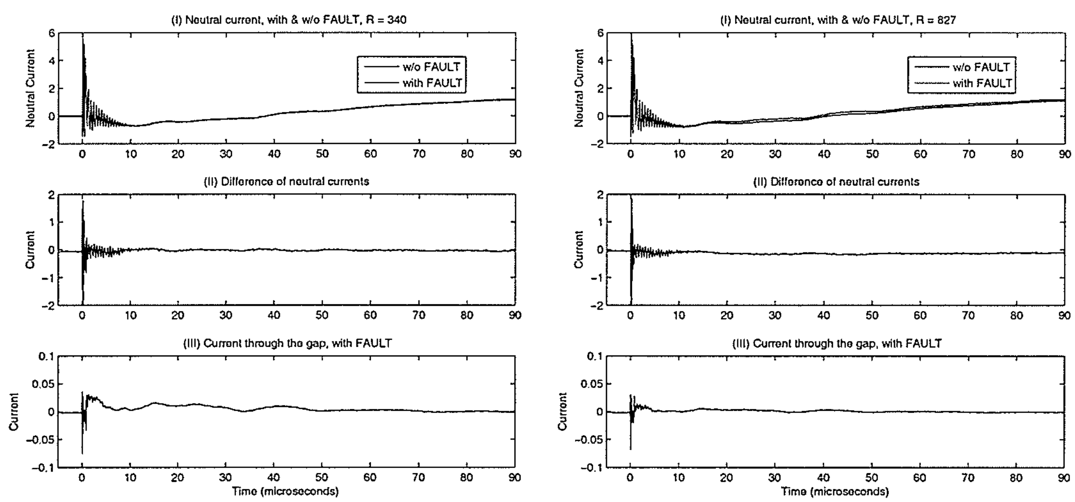

(a) (b)

Figure 6.9: Neutral current waveforms, without and with a fault; (a) 340 Ω resistor in series, (b) 827 Ω resistor in series.

As discussed earlier, the first 2 μs of the neutral current trace cannot be expected to be matched (reduced & full-wave) because of the great probability of voltage pick-up from the high-voltage circuits [4].

Fig. 6.8(b), 6.9(a), and 6.9(b) show waveforms of a fault that lasted for a short time compared to the duration of the applied impulse voltage. The faults were created by connecting a sphere gap and three different values of series resistors between sections #7 and #8. As the duration of the fault current decreases, its effect on the neutral current is reduced. As seen from Fig. 6.8(b),6.9(a), and 6.9(b) application of the neutral-current method does not indicate the presence of a fault.

6.1.6 Summary

In this section a HV experimental setup has been used to create temporary faults on an actual coil removed from a transformer. These faults were created by using a sphere gap with a resistor in series.

When faults were created with only sphere gaps, the faults lasted for a long time compared to the duration of the applied impulse voltage, and resulted in an increased current and a displacement of the current curve with respect to the zero line. Faults created in this manner can be detected by application of the conventional neutral-current method.

When a resistor was connected in series with the gap, the current through the fault lasted for a short time compared to the duration of an impulse voltage wave. In the present work it was decided to connect a 340 Ω resistor in series with the sphere gap because with this arrangement, the neutral current waveform, following the sparkover, matches the unfaulted waveform.

This method of fault creation resulted in a singularity (spike) in the neutral current due to the fault. Since wavelet-based techniques are suitable for signals which are characterized by local features, such as peaks, edges, and breakdown points, this proposed method is an acceptable approach for investigative work that evaluates the application of wavelets for fault detection. Furthermore, faults created by the proposed method provide a useful indication of results which might be obtained in practice.

6.2 Fault detection via Wavelet-based Techniques

In published work, researchers have used CWT [12,13,15], DWT [17] and MSD [13] for fault detection. They are based on either simulated waveforms, or experimental work that was based on permanent faults. In this section, these wavelet-based methods are investigated using HV experimental waveforms. These waveforms represent minor faults that lasted for short time compared to the duration of the impulse voltage wave and occurred within the first 2 μs of the neutral current waveform.

6.2.1 Description of the Impulse Tests

The sequence of impulse tests that was considered in this section are one reduced full impulse (RFW), and two full impulses (FW1, FW2). These tests were conducted using the HV test setup described in Section 6.1. The impulse test levels and description of each impulse test are given in Table 6.1. Impulse test voltages of FW1 and FW2 were 19.5 KV and 19.6 kV respectively. Impulse test voltage of RFW was 16.0 kV, which is approximately 82% of the full impulse. The first two tests, RFW and FW1, were without a fault. In the third test, FW2, a temporary fault was created between sections #7 and #8 using a sphere gap and a series resistance of 340 Ω.

Fig. 6.10 shows the neutral current waveforms recorded during the three impulse

Table 6.1: Sequence of impulse tests.

Wave type	Test voltage (kV)	Description
RFW	16.0	Reduced Full-wave w/o fault
FW1	19.5	Full-wave w/o fault
FW2	19.6	Full-wave with a fault

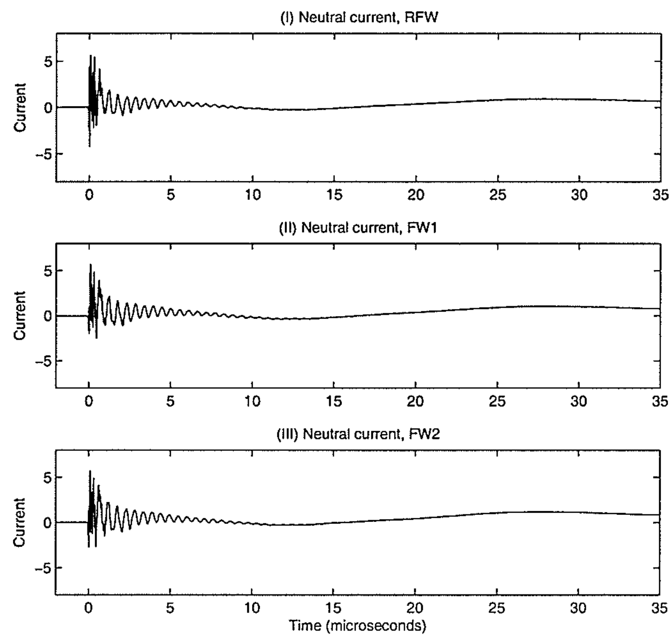

Figure 6.10: Neutral current waveforms of three impulse tests.

tests. Plots (I), (II), and (III) show recorded neutral currents derived from impulse tests conducted with RFW, FW1, and FW2 respectively. Examination of these plots shows that there is no obvious indication of an impulse test failure. These waveforms were denoised using the procedure described in Section 5.4.

6.2.2 Continuous Wavelet Transform

The CWT is used for signal analysis, such as self-similarity analysis and time-frequency analysis. The CWT adds information redundancy because the number of resulting

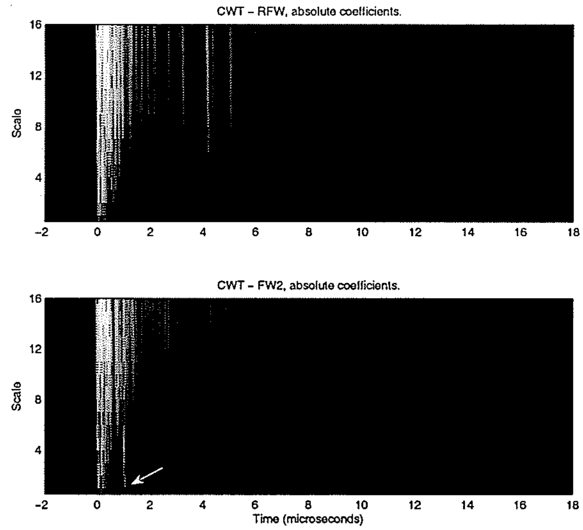

Figure 6.11: Scalogram for the CWT analysis of neutral currents; RFW and FW2.

wavelet coefficients in the time-scale domain is larger than the number of samples in the original signal. Excess redundancy generally is not desirable because more computations and memory are required to process the signals. This was cited as the reason for the author in [13], proposing use of MSD over CWT. However, excess redundancy can be helpful for applications such as time- frequency analysis of nonstationary signals.

Fig. 6.11 shows the results of analysis obtained by application of CWT to neutral currents derived from impulse tests conducted with RFW and FW2. Wavelet coefficients are calculated by shifting the wavelet function ('db4') continuously along the time axis and computing the inner product of each shifted wavelet with the neutral current. In this particular case the wavelet function was dilated on the scale of 1 to 16 in steps of 1. In Fig. 6.11, the x-axis represents time, y-axis represents scale, and the colour at each x-y point represents the magnitude of the wavelet coefficients, which reflects the similarity between the analyzed neutral current and the wavelet function.

In wavelet analysis the scale is related to the frequency of the signal. The lower scales corresponds to the most compressed wavelets. Therefore lower scales are compared to rapidly changing details of the signal, and thus correspond to high frequency components of the signal. Darker shades of the scalogram of the neutral current represent relatively low values of the amplitude of the wavelet coefficients, and lighter shades represent relatively high wavelet coefficients. When the two scalograms in Fig. 6.11 are compared, relatively high wavelet coefficients are present at approximately 1 μs. These coefficients indicate a sudden change in the neutral current due to an artificially created fault.

6.2.3 Discrete Wavelet Transform

The DWT is used for both signal analysis and signal processing, such as noise reduction, data compression, and detection of singularity. The DWT is functionally different from the CWT. The coefficients are calculated by passing the neutral current through a *low-pass* and *high-pass* filters. The scaling function, $\phi(t)$, and the wavelet function, $\psi(t)$, of 'db4' form these filters. The DWT was calculated for 5 different scales (1, 2, 4, 8, and 16).

Fig. 6.12 shows the results of analysis obtained by application of DWT to neutral currents derived from impulse tests conducted with RFW and FW2. In this figure, the x-axis represents time, y-axis represents scale, and the colour at each x-y point represents the magnitude of the wavelet coefficient. Darker shades of the scalogram of the neutral current represent relatively low values of the amplitude of the wavelet coefficients, and lighter shades represent relatively high wavelet coefficients. When the two scalograms in Fig. 6.12 are compared; relatively high wavelet coefficients are present at approximately 1 μs, which is an indication of a fault.

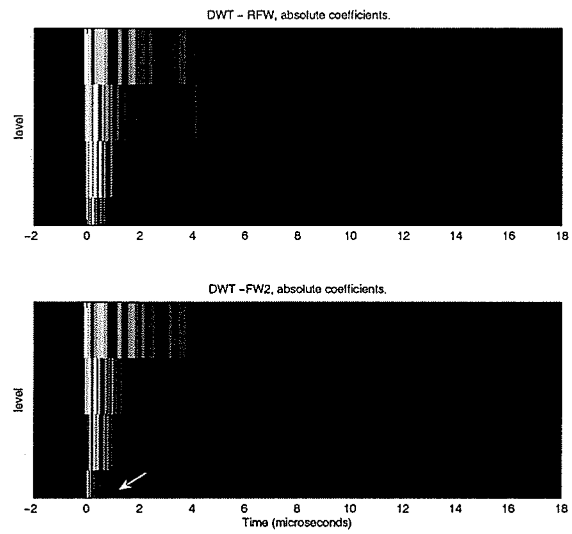

Figure 6.12: Scalogram for the DWT analysis of neutral currents; RFW and FW2.

6.2.4 Multiresolution Signal Decomposition

The MSD technique decomposes a given signal into the detailed and approximated versions. Due to minor insulation failures, the neutral current may contain singularities. By using the MSD technique, the neutral current was decomposed into two other signals; one was the approximated version of the neutral current signal, and the other was the detailed version of the neutral current that contains singularities. Therefore, the MSD technique discriminates disturbance from the original signal, and then analyzes them separately.

In this section, the MSD technique and quadrature mirror filter banks are applied to decompose the neutral current with and without fault into a localized and detailed representation in the form of wavelet coefficients. Daubechies 4 wavelet ('db4') is used for the mother wavelet and the neutral current was decomposed to 3 levels. At the lowest scale, that is scale 1, the mother wavelet is most localized in time and

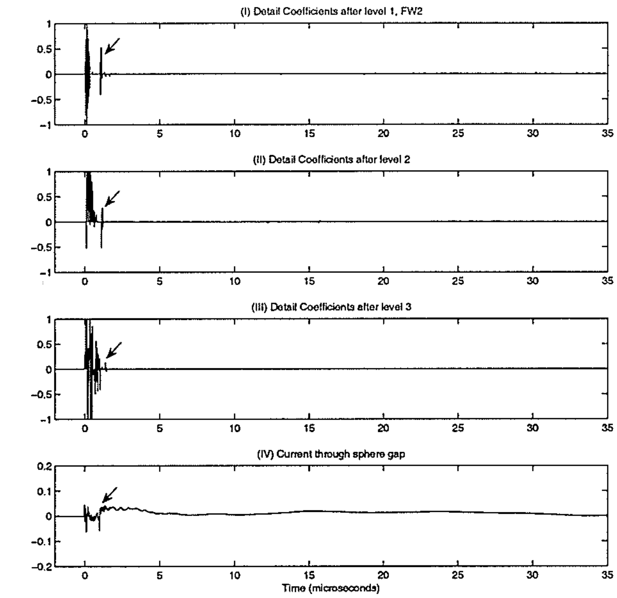

Figure 6.13: MSD of neutral current with a fault (FW2) using the Daubechies 'db4'.

oscillates most rapidly within a very short period of time. As the wavelet goes to higher scales, the analyzing wavelets become less localized in time and oscillate less due to the dilation nature of the wavelet transform analysis. As a result of higher scale signal decomposition, fast and short transient disturbances will be detected at lower scales, whereas slow and long transient disturbances will be detected at higher scales. Hence, one can detect both fast and slow transients with a single type of analyzing wavelet.

Fig. 6.13 and Fig. 6.14 show decomposition of neutral current waveforms obtained under application of impulse test voltage FW2 and RFW respectively. Detailed coefficients after the wavelet decomposition of the neutral current signal at levels 1, 2, and 3 are shown in top three plots. The current through the sphere gap, which created the artificial faults is shown in the bottom-most plot.

In Fig. 6.13, the detailed coefficients after level 1 and 2 have relatively high wavelet

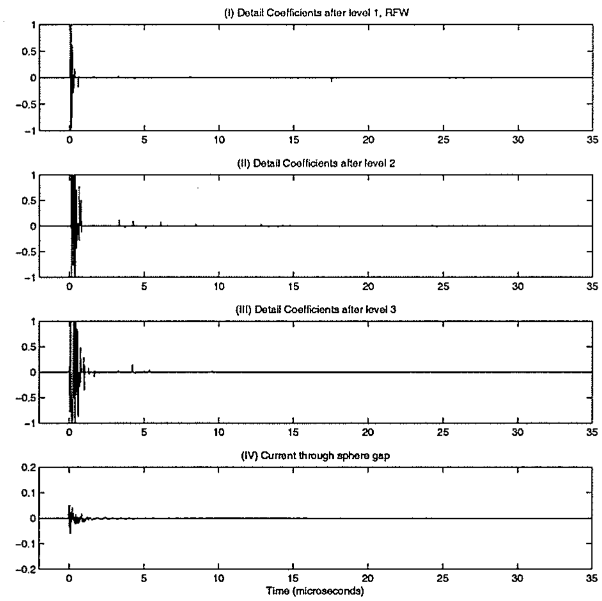

Figure 6.14: MSD of neutral current without a fault (RFW) using the Daubechies 'db4'.

coefficients at approximately 1 μs; this corresponds to the fault as evidenced from the current through the sphere gap. Such details are absent in Fig. 6.14 indicating that MSD was successful in the detection of the fault. In this particular case detailed coefficients are localized in time, enabling the time of occurrence of the fault to be found accurately, and this information may be used to locate the position of the fault within the transformer.

6.2.5 Summary

In this section, temporary faults that lasted for a short time relative to the duration of the applied impulse voltage wave were analyzed using wavelet-based techniques. Perturbation due to the fault occurred within the first 2 μs of the neutral current trace, which cannot be expected to be matched (reduced & full-wave) because of the great probability of voltage pick-up from the high-voltage circuits.

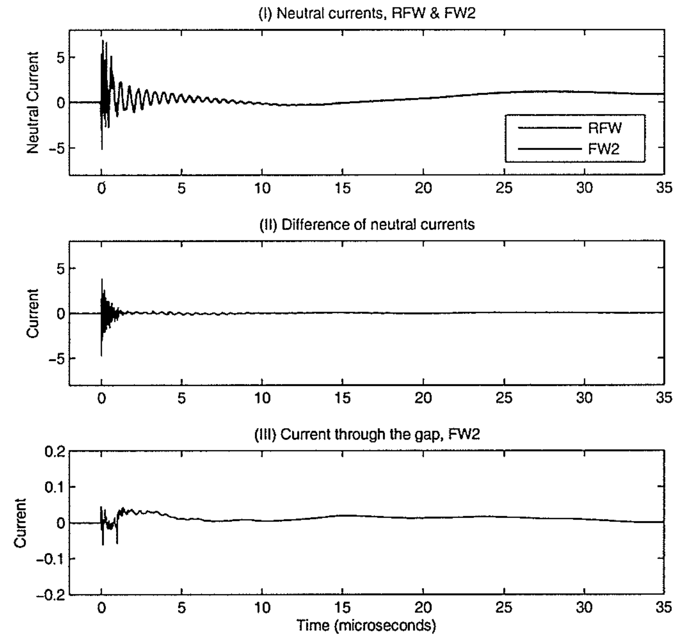

Figure 6.15: Neutral-current Method: Comparison of RFW and FW2.

The results in this section show that wavelet-based techniques can detect such faults with adequate sensitivity. The CWT based method requires some expertise to interpret the scalogram and does not yield accurate information on the time of occurrence of the fault. With the MSD technique the detailed coefficients are much more localized in time resulting in more accurate information on the time of occurrence of the fault.

6.3 Fault Detection in Time-domain

The neutral current waveforms shown in Fig. 6.15 were recorded during impulse tests conducted with impulse voltages RFW and FW2. Plot (I) shows the neutral current waveforms for the two impulse tests. RFW was normalized so that two waveforms can be compared on the same plot. Plot (II) shows the difference in the neutral currents.

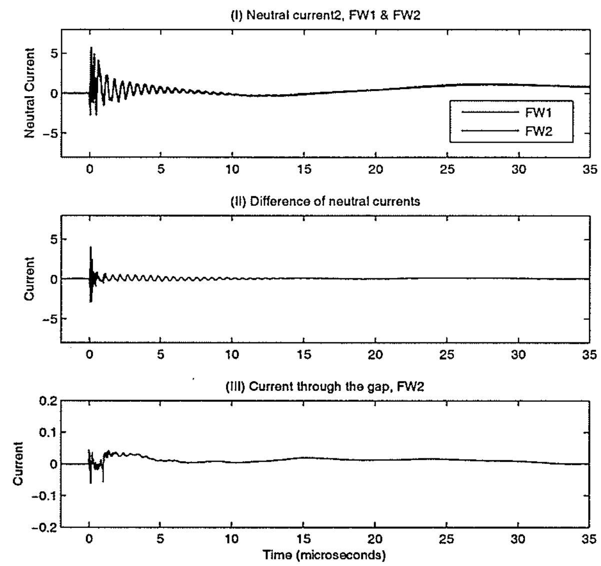

Figure 6.16: Neutral-current Method: Comparison of FW1 and FW2.

Plot (III) shows the current through the sphere gap during the fault between sections #7 and #8. A sudden change in the current due to the fault is visible at approximately 1 μs in plot (III).

The neutral current waveforms shown in Fig. 6.16 were recorded during impulse tests conducted with FW1 and FW2. In this case neutral current waveforms obtained by applying two 100% full waves are compared. Plot (I) shows the neutral current waveforms obtained from the two impulse tests. FW1 was normalized so that two waveforms can be compared on the same plot. The difference between the neutral currents and the current through the sphere gap are shown in plots (II) and (III) respectively.

Comparison of neutral currents recorded during impulse tests conducted with RFW and FW1 are shown in Fig. 6.17. In this case neutral current waveforms obtained by applying reduced full wave and a 100% full waves were compared.

In this particular sequence of tests, neutral-current method could not detect the

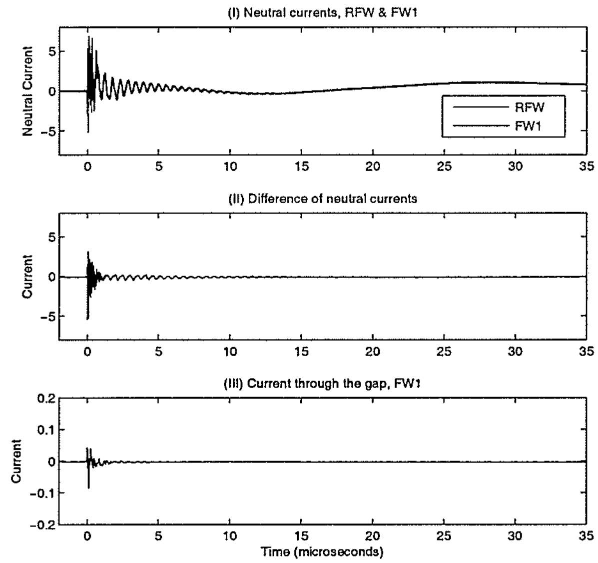

Figure 6.17: Neutral-current Method: Comparison of RFW and FW1.

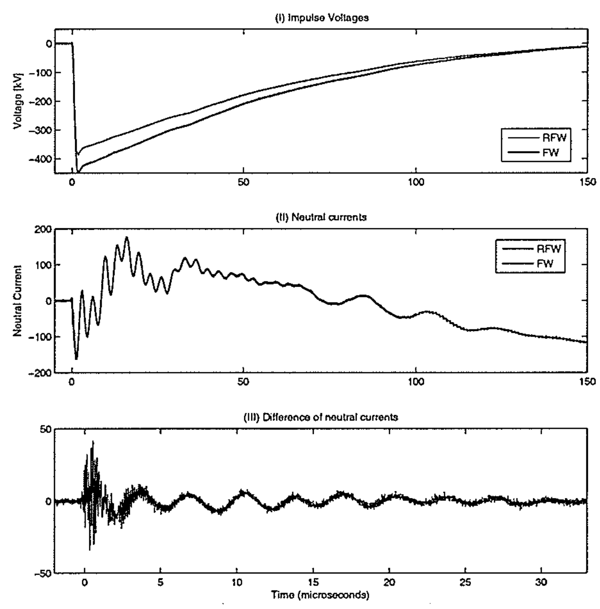

Figure 6.18: Actual impulse test data, 240 MVA, 132/79 kV transformer.

fault between the sections. Furthermore, the first 2 μs of the neutral current trace cannot be expected to be matched (reduced & full-wave) because of the great probability of voltage pick-up from the high-voltage circuits [4]. This is illustrated in Fig. 6.18, which shows test results of an actual impulse test on a 240 MVA, 132/79 kV transformer, which passed the impulse test. Applied voltage was measured using a voltage divider and the current was measured using a 1 Ω noninductive shunt. The waveforms were captured using a commercially available impulse measuring system. The digitizer used in the system has 10-bit resolution and a sampling rate of 30 Ms/cycle. The test system is similar to that shown in Fig. 2.5. Plot (I) shows applied impulse voltages for reduced full-wave and full-wave impulse tests. Plot (II) shows the neutral current waveforms obtained from the two impulse tests. Reduced full-wave was normalized so that two waveforms can be compared on the same plot. Plot (III) shows the difference between the neutral currents. Time scale of the plot in (III) was reduced to highlight the fact that the first 2 μs of the neutral current trace cannot be expected to be matched.

Therefore, if a fault occurs within the first 2 μs, which is the case in the presented work, under application of impulse FW2, the fault cannot be detected using the neutral-current method.

6.4 Fault Detection in Frequency-domain

The transfer-function is calculated as the quotient of the neutral current spectrum and the impulse test voltage spectrum. It reflects the electrical characteristics of the winding and reveals its natural oscillations. Each resonant pole on the transfer function plotted against frequency corresponds to a natural resonance of a winding section. In practise the two obtained transfer functions of the full and reduced levels

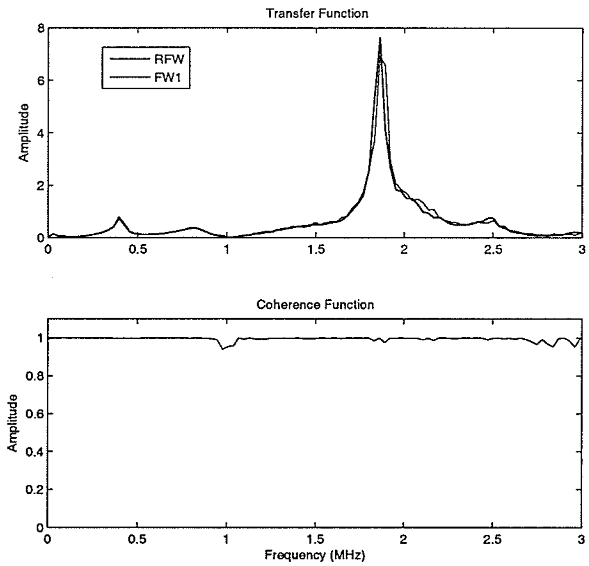

Figure 6.19: Transfer-function analysis during the lightning impulse tests; RFW and FW1.

are superimposed. Neither the amplitude nor the shape of the generated wave form affect the shape of the transfer function. In other words the transfer function shows a fingerprint of the test object which is independent of the generated wave form.

In Fig. 6.19, plot (I) the transfer-function of the winding obtained with the application of reduced full-wave (RFW) is compared to that at full-wave (FW1). There is no clear evidence of a frequency shift or pole-height attenuation in the transfer-functions, which indicates that application of FW1 did not result in an impulse test failure. These plots show the frequency response of the windings up to 3 MHz. The transfer functions calculated beyond approximately 3 MHz diverge which is caused by a decrease in the spectral harmonics of the test voltage and current below the noise level, which imposes an upper frequency limit on the reliable calculation of the transfer function.. However, information about the fault between turns or discs is contained in the high frequency spectral components (usually between 0.5 MHz to

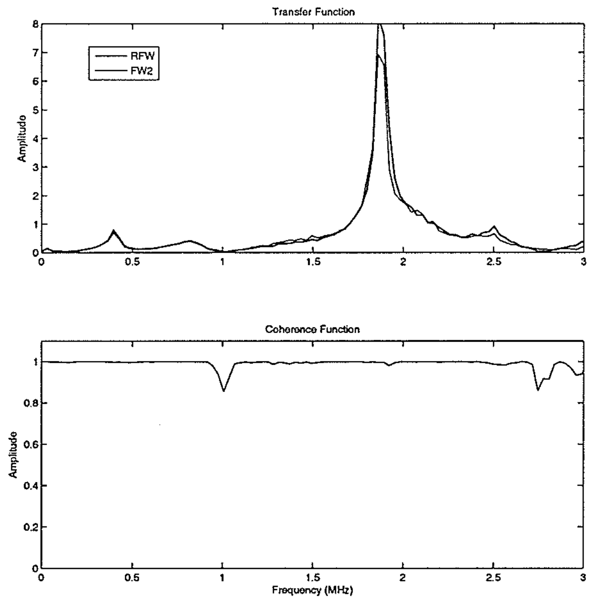

Figure 6.20: Transfer-function analysis during the lightning impulse test; RFW and FW1.

2.5 MHz) of the neutral current and voltage test records [11]. The coherence function between RFW and FW1 is shown in plot (II). The coherence-function attains a value of unity when the set of voltages and currents recorded on the same winding have not changed during the impulse test, and when the records are free from interference. An interference imposed on the test records decreases the coherence, attaining value zero when the signals are completely masked by noise. A low coherence region should not be considered as reliable information for detection of the faults in the winding under examination.

In Fig. 6.20, plot (I) the transfer function of the winding obtained in the presence of a minor insulation failure under the application of FW2 is compared to that obtained by application of impulse voltage RFW in the absence of a fault. The two responses differ clearly; a difference in the pole height is evident at approximately 1.8 MHz. The coherence function between RFW and FW2 is shown in plot (II), which indicates that the voltages and currents had not changed during the impulse tests, and the records were free from interference.

According to the transfer-function theory, a minor insulation failure of the transformer will result in shifting the resonant pole to another frequency or creation of a new pole. In current study, minor insulations failures resulted in changes to the pole height only. It is quite possible, that a new pole may have been created; however, the 9-bit digitizer used in the study was not sufficiently sensitive to detect such changes. It has been reported that the transfer function obtained with the full lightning impulse can be reliably calculated up to approximately 1 MHz using the digital records of voltage and current taken with a 10-bit, 30 MHz dual-channel digitizer. The same instrumentation allows the transfer function to be calculated from the records obtained during the chopped-impulse test, up to approximately 2.2 MHz [10].

6.5 Fault Detection via WPD

6.5.1 Introduction

The wavelet packet decomposition (WPD) of a signal can be viewed as a step by step transformation of the signal from the time domain to the frequency domain. The top level of the WPD is the time representation of the signal. As each level of the decomposition is calculated there is an increase in the trade-off between time and frequency resolution. The bottom level of a fully decomposed signal is a frequency representation.

In this thesis, WPD of the neutral current is proposed instead of MSD for detection of minor insulation failures during impulse tests. In MSD, each level is calculated by passing the previous approximation coefficients though a high and low pass filters.

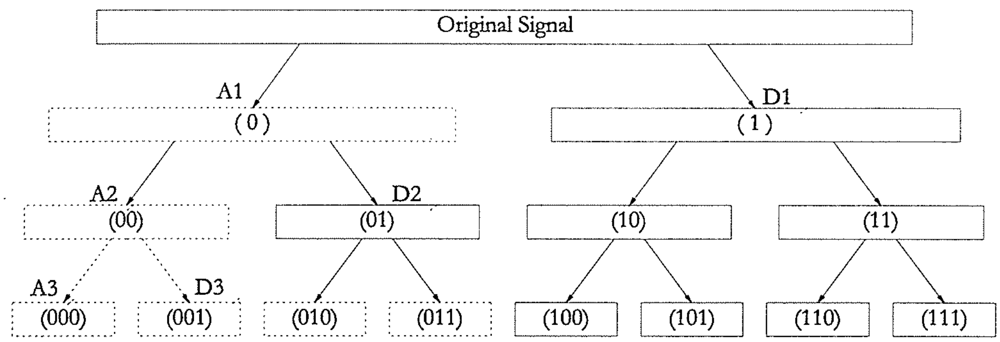

Figure 6.21: WPD over 3 levels

However in the WPD, both the detailed and approximation coefficients are decomposed as shown in Fig. 6.21. The alphanumerics indicate the wavelet coefficients which correspond to MSD. The numbers (i.e. 0, 10, 110 etc.) indicate the path of each packet. The path is a combination of the characters 0 and 1, where 0 represents low-pass filtering (approximate) followed by a decimation by a factor of two, and 1 represents high-pass filtering (detailed) followed by a decimation by a factor of two. Based on Fig. 6.21, the signal can be represented with different sets of sequences, or different decomposition schemes, such as (1, 01, 001, 000), (1, 00, 010, 011), or (000, 001, 010, 011, 100, 101, 110, 111). As the decomposition level increases, the number of different decomposition schemes also increases. In this thesis, decomposition scheme (1, 01, 10, 11, 100, 101, 110, 111) is proposed for detection of impulse test failures.

6.5.2 Example of WPD for Fault Detection

This section demonstrates the application of WPD for fault detection using impulse test records obtained by using HV impulse tests as described in Table 6.1.

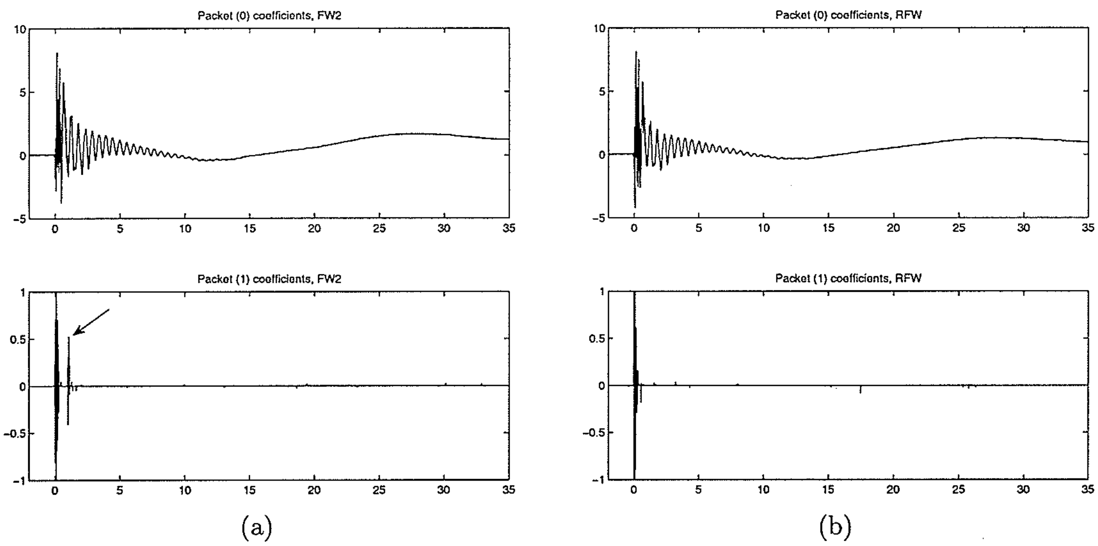

Figure 6.22: The WPD over 1 level for RFW and FW2

Fig. 6.22 shows the results of application of WPD, at level 1, to neutral currents obtained with and without a fault. Packet (1) clearly detects the fault at approximately 1 μs. At level 1 both MSD and WPD gives similar results i.e. packet (1) and D1 are the same.

Fig. 6.23 shows the WPD of neutral current with and without a fault at level 2. Packets (10, 11) clearly detect the fault at approximately 1 μs. Packet (01) also can be used for detection of the fault. At This level of decomposition, MSD and WPD yield different results. With MSD, one would have only packet (01), i.e. coefficients related (01) and D2 are identical. Therefore, when using MSD valuable information regarding the fault could be lost.

At the WPD of neutral current with and without a fault at level 3, difference between MSD and WPD is very significant, which is shown in Fig. 6.24 and Fig. 6.25. The MSD of neutral current with fault would give results of packets (000, 001) as shown in Fig. 6.24(a). These packets do not provide useful information relevant to detect the fault. Packets (100, 101, 110, 111) as shown in Fig. 6.25(a)clearly identify

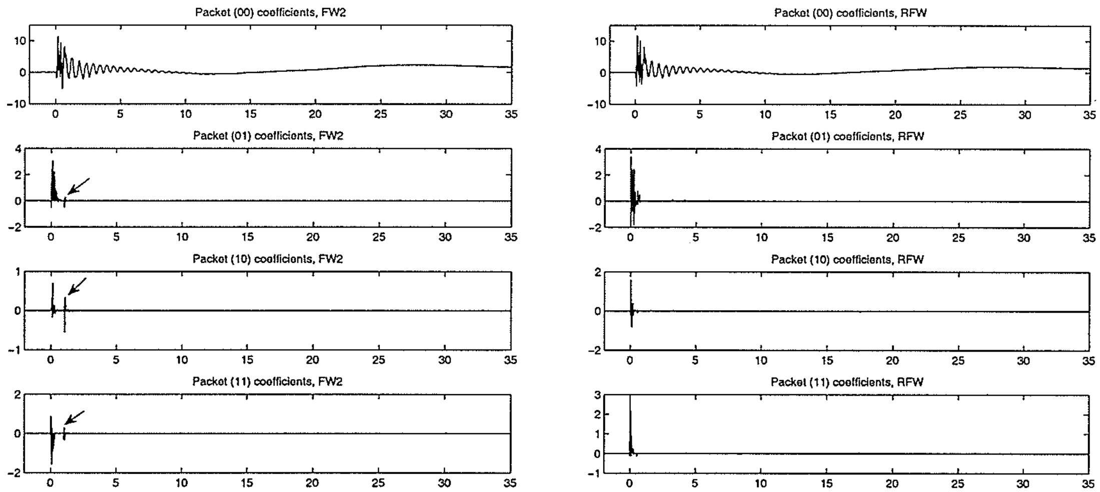

(a) (b)

Figure 6.23: WPD over 2 levels for RFW and FW2

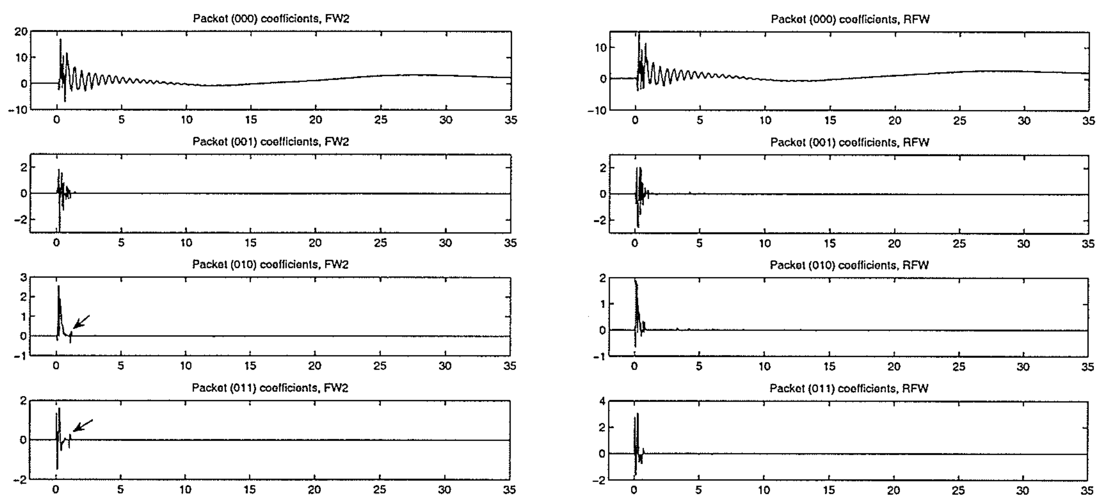

(a) (b)

Figure 6.24: WPD over 3 levels for RFW and FW2

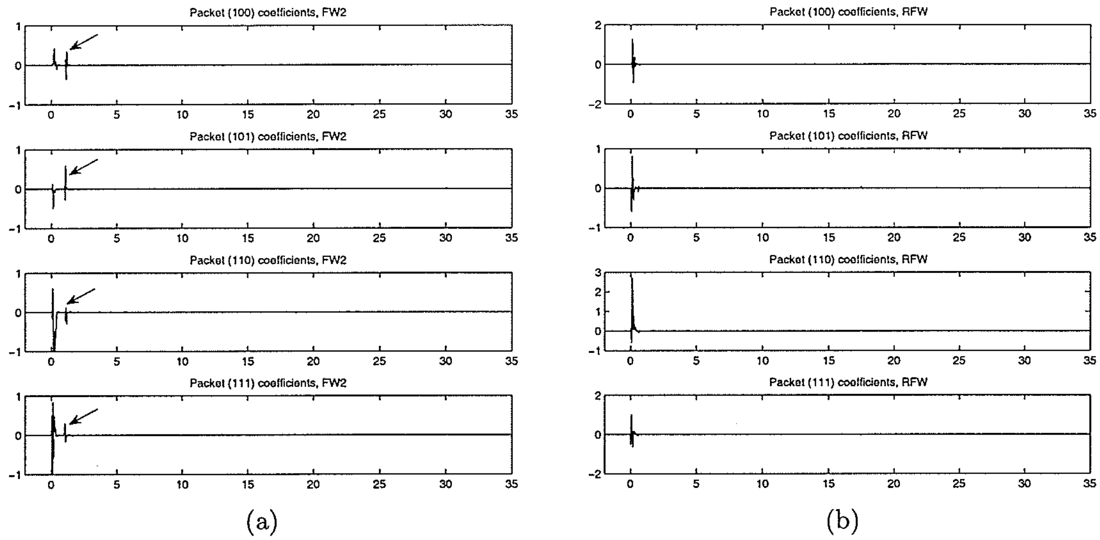

Figure 6.25: The WPD over 3 levels for RFW and FW2

the impulse test failure.

The above results show that WPD is superior to MSD since it provides additional information which can be used to detect minor faults.

6.6 Detection of Turn-to-turn Faults

As discussed earlier, during impulse testing, waveforms were captured at different applied voltages, and faults were simulated at different locations along the coil. Artificial faults between sections were created by using a sphere gap in series with a resistor. Due to the low magnitude of the voltage between certain sections, it was not possible to create faults using sphere gaps. Therefore, faults between these sections were created by use of a neon lamp.

Fig. 6.26 shows analysis of neutral currents obtained with a short duration fault between sections #4 and #5. This is representative of creating a turn-to-turn fault on the top portion of the winding (Fig. 6.3). Fig. 6.26(a) shows the comparison of

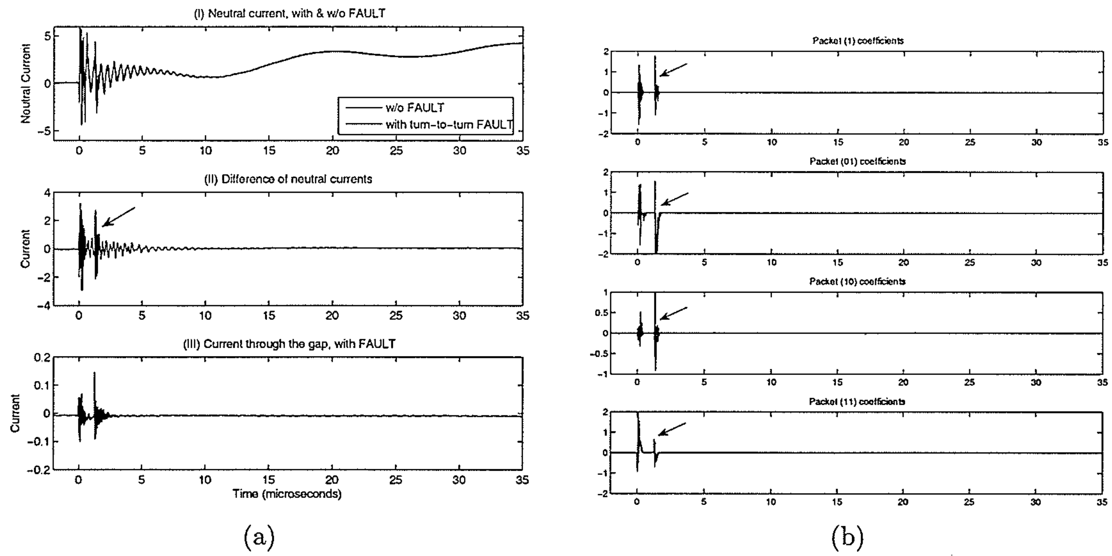

Figure 6.26: Detection of fault between sections #4 and #5 (a) Neutral-current method, and (b) WPD.

the neutral current with and without the fault. The fault can be easily identified by comparison of neutral currents. Fig. 6.26(b) shows the analysis of the neutral current with fault between #4 and #5 using WPD over 2 levels.

Fig. 6.27 shows analysis of neutral currents obtained with a short duration fault between sections #25 and #26. These sections are close to the voltage taps, and number of turns between the sections are approximately four. Fig. 6.26(a) shows the comparison of the neutral current with and without the fault. The peak of the perturbation due to the fault is approximately 3.7% of the maximum amplitude of the neutral current. Fig. 6.27(b) shows the analysis of the neutral current with fault between #25 and #26 using WPD over 2 levels. In this particular case, WPD appears to be more sensitive to this particular type of fault compared to the neutral-current method.

The authors in [12, 13] have analyzed simulated neutral currents to conclude that wavelet-based techniques are suitable for detection of faults that could not be de-

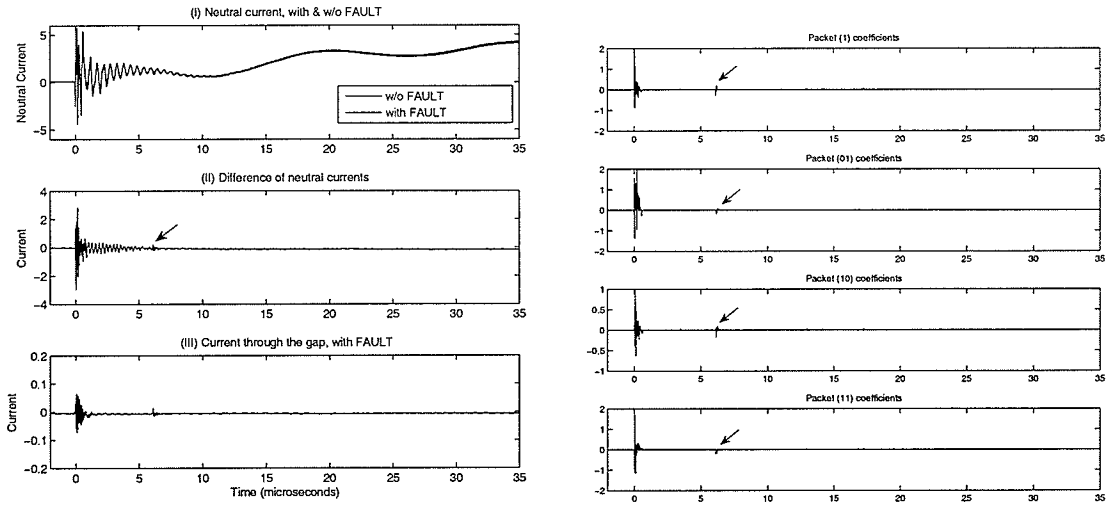

(a) (b)

Figure 6.27: Detection of fault between sections #25 and #26 (a) Neutral-current method, and (b) WPD.

tected by comparison of neutral currents. In their work, neutral current of a transformer which failed the impulse test was simulated by superposing a short-duration (exponentially decaying) oscillating transient onto the neutral current of a healthy transformer. The peak of the superposed transient signal was 7.5% of the neutral peak. As shown in above results, neutral-current method was able to detect a minor fault even when the fault created a perturbation in the neutral current as low as 3.7% of the neutral peak.

6.7 Sensitivity Analysis

In the current research, low-voltage and high-voltage experimental setups have been used to create minor faults with a model transformer and an actual transformer coil. During the experimental work, faults were created between sections at different locations and at different voltages. Experimental waveforms were analyzed using (a) neutral-current method, (b) transfer-function method, and (c) wavelet-based techniques (CWT, MSD, and WPD). Sensitivity of these methods in detecting minor faults created in the experiential work is discussed below.

6.7.1 Duration of the Fault Current

Wavelet-based techniques are suitable for the detection of minor faults that last for a short time compared to the duration of an impulse voltage wave. Due to the short duration of the fault, the shape of the neutral current wave is dominated by the change of capacitance which result in a high frequency transients for few microseconds.

However, if the fault lasts for a longer time, then the effect of the change of inductance makes its presence felt. Therefore, a fault of short duration will cause minor distortion in the shape of the neutral current, and a longer fault will result in an increased current and displacement of the current curve with respect to zero line. These faults can be detected by neutral-current method without any difficulty.

6.7.2 Time Instance of the Fault on the Neutral Current

The results show that the wavelet-based techniques can be successfully applied to detect short-duration temporary faults, which occur within the first 2 μs of the neutral current waveforms; this is not possible by the use of the conventional neutral-current method. The first 2 μs of the neutral current trace cannot be expected to be matched (reduced & full-wave) because of the great probability of voltage pick-up from the high-voltage circuits.

Turn-to-turn faults can be detected using neutral-current method. The results found in this research work do not support the conclusions in some published literature that wavelets can detect minute faults that cannot be detected by the neutral-current method.

6.7.3 Physical Location of the Fault

The results show that the wavelet-based techniques could be successfully applied to detect short-duration temporary faults, which occurred within the first 2 μs of the neutral current waveforms. These minor faults were created close to the line-end in the HV coil.

Faults created close to the voltage taps (#25 and #26) resulted in a perturbation in the neutral current which was approximately 3.7% of the neutral peak. In this case, wavelet-based techniques (particularly WPD) show higher sensitivity in detecting the fault compared to the neutral-current method.

6.7.4 Different Wavelet-based Techniques

The CWT adds information redundancy because the number of resulting wavelet coefficients in time-scale domain is larger than the number of samples in the original signal. Excess redundancy prove higher sensitivity in detecting the faults. However, the CWT based method requires some expertise to interpret the scalogram and does not yield accurate information on the time of occurrence of the fault.

With the MSD and WPD techniques the detailed coefficients are much more localized in time resulting in more accurate information on the time of occurrence of the fault.

In the MSD, each level is calculated by passing the previous approximation coefficients though a high and low pass filters. However in the WPD, both the detailed and approximation coefficients are decomposed. Therefore, WPD shows higher sensitivity in detecting minor faults compared to MSD.

6.8 Summary

In this chapter impulse test records were analyzed to detect faults using (a) conventional neutral-current method, (b) wavelet-based methods, and (c) the transfer-function method.

Impulse test records were generated using a HV experimental setup discussed in Section 6.1.2. These temporary faults lasted for a short time relative to the duration of the applied impulse voltage wave. Since the fault lasted for short time, there was not any displacement of the neutral current curve with respect to the zero line.

The recorded neutral currents were analyzed using previously proposed wavelet-based techniques. Both CWT and DWT can detect faults with adequate sensitivity. The MSD technique has an advantage in that it may be used to identify the time of occurrence of the fault more accurately than possible with the continuous wavelet transform. The results show that the two techniques compliment one another and may be used as effective tools in practice.

The recorded neutral currents were also analyzed using WPD. Results show WPD to be superior in detecting faults when compared to MSD. WPD is proposed as the preferred wavelet-based method for detecting minor faults.

The reported results show that the wavelet transform can be successfully applied to detect short-duration temporary faults, which occur within the first 2 μs of the neutral current waveforms; this is not possible by the use of the conventional neutral-current method.

The results presented in this thesis do not support the conclusions in some published literature, which have claimed that wavelets can detect minute faults that cannot be detected by the neutral-current method. However, the improved time-frequency resolution of WPD is significant when perturbation is small or in cases where comparison of neutral current is difficult when the applied impulse voltage wave shape is not the same.

The transfer-function method was capable of identifying the fault. However, the transfer-function theory states that a minor insulation failure of the transformer will result in shifting the resonant pole to another frequency or creation of a new pole. The calculated transfer-function shows that the pole height has changed. It is quite possible, that new poles may have been created, however, the 9-bit digitizer used in the present study may not have been sufficiently sensitive to detect such changes.

Chapter 7

Conclusions

7.1 General Conclusions

This thesis presented investigative research work on application of wavelets to detect minor insulation failures during impulse tests on large power transformers. The investigation was based on (a) experimental work using a RSG with artificial faults created using neon lamps, and (b) experimental work using a IG with artificial faults created using small spark gaps. The results and analysis highlight the importance and limitations of wavelet-based techniques for the detection of minor faults.

In Chapter 5, the suitability of wavelet-based techniques to detect minor faults was investigated by using experimental research work at reduced voltage. The neutral currents with minor faults were artificially created using a neon lamp and a model transformer. These temporary faults lasted for a short time relative to the duration of the applied impulse voltage wave.

The recorded neutral currents were analyzed using wavelet-based techniques. Test results show that the CWT can detect faults with adequate sensitivity. However, these faults could have been located using neutral-current method as well. Furthermore, analysis of neutral currents with temporary faults do not support the conclusions in some published literature that wavelets can detect minute faults that might not be detected by the neutral-current method.

The CWT analysis of neutral current with faults has demonstrated that the physical location of the fault in the winding can be estimated provided that the transient behaviour of the winding is known.

The application of MSD or WPD techniques did not result in successful detection of some of these faults. This highlights one of the limitations of the wavelet based techniques. That is, selection of the wavelet function is crucial for the wavelet-based method to detect minor faults. Furthermore, the CWT adds information redundancy because the number of resulting wavelet coefficients in time-scale domain is larger than the number of samples in the original signal. Excess redundancy generally is not desirable because more computations and memory are required to process the signals. In this particular case, excess redundancy was helpful in detecting the fault.

It is also shown that the use of permanent faults to create faulted neutral currents in transformer windings is not the correct approach for investigative studies that involve the use of wavelets. This is important since other researchers have used permanent faults to justify the wavelet-based techniques to detect minor faults.

A quantitative method to select the appropriate wavelet function for this particular application is proposed. The techniques suggested by (5.1) was used in the present work resulting in the choice of 'db4' as a suitable basis function. Although faults created by a spark gap in air do not replicate actual conditions, and the shape of the perturbation may not be same as one would expect in practice, results of the current research work suggest that 'db4' to be acceptable for fault detection.

Since the captured neutral current waveforms are contaminated with noise, sometimes, signal processing is required prior to the application of WT for fault detection. A wavelet-based method, which is suitable for reducing noise in the neutral current waveforms is also reported.

In the experimental work at reduced voltage, the magnitude of the neutral current is low compared to noise present in the signal. Wavelet-based techniques were not able to detect certain faults that resulted in small perturbations on the neutral current. To overcome this limitation, it was decided to conduct HV experiments on an actual coil removed from a transformer.

In Chapter 6, the applicability of wavelet-based techniques for detection of minor insulation failures during impulse tests was investigated by using a HV experimental setup. The neutral currents with minor insulation failures (faults between sections with multiple turns) were artificially created using small-size sphere gaps on a HV transformer coil. A neon lamp was used to create faults between certain sections because the voltage across these sections was insufficient to cause spark gap operation. In one such case, a fault was created involving only one turn.

The results show that the wavelet transform can be successfully applied to detect short-duration temporary faults, which occur within the first 2 μs of the neutral current waveforms; this is not possible by the use of the conventional neutral-current method. These faults were located physically near the line-end of the high-voltage coil.

It was found that apart from short-duration temporary faults, which occur within the first 2 μs, even turn-to-turn faults can be detected using neutral-current method. The results found in the current research work do not support the conclusions in some published literature that wavelets can detect minute faults that can not be detected by the neutral-current method.

The neutral current waveforms were analyzed using WPD, which has not been proposed in any of the published literature. The results and analysis of neutral currents with WPD have shown that WPD has a better sensitivity to detect minor faults when compared to MSD.

A common feature in all the tests performed was that the continuous wavelet transform method could detect faults with adequate sensitivity in the low-voltage tests; the opposite was true in the high-voltage tests. This could be due to the fact that neon lamps and sphere gaps have different breakdown characteristics and the perturbation caused is different as well. These results imply that the selection of the particular wavelet function is very important.

Both the low-voltage and high-voltage test results show that the CWT can detect faults with adequate sensitivity. The MSD and WPD techniques have an advantage because of the their application to identify the time of occurrence of the fault more accurately than possible with the CWT. The results show that the CWT and WPD techniques compliment one another and may be used as effective tools in practice. However, this investigative study found no evidence to suggest that the wavelet transform is superior to the neutral current method with one exception, that is, short-duration temporary faults, which occur within the first 2 μs.

Based on reduced voltage and HV experimental data and analysis presented in this thesis, following specific conclusions can be drawn:

1. The results show that the wavelet transform can be successfully applied to detect short-duration temporary faults, which occur within the first 2 μs of the neutral current waveforms; this is not possible by the use of the conventional neutral-current method.

2. It was found that apart from short-duration temporary faults which occur within

the first 2 μs, even a turn-to-turn faults can be detected using neutral current method. The results found in this research work do not support the conclusions in some published literature that wavelets can detect minute faults that can not be detected by the neutral-current method.

3. Finally, CWT and WPD are proposed for detection of minor faults. As stated earlier, no evidence was found to support the claim that wavelet-based techniques are superior to the neutral-current method except in the case of short-duration temporary faults which occur within the first 2 μs. However, the improved time-frequency resolution of wavelets is significant when the perturbation is small or when comparison of neutral currents is difficult when the applied impulse voltage wave shape is not the same.

7.2 Contributions

The main contributions of the work presented in this thesis are as follows.

- Investigated the suitability of wavelet based methods for fault detection using an experimental setup at reduced voltage. Results show that the use of permanent faults to create faulted neutral currents in transformer windings is not the correct approach for investigative work that involves use of wavelets.

- Investigated the suitability of wavelet based methods for fault detection using a HV experimental setup. The results showed that (a) the wavelet transform can be successfully applied to detect short-duration temporary faults, which occur within the first 2 μs of the neutral current waveforms; this is not possible by the use of the conventional neutral-current method, and (b) contrary to published literature, wavelet transform did not detect minute faults that cannot be detected by the neutral-current method.

- Proposed WPD for fault detection. The improved time-frequency resolution of WPD is significant when perturbation is small or the comparison of neutral current is difficult when applied impulse voltage wave shape is not the same.
- Development and implementation of statistical analysis technique to select the best basis for fault detection.
- Development and implementation of algorithm for denoising of experimental waveforms.

These contribution have led to the following publications;

- S. N. Fernando, M. R. Raghuveer, and W. Ziomek, "Optimal wavelet selection to identify faults during impulse tests," in IEEE Conference on Electrical Insulation and Dielectric Phenomena, Kansas City, Missouri, USA, Oct. 2006
- S. N. Fernando and M. R. Raghuveer, "Application of wavelets to identify faults during impulse tests," in IEEE Conference on Electrical Insulation and Dielectric Phenomena, Nashville, TN, USA, Oct. 2005, vol. 4, pp. 581 584
- S. N. Fernando, M. R. Raghuveer, and W. Ziomek, "Detection of temporary faults during impulse tests using wavelets," in IEEE Conference on Electrical Insulation and Dielectric Phenomena, Albuquerque, NM, USA, Oct. 2003, vol. 4, pp. 478 481.

7.3 Suggestions for Future Research

Comparison of neutral current during chopped impulse tests is not possible due to the uncertainties of the chopped time. It is possible that wavelets may be able to locate such faults. Further research is required to investigate the use of wavelets to detect faults that occur during chopped impulse tests.

Appendix A

HV Coil

Table A.1: HV Coil Design and Calculation Sheet.

Insulation level [kV]	161		
LIL - FW [kV]	650/110		
Rated Voltage [kV]	138		
Winding type	HV - Center Fed, Disc Spiral		
Conductor length/leg [in]	4949		
MVA & position	100@DTC1	100@DTC3	100@DTC5
Line voltage [kV] & position	144.90	138.00	131.10
No. of turns	376	358	340
Turns/leg	376		
Discs	$2 \parallel \times 52$		
Layers × turns/sect	7.857		
Volts between discs [V]	3498		
Winding height [in]	$56.93 \Rightarrow$ **57.00**		
Coil dimensions [in]	44.32 ID $\times$ 55.98 OD		

Appendix B

Measuring System

B.1 Digital Oscilloscope

Table B.1: TDS 3054 - Electrical Characteristics.

Bandwidth	500 MHz
Channels	4
Sample rate range	100 S/s to 5 GS/s
Maximum Record Length	10,000 points
Digitizers	9-bit resolution, separate digitizers for each channel sample simultaneously
Vertical Sensitivity (/div)	1 mV-10 V
Vertical Accuracy	$\pm$ 2%
BW Limit	Selectable between 20 MHz, 150 MHz
Input impedance, DC coupled	1 MΩ $\pm$1% in parallel with 13 pF $\pm$2 pF 50 Ω $\pm$1%; VSWR$\leq$ 1.5:1 from DC to 500 MHz
Time Base:Range (/div), Accuracy	1 ns - 10 s/div, 200 ppm

B.2 Probes

Table B.2: Tektronix P6015A High Voltage Probe - Electrical Characteristics.

Voltage	20 kV DC, 40 kV Peak (100 ms Pulse Width)
Bandwidth	75 MHz
Loading	100 MΩ 3 pF
Compensation Range	7 to 49 pF
Rise Time	4.0 ns
Attenuation	1000X

Table B.3: High Frequency Current Monitor - Electrical Characteristics.

Sensitivity	0.01V/A into 50 Ω
Maximum Current	50 kA
Droop	0.004 Percent/μ sec
$\int$ Idt	1 A sec

B.3 50 kV Impulse Generator

Table B.4: Impulse Generator - Circuit Parameters.

Discharge Capacitance, C1	0.25 μF
Load Capacitance, C2	0.33 μF (Three 1 μF in series)
Front Resistance, R1	37.9 Ω
Discharge Resistance, R2	208.6 Ω

Acronyms

AC	Alternating Current
BIL	Basic Lightning Impulse Insulation Level
BSL	Basic Switching Impulse Insulation Level
CIGRE	International Council on Large Electric Systems
CW	Chopped Wave
CWT	Continuous Wavelet Transform
DC	Direct Current
DWT	Discrete Wavelet Transform
EHV	Extra High Voltage
FFT	Fast Fourier Transform
FOW	Front of Wave
FW	Full Wave
GIS	Gas Insulated Substations
HV	High Voltage
IEC	International Electrotechnique Commission
IEEE	Institution of Electrical and Electronics Engineers
IG	Impulse Generator
LV	Low Voltage
MRA	Multiresolution Analysis
MSD	Multiresolution Signal Decomposition
PD	Partial Discharge
RFW	Reduced Full Wave
STFT	Short Time Fourier Transform
TF	Transfer Function
VFT	Very-fast-front Transients
WPD	Wavelet Packet Decomposition

Reference

[1] L. L. Grigsby, *The Electrical Engineering Handbook.* IEEE, 1989.

[2] IEEE, *Standard General Requirements for liquid-immersed distribution, power, and regulating transformers, IEEE Std C57.12.00-2000.* Institue of Electrical and Electronics Engineers, Piscataway, NJ, USA, 2000.

[3] IEEE, *Standard Test Code for liquid-immersed distribution, power, and regulating transformers, IEEE Std C57.12.90-1999.* Institue of Electrical and Electronics Engineers, Piscataway, NJ, USA, 1999.

[4] IEEE, *Guide for Transformer Impulse testing, IEEE Std. C57.98-1993.* Institue of Electrical and Electronics Engineers, Piscataway, NJ, USA, 1993.

[5] IEC, *Power Transformers - Insulation levels, dielctric testing and external clearance in air, IEC 60076-3.* International Electrotechnique Commission, Geneva, Switzerland, 2000.

[6] IEC, *Guide to the lighting impulse and switching impulse testing - Power Transformers and reactors, IEC 60076-4.* International Electrotechnique Commission, Geneva, Switzerland, 2002.

[7] CSA, *Power Transformers and Reactors, CAN/CSA-C88-M90.* Canadian Standards Associations, Toronto, Canada, 2004.

[8] F. J. Vogel and V. M. Montsinger, "Progress report on impulse testing of commercial transformers," *AIEE Transactions*, vol. 52, pp. 409–10, 1933.

[9] K. Karsai, D. Kerenyi, and L. Kiss, *Large Power Transformers.* Elsevier Science Publishing Company, Inc., 1986.

[10] R. Malewski and B. Poulin, "Impulse testing of power transformers using the transfer function method," *IEEE Trans. on Power Delivery*, vol. 3, pp. 476–489, April 1988.

[11] R. Malewski, E. Gockenbach, R. Maier, K. H. Fellmanu, and H. Claudi, "Five years of monitoring the impulse test of power transformers with digital recorders and the transfer function method," Paper 12-201, CIGRE, Paris, August-September 1992.

[12] L. Satish, "Short-time Fourier and wavelet transforms for fault detection in power transformers during impulse tests," *IEE Proc. Sci. Meas. Technol.*, vol. 145, pp. 77–84, March 1998.

[13] S. K. Pandey and L. Satish, "Multiresolution signal decomposition: A new tool for fault detection in power transformers during impulse tests," *IEEE Trans. on Power Delivery*, vol. 13, pp. 1194 –1200, Oct. 1998.

[14] G. G. Karady, M. Reta-Hernandez, F. Amarh, and G. McCulla, "Improved technique for fault detection sensitivity in transformer impulse test," in *Power Engineering Society Summer Meeting*, vol. 4, (Seattle, WA, USA), pp. 2412–2416, IEEE, July 2000.

[15] M. R. Rao and B. P. Singh, "Detection and localization of interturn fault in the hv winding of a power transformer using wavelets," *IEEE Trans. on Dielectrics and Electrical Insulation*, vol. 8, pp. 652 –657, Aug. 2001.

[16] A. Bhoomaiah, P. K. Reddy, K. S. L. Murthy, P. A. Naidu, and B. P. Singh, "Measurement of neutral currents in a power transformer and fault detrection

using wavelet techniques," in *Conference on Electrical Insulation and Dielectric Phenomena*, vol. 2, (Boulder, Colorado, USA), pp. 170 – 173, IEEE, Oct. 2004.

[17] N. P. Kumar, J. Amaranath, K. D. Shrivastava, and B. P. Singh, "Identification of winding faults in power transformers by low voltage impulse test and neutral current method using wavelet transform approach," in *Conference on Electrical Insulation and Dielectric Phenomena*, vol. 2, (Nashville, TN, USA), pp. 140 – 143, IEEE, Oct. 2005.

[18] IEC, *Insulation co-ordination Part 1: Definitions, principles and rules, IEC 60071-1*. International Electrotechnique Commission, Geneva, Switzerland, 2006.

[19] R. Degeneff, W. McNutt, W. Neugebauer, J. Panek, M. Mccallum, and C. Honey, "Transformer response to system switching voltages," *IEEE Transaction on on Power Apparatus and Systems*, vol. PAS-101, pp. 1457 – 1470, June 1982.

[20] L. L. Grigsby, *The Electric Power Engineering Handbook*. CRC Press LLC, 2001.

[21] R. Kaufman and J. Meador, "Dielectric tests for ehv transformers," *IEEE Trans. on Power Apparatus and Systems*, vol. PAS-87, pp. 135–145, Jan. 1968.

[22] A. J. Vandermaar, M. Wang, J. B. Neilson, and K. D. Srivastava, "The electrical breakdown characteristics of oil-paper insulation under steep front impulse voltages," *IEEE Transaction on Power Delivery*, vol. 9, pp. 1926–1933, October 1994.

[23] C. W. G. 33/13-09, "Very fast transient phenomena associated with gas insulated substations," *CIGRE, Paper 33-13*, Paris, 1988.

[24] L. F. Blume, A. Boyajian, G. Camilli, T. C. Lennox, S. Minneci, and V. M. Montsinger, *Transformer Engineering*. John Wiley & Sons, INC, 1951.

[25] T. K. Ganguli, M. V. Prabhakar, S. K. Gupta, R. K. Singh, and K. G. Krishnana, *Transformers.* Tata McGraw-Hill Publishing Company Limited, 2003.

[26] A. Padersen, "On the response of interleaved transformer windings to surge voltages," *IEEE Trans. on Power Apparatus and Systems*, vol. PAS-82, pp. 349–356, June 1963.

[27] R. C. Degeneff and W. N. Kennedy, "Calculation of initial, pseudo-final, and final voltage distributions in coils using matrix techniques," in *IEEE Summer Power Meeting*, (San Francisco, CA, USA), IEEE, 1975.

[28] J. H. Harlow., *Electric power transformer engineering.* CRC Press LLC, 2004.

[29] R. Degeneff, "A general method for determining resonances in transformer windings," *IEEE Transaction on on Power Apparatus and Systems*, vol. PAS-96, pp. 423–430, March/April 1977.

[30] M. Vaklian, R. C. Degeneff, and M. Kupferschmid, "Computing the internal transient voltage response of a transformer with a nonlinear core using gears method part 1: Theory," *IEEE Transaction on Power Delivery*, vol. 10, p. 18361841, October 1995.

[31] M. Vaklian, R. C. Degeneff, and M. Kupferschmid, "Computing the internal transient voltage response of a transformer with a nonlinear core using gears method part 2: Verification," *IEEE Transaction on Power Delivery*, vol. 10, p. 702708, May 1995.

[32] F. de Leon and A. Semlyen, "Complete transformer model for electromagnetic transients," *IEEE Transaction on Power Delivery*, vol. 9, p. 231239, January 1994.

[33] H. Dommel, "Digital computer solution of electromagnetic transients in single and multiphase networks," *IEEE Transaction on on Power Apparatus and Systems*, vol. PAS-88, p. 388399, April 1969.

[34] R. Degeneff, M. Vakilian, M. Gutierrez, P. Mckenny, R. Girgis, J. Schneider, J. Provanzana, and P. Soderberg, "Modeling power transformer for transient voltage calculations," *CIGRE, paper 12-304*, 1992.

[35] R. Malewski, K. Drazba, S. Sieradzki, and M. Borecki, "A digital assessment technique of transformer winding oscillations," *CIGRE, paper 12/33-07*, 2000.

[36] IEEE, *Techniques for High-Voltage Testing, IEEE Std. 4-1995.* Institue of Electrical and Electronics Engineers, Piscataway, NJ, USA, 1995.

[37] R. Kaufman, "Dielectric tests and test procedures for ehv transformers protected by modern surge arresters and operated on effectively grounded systems 345 kv through 765 kv," *IEEE Trans. on Power Apparatus and Systems*, vol. PAS-92, pp. 1752–1762, Sept. 1973.

[38] H. Aeschlimann, "Modeling power transformer for transient voltage calculations," *CIGRE, Report 126*, 1954.

[39] F. J. Vogel, "Discussion on the paper... dielectric tests for ehv transformers," *IEEE Trans. on Power Apparatus and Systems*, vol. PAS-87, pp. 141–142, Jan. 1968.

[40] G. Karady, "The stress produced by chopped-wave tests in different transformer connecctions and their variation with wave duration," *CIGRE Report*, vol. 114, 1958.

[41] V. M. Montsinger, "Coordination of power transformers for steep-front impulse waves," *AIEE Transactions*, vol. 57, pp. 183–195, April 1938.

[42] P. L. Bellaschi, "Impulse test requirements for generator transformers and for tertiary windings," *IEEE Trans. on Power Apparatus and Systems*, vol. 88, pp. 1183–1186, August 1969.

[43] R. Malewski, A. Claudi, C. Josephy, and S. Jud, "Checking electromagnetic compatibility. of a hv impulse measuring circuit with. coherence functions," in *High Voltage Measurements and Calibration*, (Arnhem, Netherlands), pp. P8.1–P8.11, ERA Technology Conference, October 1994.

[44] N. R. Hylten-Cavallius and T. N. Giao, "Floor net used as ground return in high-voltage test areas," *IEEE Trans. on Power Apparatus and Systems*, vol. PAS-88, pp. 996–1005, July 1971.

[45] K. Fowler, "Grounding and shielding, part 1-noise," *IEEE Instrumentation and Measurement Magazine*, vol. 3, pp. 41 –44, June 2000.

[46] IEC, *Instruments and software used for measurement in high-voltage impulse tests - Part 1: Requirements for instruments, IEC 61083-1.* International Electrotechnique Commission, Geneva, Switzerland, 2001.

[47] IEC, *High-Voltage Test Techniques Part 2: Measuring Systems-Second Edition; Amendment 1-1996, IEC 60060-2.* International Electrotechnique Commission, Geneva, Switzerland, 1994.

[48] G. Karady and N. Hylten-Cavallius, "Electromagnetic shielding for high voltage laboratories," *IEEE Trans. on Power Apparatus and Systems*, vol. PAS-90, pp. 1400–1406, June 1971.

[49] F. Rizk, Y. Gervais, and H. Luhrmann, "Performance of electromagnetic shields in high voltage laboratories," *IEEE Trans. on Power Apparatus and Systems*, vol. PAS-94, pp. 2077–2083, Nov./Dec. 1975.

[50] R. Malewski, "Wirewound shunts for measurement of fast current impulses," *IEEE Trans. on Power Apparatus and Systems*, vol. PAS-103, pp. 2927–2933, October 1984.

[51] A. J. Schwab, "Low-resistance shunts for impulse currents," *IEEE Trans. on Power Apparatus and Systems*, vol. PAS-90, pp. 2251–2257, October 1971.

[52] T. McComb, J. Kuffel, R. Malewski, and K. Schon, "Qualifying an impulse digitizer for measurements in hv impulse tests," *IEEE Transactions on Power Delivery*, vol. 5, pp. 1256–1265, July 1990.

[53] IEEE, *Standard for digital recorders for measurement in high-voltage impulse tests, IEEE Std 1122-1998.* Institue of Electrical and Electronics Engineers, Piscataway, NJ, USA, 1998.

[54] K. E. Stenkvist, "Study of fault detection and failure location during surge testing of transformers," *CIGRE, Report 129*, 1952.

[55] W. Rabus, "The impulse voltage difference method for the detection and location of faults during full wave impulse tests on transformers," *CIGRE, Report 139*, 1954.

[56] J. H. Hagenguth, "Progress in impulse testing of transformers," *AIEE Transactions*, vol. 63, pp. 999–1005, 1944.

[57] M. E. Beavers, J. E. Holcomb, and L. C. Leoni, "Magnetization of transformer cores during impulse testing," *AIEE Transactions*, vol. 74, pp. 118–123, April 1955.

[58] F. Beldi, "Impulse testing of transformers, measuring procedures and test circuits," *CIGRE, Report 112*, 1952.

[59] J. G. Anderson, "Ultrasonic detection and location of dielectric discharges in insulating structures," *AIEE Transactions*, vol. 75, no. 3, pp. 1193–1198, 1956.

[60] A. C. Franklin, *The J & P transformer book.* Butterworth & Co. Ltd., 1983.

[61] I. C. Report, "Switching surge tests for oil-insulated power transformers," *IEEE Trans. on Power Apparatus and Systems*, vol. PAS-86, pp. 247–249, Feb. 1967.

[62] I. C. Report, "Switching surge tests for oil-insulated power transformers," *IEEE Trans. on Power Apparatus and Systems*, vol. PAS-87, pp. 405–407, Feb. 1968.

[63] K. Ramchandran, M. Vetterli, and C. Herley, "Wavelets, subband coding, and best bases," *Proceedings of the IEEE*, vol. 84, pp. 541 –560, April 1996.

[64] I. Daubechies, "The wavelet transform, time-frequency localization and signal analysis," *IEEE Transactions on Information Theory*, vol. 36, pp. 961–1004, Sept. 1990.

[65] I. Daubechies, *Ten Lectures on Wavelets.* Society for Industrial & Applied Mathematics, 1992.

[66] S. Mallat, "A theory for multiresolution signal decomposition: The wavelet representation," *IEEE Transactions Pattern Analysis and Machine Intelligence*, vol. 11, pp. 674–693, July 1989.

[67] S. Mallat, *A Wavelet Tour of Singal Processing.* Academic Press, 1999.

[68] O. Rioul and M. Vetterli, "Wavelets and signal processing," *IEEE Spectrum Magazine*, pp. 14–38, Oct. 1991.

[69] M. Farge, "Wavelet transforms and their applications to turbulance," *Annual Review Fluid Mechanics*, vol. 25, pp. 395–457, 1992.

[70] F. Truchetet and O. Laligant, "Wavelets in industrial applications: a review," *Wavelet Applications in Industrial Processing II, Proceedings of the SPIE*, vol. 5607, pp. 1–14, November 2004.

[71] A. Graps, "An introduction to wavelets," *IEEE Computational Sciences and Engineering*, vol. 2, pp. 50–61, Summer 1995.

[72] M. Sadiku, C. Akujuobi, and R. Garcia, "An introduction to wavelets in electromagnetics," *IEEE Microwave Magazine*, vol. 6, pp. 63–72, June 2005.

[73] R. Polikar, "The engineer's ultimate guide to wavelet analysis." http://users.rowan.edu/ polikar/WAVELETS/WTtutorial.html, 2001.

[74] B. Gururaj, "Simple technique of data generation for evaluation of transformer transfer function analysis software," IWD 44, CIGRE WG 33-03, Malaga Spain, 1994.

[75] L. C. Aicher, "Some aspects of ground current measurements during transformer impulse tests," *AIEE Transactions*, vol. 79, no. 3, pp. 1101–1107, 1961.

[76] B. Gururaj and L. Satish, "Detection and localization of interturn fault in the hv winding of a power transformer using wavelets," *IEEE Trans. on Dielectrics and Electrical Insulation*, vol. 9, pp. 479 –480, June 2002.

[77] C. G. A. Koreman, "Improvement in transformer testing through the use of the transfer function," in *Fifth International Symposium on High Voltage Engineering*, vol. 5, (Braunschwieg, Germany), pp. 1–4, ISH, August 1987.

[78] F. Harris, "On the use of windows for harmonic analysis with the discrete fourier transform," *Proceedings of IEEE*, vol. 66, pp. 51–83, Jan. 1978.

[79] P. T. M. Vaessen and E. Hanique, "Power quality assessment via wavelet transform analysis," *IEEE Transactions on Power Delivery*, vol. 11, pp. 924–930, April 1996.

[80] X. Ma, C. Zhou, and I. J. Kemp, "Automated wavelet selection and thresholding for PD detection," *IEEE Electrical Insulation Magazine*, vol. 18, pp. 37–45, Mar/Apr 2002.

[81] L. Satish and B. Nazneen, "Wavelet-based denoising of partial discharge signals buried in excessive noise and interference," *IEEE Trans. on Dielectrics and Electrical Insulation*, vol. 10, pp. 354 –367, April 2003.

[82] X. Ma, C. Zhou, and I. J. Kemp, "Interpretation of wavelet analysis and its application in partial discharge detection," *IEEE Trans. on Dielectrics and Electrical Insulation*, vol. 9, pp. 446–457, June 2002.

[83] M. Jansen, *Noise Reduction by Wavelet Thresholding.* Springer-Verlag, 2001.

[84] G. Keppel and S. Zedeck, *Data Analysis for Research Designs – Analysis of Variance and Multiple Regression/Correlation Approaches.* W.H. Freeman and Company, 1989.

[85] C. Taswell, "The what, how, and why of wavelet shrinkage denoising," *Computing in Science and Engineering*, vol. 3, pp. 12–19, May/Jun 2000.

[86] D. Donoho and I. Johnstone, "Threshold selection for wavelet shrinkage of noisy data," *Proceedings of the 16th Annual International Conference of the IEEE*, vol. 1, pp. A24–A25, Nov 1994.

[87] D. Donoho, "De-noising by soft-thresholding," *IEEE Trans. on Information Theory*, vol. 41, pp. 613–627, May 1995.

[88] D.-F. Guo, W.-H. Zhu, Z.-M. Gao, and J.-Q. Zhang, "A study of wavelet thresholding denoising," in *Signal Processing Proceedings, 2000. WCCC-ICSP 2000. 5th International Conference on*, vol. 1, (Beijing, China), pp. 329–332, IEEE, Aug. 2000.

[89] A. Miki, T. Hosoya, and K. Okuyama, "a calculation method for impulse voltage distribution and transferred voltage in transformer windings," *IEEE Trans. on Power Apparatus and Systems*, vol. 97, pp. 930–939, May/June 1978.

[90] L. L. Preston, "Chopped wave impulse testing of transformers," *CIGRE, Report 131*, 1956.

[91] R. Elsner, "Detection of insulation failures during impulse testing of transformers," *CIGRE, Report 101*, 1954.

[92] P. G. Provoost, "Impulse testing of transformers," *CIGRE, Report 115*, 1954.

[93] T. W. Liao and J. G. Anderson, "Propagation mechanism of impulse corona and brakdown in oil," *Trans. AIEE*, vol. 72, pp. 641 –648, November 1953.

[94] F. A. M. Rizk. private communication, 2006.